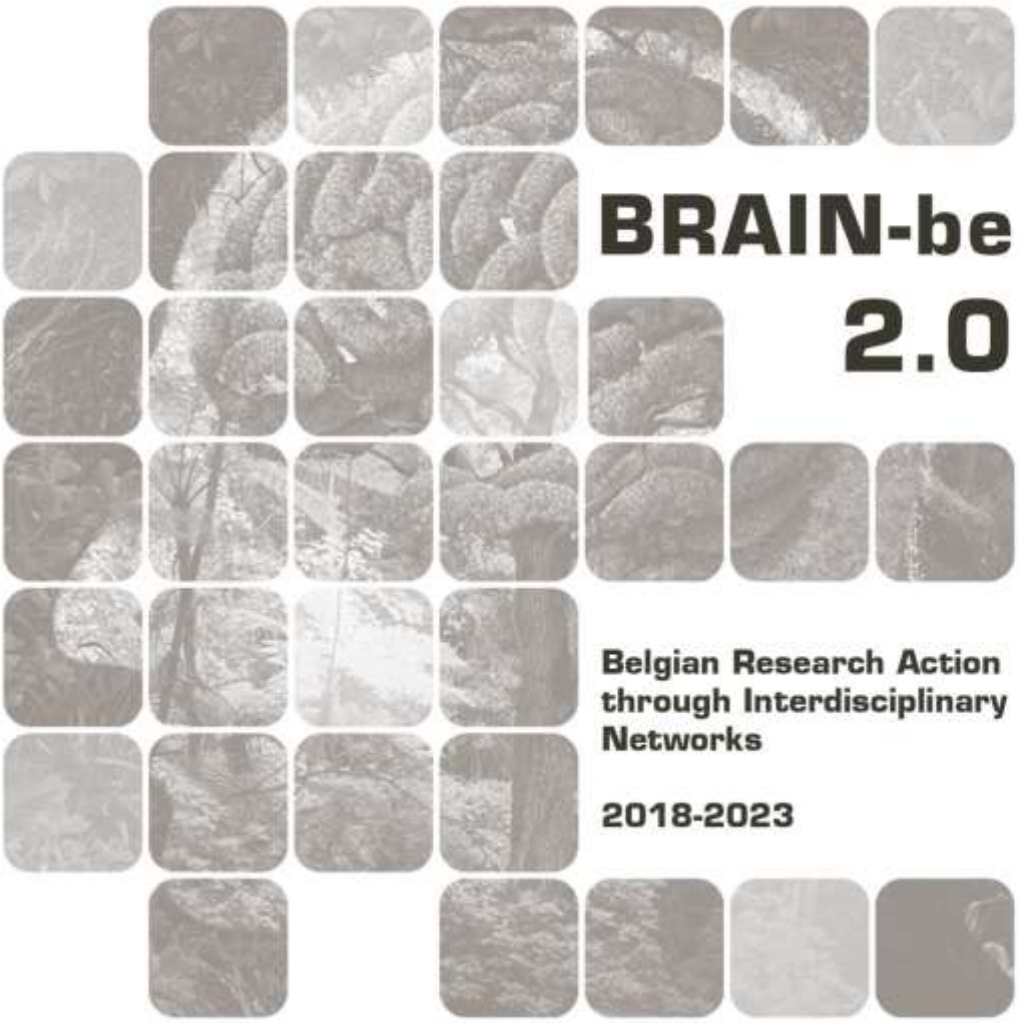

DESIRED

Tracing differentiation processes through siderophile elements, from meteorites to giant ore deposits

Sophie DECRÉE (Institute of Natural Sciences) – Vinciane DEBAILLE (ULB) – Steven Goderis (VUB) – Lisa KRÄMER RUGGIU (VUB) – Gabriel PINTO MORALES (ULB) – Marleen DE CEUKELAIRE (Institute of Natural Sciences)

belspo .be

NETWORK PROJECT

DESIRED

Tracing differentiation processes through siderophile elements, from meteorites to giant ore deposits

Contract - B2/191/P1/DESIRED

FINAL REPORT

PROMOTORS: Sophie DECRÉE (Institute of Natural Sciences)
Vinciane DEBAILLE (ULB)
Steven Goderis (VUB)

AUTHORS: Sophie DECRÉE (Institute of Natural Sciences)
Vinciane DEBAILLE (ULB)
Steven Goderis (VUB)
Lisa KRÄMER RUGGIU (VUB)
Gabriel PINTO MORALES (ULB)
Marleen DE CEUKELAIRE (Institute of Natural Sciences)

ULB VUB natural sciences .be belspo .be

Published in 2026 by the Belgian Science Policy Office
WTCIII
Simon Bolivarlaan 30 bus 7
Boulevard Simon Bolivar 30 bte 7
B-1000 Brussels
Belgium
Tel: +32 (0)2 238 34 11
http://www.belspo.be
http://www.belspo.be/brain-be

Contact person: Koen Lefever
Tel: +32 (0)2 238 35 51

Sophie DECRÉE (Institute of Natural Sciences), Vinciane DEBAILLE (ULB), Steven Goderis (VUB), Lisa KRÄMER RUGGIU (VUB), Gabriel PINTO MORALES (ULB), Marleen DE CEUKELAIRE (Institute of Natural Sciences). ***Tracing differentiation processes through siderophile elements, from meteorites to giant ore deposits***. Final Report. Brussels: Belgian Science Policy Office 2026 – 93 p. (BRAIN-be 2.0 - (Belgian Research Action through Interdisciplinary Networks))

TABLE OF CONTENTS

ABSTRACT

Context

The DESIRED project investigates how moderately to highly siderophile elements—including Au, PGE (Os, Ir, Ru, Rh, Pt, Pd), Re, and companion metals such as Cr, Co, Ni, Mo, and W—are distributed in both terrestrial and extraterrestrial materials. These metals preferentially partition into metallic phases during planetary differentiation and therefore became sequestered into Earth's core early in its history. Their pronounced depletion in the crust and mantle relative to solar abundances explains their status as precious metals and their tendency to form economically significant deposits only when specific geodynamic or surface processes concentrate them, often through the erosion of (ultra)mafic rocks that sample chemically distinct mantle reservoirs.

Understanding siderophile element behaviour provides a window into the earliest stages of Earth's accretion. Distinct suites of elements with particular metal affinities have proven especially useful for reconstructing the isotopic composition of the planet's building material through time. A key concept here is the **late veneer**, a final influx of meteoritic matter that arrived after core–mantle differentiation and enriched Earth's silicate reservoirs in highly siderophile elements (HSE). By determining the relative contributions and isotopic fingerprints of late-veneer versus pre-late veneer material, it becomes possible to identify the abundances and type of meteoritic inputs, refine models of planetary growth, and reconcile diverging isotopic observations—such as those suggesting either volatile-rich or extremely dry accreting components. These insights may be helpful to explain the formation of giant PGE-rich deposits and other Earth's defining features, such as liquid water, volatile budgets, a protective magnetic field, mantle convection, and the evolution of life.

Objectives

- **Origin of precious-metal deposits in the Kaapvaal Craton**
  Analyse ~3.5–2.0 Ga mafic magmatic rocks and associated shales to determine how Au and PGE were transferred from mantle reservoirs into the crust. The Kaapvaal Craton hosts globally unparalleled mineral endowments: the Witwatersrand Basin has produced roughly one-third of all gold ever mined, and the nearby Bushveld Complex is the dominant source of global PGE. Despite this extraordinary concentration of precious metals, no unified genetic model exists. This objective aims to test whether these deposits reflect isotopic signatures characteristic of late-veneer additions or earlier, pre-late veneer mantle heterogeneities possibly tied to incomplete early core formation or later additions of undifferentiated extraterrestrial material.
- **Meteorite constraints on pre-late veneer and late-veneer isotopic signatures**
  Characterize selected meteorites—especially enstatite meteorites and carbonaceous chondrites—to determine what each isotopic proxy (Cr, Ni, Mo, Ru, Os, W) records. Concentration data, isotopic ranges, and experimentally determined high-pressure, high-temperature partition coefficients are used to discriminate between materials incorporated early in Earth's accretion and those added in the late veneer. Existing work suggests that early accreting matter was dominantly enstatite-like, whereas late-accreting matter may resemble CI carbonaceous chondrites. This implies a late veneer sourced from further out in the Solar System and potentially smaller in mass than previously estimated.
- **Preservation of extraterrestrial signals in Belgian Phanerozoic limestones**
  Apply the isotopic tools developed in the first two objectives to Phanerozoic limestone successions showing chromium enrichments and indications of extraterrestrial inputs, such as cosmic dust. This objective tests whether isotopic signatures of meteorite bombardments can survive diagenesis and long-term geological processes, thereby allowing reconstruction of ancient fluxes of extraterrestrial material and improving interpretation of sedimentary archives.
- **Expansion and curation of the Antarctic meteorite collection at RBINS**
  Enhance the size, quality, and scientific utility of the RBINS Antarctic meteorite repository through targeted collection missions (BELARE 2022–2023; 2024-2025 and beyond). The expanded collection—already exceeding 1,450 specimens—provides sufficiently large samples for high-precision isotopic

analyses required for Objective 2. Improved curation protocols further support long-term accessibility and reliability of these key extraterrestrial samples.

Conclusions

During the project period, substantial progress was achieved across all major research axes, beginning with extensive work on the Kaapvaal Craton, where electron microprobe and LA-ICP-MS analyses of silicates, sulphides, oxides, and phosphates revealed significant mineralogical diversity and clear evidence of post-crystallization alteration, emphasizing the potential impact of metamorphic processes on siderophile element distributions and isotopic systems. The completed digestion and chromatographic separation of eight Kaapvaal samples were validated against previously reported datasets and reveal HSE variability driven primarily by petrology, likely dominated by small-scale heterogeneity. The newly established microdistillation-TIMS method for Os isotope measurements, obtaining DROSS standard values consistent with published data (differences <0.007 in $^{187}Os/^{188}Os$). Because such analyses are extremely time-consuming, further study is ongoing. The paper related to the characterization of in situ HSE distribution in unequilibrated ordinary chondrites analysed via LA-ICP-MS is currently in preparation. Parallel efforts at VUB advanced the study of meteorite-derived signatures in terrestrial impact structures, including collaborative Ru and Cr isotope measurements. The Antarctic meteorite program also advanced significantly, with the RBINS collection now surpassing 1,450 specimens following the 2022-2023 recovery mission and the 2024-2025 field season, which yielded 110 new fragments from the Belgica Mountains. Curation, classification, and micro-CT imaging are ongoing, contributing essential data for the digitalization of the collection and future virtual exhibits, alongside publications stemming from earlier cosmic-particle analyses. Work on fossil micrometeorites from Belgian limestone deposits likewise delivered major results, with 130 kg of carbonate rock processed to recover more than 2000 micrometeorites, including rare, well-preserved silicate-bearing types, now representing one of the world's largest such collections. Comprehensive mineralogical and isotopic characterization (SEM, XRF, EMPA, LA-ICP-MS, O and Fe isotopes) enabled the reconstruction of a pronounced micrometeorite flux peak preceding the Hangenberg Event, and culminated in a publication in *Geochimica et Cosmochimica Acta* (Krämer Ruggiu et al., 2025), with a second paper on the extraction technique in preparation. Finally, community engagement was strengthened through the organization of the 86th Annual Meeting of the Meteoritical Society (27 July-2 August 2024) by the ULB-VUB team, which included a dedicated workshop on meteorite curation at RBINS, further enhancing international collaboration and visibility.

Keywords

Siderophile elements; planetary differentiation; precious metals; Kaapvaal Craton; platinum-group elements (PGE); isotopic geochemistry; osmium isotopes; meteorites; Antarctic meteorite curation; micrometeorites; Devonian-Carboniferous boundary; Hangenberg Event; ore genesis; mantle processes; LA-ICP-MS; TIMS; digital collections.

1. INTRODUCTION

Planetary differentiation represents one of the most fundamental processes in the early evolution of terrestrial bodies. During the formation of the Earth, metal-silicate segregation led to the development of a metallic core and a silicate mantle, resulting in the preferential partitioning of siderophile ("iron-loving") elements, such as Cr, Co, Ni, Ga, Mo, W, Re, Au and the platinum-group elements (PGE: Os, Ir, Ru, Rh, Pt, Pd), into the metallic phase (Jones & Drake, 1986; Wood et al., 2006; Righter et al., 2015). As a consequence, these elements are present in the silicate Earth at concentrations several orders of magnitude lower than in chondritic meteorites (Kimura et al., 1974; McDonough & Sun, 1995). Their distribution and isotopic compositions therefore provide key constraints on the timing, mechanisms and sources of planetary accretion and core formation (Walker, 2009; Dauphas et al., 2014; Fischer-Gödde & Kleine, 2017).

Despite their strong siderophile behaviour, highly siderophile elements (HSEs) display near-chondritic relative abundances in the Earth's mantle (Becker et al., 2006; Day et al., 2016). This apparent paradox has long been interpreted as evidence for a "late veneer", a small mass of chondritic material accreted to the Earth's mantle after core formation ceased (Chou, 1978; Walker, 2009; Fischer-Gödde & Kleine, 2017). The late veneer hypothesis provides a framework for understanding not only the HSE budget of the mantle, but also the volatile and water content of the Earth (Dauphas, 2017). However, the precise nature, isotopic composition and contribution of this late accreted material remain debated. Recent isotopic evidence from Fe, W, Ru, Mo and Ni systems has shown that the Earth's mantle may have incorporated material from distinct meteorite reservoirs at different stages of its accretion (Kruijer et al., 2017; Fischer-Gödde et al., 2020; Hopp et al. 2025).

The study of siderophile element systematics and isotopic signatures thus bridges planetary science and ore geology. Large-scale enrichments of Au and PGE in the Earth's crust, particularly within Archean cratons, provide an opportunity to investigate the link between deep-Earth geochemical reservoirs and ore-forming processes. The Kaapvaal Craton (South Africa) hosts the world's largest Au and PGE deposits, namely the Witwatersrand Basin and the Bushveld Complex, which together account for a major proportion of global precious metal production (Frimmel, 2005; Maier et al., 2013). Yet, the genetic relationship between mantle heterogeneity, crustal magmatism and metal endowment remains poorly constrained.

Within this context, the **DESIRED project ("Tracing differentiation processes through siderophile elements, from meteorites to giant ore deposits")** aimed to decipher the geochemical pathways and isotopic fingerprints of siderophile elements from planetary differentiation to crustal ore formation. By integrating high-precision elemental and isotopic analyses of terrestrial and extraterrestrial materials, DESIRED sought to constrain the sources, transfer processes and temporal evolution of siderophile elements in the Earth and to reinforce Belgium's expertise and infrastructure in planetary and metallogenic geochemistry.

2. STATE OF THE ART AND OBJECTIVES

Prior to the DESIRED project, several outstanding questions remained unresolved in the field of siderophile element geochemistry and isotope systematics. Although the late veneer hypothesis successfully explained the near-chondritic HSE pattern of the mantle, isotopic studies using W, Mo, Ru, Cr and Ni had revealed that the early solar system was characterised by a pronounced dichotomy between **non-carbonaceous (NC)** and **carbonaceous (CC)** meteorite reservoirs (Trinquier et al., 2009; Warren, 2011; Budde et al., 2016; Kruijer et al., 2017). These reservoirs are thought to have formed at different heliocentric distances and remained isolated after the accretion of Jupiter (Kruijer et al., 2017; Burkhardt et al., 2019). The isotopic composition of the Earth is closer to the NC reservoir, suggesting that most of the accreted material originated from the inner solar system (Dauphas, 2017). However, some isotopic systems (e.g., Mo, Ru, W) show minor CC-like signatures in the mantle, possibly reflecting late delivery of volatile-rich material from the outer solar system (Fischer-Gödde & Kleine, 2017; Budde et al., 2019). Moreover, since the start of this project, it has been proposed based on high-precision Fe isotope systematics that Ryugu/Ivuna-type carbonaceous chondrites (Cis) are unique meteorites representing an isotopically distinct third reservoir located beyond the orbit of Saturn, thus suggesting the existence of an isotopic trichotomy between NC, CC, and CI meteorites (Hopp et al. 2022) although this observation remains debated.

At the same time, the isotopic record of early terrestrial differentiation is still incomplete. Chromium (Cr), nickel (Ni) and tungsten (W) isotopes are particularly valuable tracers of early core–mantle segregation and late accretion. Radiogenic ^{182}W variations, inherited from the decay of ^{182}Hf during the first ~60 Myr of the solar system, record the timing of metal-silicate separation (Kleine et al., 2005; Touboul et al., 2012). Combined with nucleosynthetic isotope anomalies in Cr, Mo and Ru, these data offer a multi-proxy framework for identifying distinct mantle domains and potential late accretionary components (Dauphas et al., 2014; Fischer-Gödde et al., 2020). However, the relative contribution of pre- and post-late-veneer components to mantle heterogeneity has rarely been addressed in a single integrated study.

From a metallogenic perspective, the Kaapvaal Craton presents a unique natural laboratory for investigating the deep-Earth sources of precious metals. The coexistence of the Witwatersrand Au deposits (~30% of all gold ever mined; Frimmel, 2005) and the Bushveld Complex (the largest global PGE resource; Maier et al., 2013) suggests a long-lived geochemical anomaly in the underlying mantle. Yet, no unified genetic model exists to explain their extraordinary metal endowment. Previous work had mainly focused on crustal processes such as magmatic differentiation or hydrothermal remobilization, whereas the isotopic nature of the mantle source remained unexplored.

Furthermore, the isotopic signatures of extraterrestrial material preserved in sedimentary archives offered a complementary perspective on the Earth's interaction with cosmic dust and meteorite influxes through time. Chromium-rich spinel grains preserved in Phanerozoic limestones and shales have been proposed as potential indicators of enhanced extraterrestrial fluxes (Schmitz et al., 2001; Schmitz et al., 2003; Peucker-Ehrenbrink, 2013), but their isotopic characteristics and possible links with biotic crises remain poorly constrained. Belgium's stratigraphic record, with for example well-documented Devonian sections, provided an ideal setting for testing these hypotheses.

Finally, at the institutional level, the Royal Belgian Institute of Natural Sciences (RBINS) has established one of Europe's largest Antarctic meteorite collections (>1,450 specimens) through multiple Belgian–

Japanese recovery missions (Goderis et al., 2019). This collection provided an exceptional opportunity to apply state-of-the-art isotopic analyses to pristine meteorites, while simultaneously reinforcing RBINS as an internationally recognised curation center.

Against this scientific and institutional backdrop, the **DESIRED project** was designed with four main objectives:

1. **To determine the origin of the world-class precious metal deposits (Au and PGE) in the Kaapvaal Craton (South Africa)** by analysing mafic magmatic rocks and related shales (3.5-2.0 Ga) for their siderophile element abundances and multi-isotopic compositions (Cr, Ni, Mo, Ru, Os, W) (WP1)

2. **To calibrate and interpret isotopic tracers of pre- and post-late-veneer material** through high-precision isotope measurements of selected meteorites (carbonaceous, enstatite and achondritic types), focusing on nucleosynthetic anomalies and element partitioning at high pressure and temperature (WP2)

3. **To assess the preservation of extraterrestrial isotopic signatures in the geological record**, by analysing Cr- and spinel-rich Belgian limestones corresponding to major extinction intervals (Ordovician–Silurian, Frasnian–Famennian) (WP3)

4. **To strengthen Belgium's international role in meteorite curation and analytical geochemistry**, through two new Antarctic recovery missions and the valorisation of the RBINS meteorite collection for high-precision isotopic research (WP4)

By integrating these objectives, DESIRED established a coherent framework linking mantle differentiation, late accretion, and crustal metal enrichment. The project thereby advanced both fundamental planetary science and applied metallogeny, while consolidating Belgium's position as a European hub for geochemical and meteoritic research.

3. METHODOLOGY

3.1. WP1. Unravelling the origin of gold (Au) and the PGE in the Kaapvaal Craton (South Africa)

3.1.1. Selection of samples

This Work Package focused on the petrological and geochemical investigation of mafic magmatic rocks from the Kaapvaal Craton (South Africa), in order to constrain the evolution of their mantle source and the processes leading to the enrichment of highly siderophile elements (PGE, Au, Re, Os). The study combined petrographic, mineralogical, and geochemical analyses of representative rock suites and derivative shales, with the aim of tracing possible secular variations in mantle composition and isotopic signatures through geological time.

The sample selection was conducted in collaboration with Prof. Hartwig Frimmel (University of Würzburg) and Prof. Glen Nwaila (University of the Witwatersrand). The studied samples encompassed a temporal spectrum from ~3.5 Ga komatiites (Komati Formation; Fig. 1) to ~2 Ga mafic rocks of the Bushveld Complex (Fig. 1) and carbonatites (and associated rocks) of the Phalaborwa Complex, including ~3 Ga metagabbros and (meta)basalts dated at ~2.7 and ~2.2 Ga. Complementary shale samples, interpreted as sedimentary derivatives of mafic magmatic sources, covered similar age intervals (3.5-3.1 Ga, 2.9-2.7 Ga, ~2.2 Ga). This broad age range enabled the documentation of chemical and isotopic variations before and after the late veneer and the main episodes of core formation (4.5-3.8 Ga). Representative samples were selected to ensure a balanced temporal and lithological distribution (Table 1).

Figure 1. Hand specimens of a ~3.5 Ga komatiite (from the Barberton Belt, on the left side) and a pyroxenite above an anorthosite from the Bushveld Complex (~2 Ga, on the right side)

3.1.2. Brief petrographic characterization

A detailed sample characterization was performed to (i) identify all mineral phases present, (ii) study the textures and crystallographic relationships, and (iii) detect any signs of post-magmatic perturbation (metamorphic, hydrothermal or weathering-related) that could have induced secondary mobility of major or trace elements. At the RBINS, petrographic descriptions (Annex A) were conducted using Environmental Scanning Electron Microscopy (ESEM-EDS; Quanta 200 ESEM (FEI) equipped with an Apollo 10 Silicon Drift EDS detector (EDAX)) at the Institute of Natural Sciences

(Brussels). Microscopic X-ray fluorescence (µXRF) element mapping at the VUB further documented the mineral distribution in flat surfaces and highlighted textural and chemical heterogeneities, particularly in Fe- and Ni-bearing minerals. For this, an M4 Tornado benchtop µXRF surface scanner (Bruker Nano GmnH, Berlin, Germany) equipped with a Rh tube as X-ray source and two XFlash 430 Silicon Drift detectors was used at the Archaeology, Environmental Changes & Geo-Chemistry AMGC Large Research Unit (VUB, Brussels). Mapping mode was selected with a spot size of 25 µm, and integration time of 1 ms. The applied methodology was similar to the one described in de Winter et al. (2017) and Kaskes et al. (2021). These observations confirmed the primary magmatic origin of the selected rocks and guided subsequent microanalytical work.

Table 1. Samples collected for the study.

Sample	Short sample name	Description	Location	More descriptions	Age
SHR 001	SHR 001	Komatiite	Komati river (tributary N. river)		~3.5Ga
BARB FC-003	BARBF-3	Fig Tree Group shales; Sheba Fm. (Barberton Supergroup)		Depth 1m	3.26-3.23 Ga
BARB FC-004	BARBF-4			Depth 1.5m	3.26-3.23 Ga
BARBMA-003	BARM-3	Moodies Group shales, Clutha Fm. (Barberton Supergroup)		Depth 1m	3.22-3.21 Ga
BARB MA-004	BARBM-4			Depth 1.5m	3.22-3.21 Ga
932	932	Moodies shales (Barberton)	From a traverse along Clutha Creek in Eureka Syncline of the BGB	Slaty fine-grained siltstone of unit Md53	3.5-3.1 Ga
BH1 - 33.35-33.50m	BH1	metagabbro < basement	Farm Rooidraai	Dominion SG	~3Ga (Frimmel et al., 2009)
CL 1	CL 1	Crown lavas sample		West Rand?	~2.9Ga (Armstrong, 1991; Humbert et al., 2021)
CL 2	CL 2	Crown lavas sample		West Rand?	~2.9Ga
D5P003463-015	D5P-15	Witwatersrand shales	Exploration drill hole near Driefontein gold mine, near Carletonville	Shales from the Roodeport Fm./ West Rand	2.9-2.7 Ga
D5P003463-016	D5P-16	Witwatersrand shales			2.9-2.7 Ga
D5P003463-017	D5P-17	Witwatersrand shales			2.9-2.7 Ga (Love & Byerly 1999)
VSKM-1270m (à 1 m du précédent)	VSKM 1 (précédent VSKM)	Klipsriviersberg metabasalt	Driefontein West-7 Shaft (Rethabile shaft)/ Borehole ID: D7P03831	Ventersdorp SG/Klipriversberg G.	~2.7 Ga
VS 1	VS 1				~2.7 Ga
SHR 002	SHR 002	Ongeluk basalt	Kalahari Mn field, Hekpoort	Flood basalt in Pretoria G./Transvaal SG	~2.2Ga
DP22-0000012	DP22-12	Pretoria (Transvaal SG) shales	Exploration drill hole near South Deep gold mine, near Westonaria	Shales from the Silverton Fm., Pretoria Group, Transvaal SG	~2.2Ga
DP22-0000014	DP22-14				
PGM501-1	PGM501	Bushveld Complex	Brits, Merensky Ree, Rustenberg Layered Suite	pyroxenite above anothosite, no chromite	~2Ga (Cawthorn & Wallravens 1998)
RR06465	RR06465	Bushveld Complex	Sekhukhuni	gabbro	~2Ga
RR06466	RR06466	Bushveld Complex	Dwarsrivier	Porphyric pyroxenite from the critical zone	~2Ga
RR00580	RR00580	Bushveld Complex	Rustenburg, Pt Mine	pyroxenite with pyrrhotite	~2Ga
RR00510	RR00510	Bushveld Complex		norite	~2Ga
GC 610	Ph2	Phalaborwa Complex	PMC	phoscorite	~2Ga (Wu et al. 2011)
GC 813	Ph6	Phalaborwa Complex	PMC	carbonatites cutting phoscorite	~2Ga
GC 815	Ph8	Phalaborwa Complex	PMC	phoscorite	~2Ga
GC 1994	Ph22	Phalaborwa Complex	Foskor	banded carbonatite cutting pyroxenite	~2Ga
GC 2707	Ph30	Phalaborwa Complex	Foskor	apatite-mica-cpx rock with fragments of mica	~2Ga

3.1.3. In-situ investigations

A detailed mineralogical study was then carried out to accurately determine the mineral composition and elemental speciation within the studied rocks, providing a robust foundation for forthcoming

isotopic analyses. Electron Microprobe Analyses (EMPA) were conducted at the Laboratoire GeoRessources - Université de Lorraine (France), offering quantitative, high spatial resolution data suitable for distinguishing mineral species (see below), identifying chemical zoning, and detecting compositional deviations related to geological processes.

- **Apatites (22 analyses):** used to track sources and a wide variety of processes (Annex B)
- **Silicates (74 analyses):** olivine, pyroxene, amphibole, biotite-phlogopite, epidote, and chlorite, used to assess primary mantle mineralogy and metamorphic overprints (Annex C, D)
- **Spinels and oxides (26 analyses):** mainly chromite and magnetite, sensitive indicators of magmatic redox state and mantle source composition, and late stage crystallization (Annex E)
- **Sulfides (33 analyses):** including pyrite, pyrrhotite, and chalcopyrite, which act as major carriers of chalcophile and siderophile elements (Annex F)

More precisely, these analyses were performed with a CAMECA SXFive TACTIS (University of Lorraine, France) equipped with five WDS spectrometers using an accelerating voltage of 15 kV, a probe current of 12 nA (an accelerating voltage of 25 kV and a probe current of 150 nA for trace elements), and a beam diameter of 1 µm. The peak and background counting times were 10 and 5 s, respectively. The following crystals were used: TA, LPET, LiF, and PET. The standards were natural minerals and synthetic oxides. Although Electron Probe Micro-Analysis (EPMA) provides high-precision major-element data, it is well known to be limited in detecting trace elements, particularly those present at sub-ppm concentrations or heterogeneously distributed among minor or accessory phases. To overcome these limitations and to obtain a more comprehensive trace-element dataset, Laser Ablation Inductively Coupled Plasma Mass Spectrometry (LA-ICP-MS) analyses were carried out at the AMCG Large Research Group (VUB) on 12-13 November 2024. The LA-ICP-MS analyses targeted 15 trace elements, encompassing siderophile (e.g., Ni, Co, PGE), chalcophile (e.g., Cu, Zn), and lithophile (e.g., Sc, Ti) groups. Measurements were performed on the same mineral phases previously examined by EPMA, including silicates (40 analyses), sulfides (24), spinels (19), and other oxides (2). The data acquired during the project require substantial post-processing, which could unfortunately not be completed within the project timeframe. This processing and full interpretation will be continued in early 2026.

Finally, beyond its element composition, in situ oxygen isotope analyses ($\delta^{18}O$) of apatite were obtained by SIMS (Annex G). These analyses usually provide crucial constraints on the mantle sources and the nature of the fluids involved in the system. Such data help to distinguish between mantle-derived, crustal, and metasomatic signatures, and to trace the interaction between magmatic, hydrothermal, or metamorphic components within the mineralizing environment. Numerous studies have demonstrated the value of this approach for elucidating the isotopic fingerprint of mantle and magmatic-hydrothermal systems (Žigaitė & Whitehouse, 2014; Chen et al., 2016; Sun et al., 2016; Zeng et al., 2016; Wotte et al., 2019; Yang et al., 2020; Decrée et al., 2020; Edwards et al., 2022). Oxygen isotope compositions were measured using a Cameca IMS 1270 E7 SIMS at CRPG Nancy. A Cs^+ primary ion beam (3.5 nA) was focused on a 15 µm area, with charge compensation via an electron gun. Negative secondary ions were collected with a mass resolution of 3000 (M/ΔM) and a 35 eV energy slit. Before each measurement, surfaces were pre-sputtered for 90 seconds to remove contaminants. Isotopic analyses were conducted in multicollection mode with Faraday collectors, with a total counting time of 150 seconds and an internal precision of ~0.1‰. Durango apatite ($\delta^{18}O$ = 9.4‰;

Trotter et al., 2008) was used for mass fractionation calibration, yielding an external 2σ precision of 0.15–0.20‰. Measured $\delta^{18}O$ values are reported relative to Standard Mean Ocean Water (SMOW).

3.1.4. Whole rock analyses

3.1.4.1. Major and trace elements

Whole-rock major and trace element concentrations were determined at the Laboratoire G-Time, Université libre de Bruxelles (ULB, Belgium). Powdered samples were prepared from 24 lithologies representative of the Kaapvaal Craton and digested by alkaline fusion method for major and trace element analyses. In brief, ~50 mg of sample was mixed with ~800 mg of lithium metaborate and ~200 mg of lithium tetraborate (both with purity > 99.999%). The mixture was heated in a muffle furnace at 1000 °C for 10 minutes in graphite crucible. After cooling, the bead was dissolved in 50 ml of HNO_3 %% using magnetic agitator for 4 hours. Major elements were measured at ULB by inductively coupled plasma-optical emission spectrometry (ICP-OES; Thermo Fisher Scientific iCAP) using Y as internal standard and a calibration curve made of synthetic standards. Three international standards (USGS BHVO-2 (basalt), USGS AGV-2 (andesite) and SBC-1 (shale)) were used for assessing precision and reproducibility, that was better than 2% (RSD). Trace elements were measured by quadrupole inductively coupled plasma-mass spectrometry (Q-ICP-MS; Agilent 7700) operated with a He collision cell. Indium was used as an internal standard. Analytical reproducibility, assessed using the three same reference material (N = 5 for each), was better than 6% relative standard deviation (RSD).

3.1.4.2. HSE abundances and Os stable isotopes

Concentrations of the HSE (Ir, Ru, Pt, Re, and Pd) were determined in eight samples by isotope dilution mass spectrometry. Samples were selected based on the distribution and abundances of moderately siderophile elements, particularly Cr and Ni, which have been used to locate the iridium-rich layer in K-Pg sections (e.g., Goderis et al., 2021; de la Parra et al., 2022). Approximately 1 g of homogenized powder was weighed into quartz tubes and spiked with an appropriate aliquot of a mixed spike enriched in ^{99}Ru, ^{106}Pd, ^{191}Ir, and ^{194}Pt, added in aqua regia (1-2 mL concentrated HCl and 2-4 mL concentrated HNO_3). Sample-spike equilibration was achieved at 250 °C and ~90 bar using a Milestone UltraWAVE microwave digestion system at VUB (de la Parra et al., 2022). After cooling, chloroform was added to partition Os, while the remaining HSE were retained in the inverse aqua regia. The HSE fraction was purified from the matrix using ion-exchange chromatography (AG 1-X8, 200-400 mesh) at ULB. After column chemistry, HSE cuts were dried down, redissolved in ultrapure HCl, and analysed on an Agilent 7700 quadrupole ICP-MS at the Laboratoire G-Time (ULB, Brussels). All samples and reference materials were blank corrected. Results for the basalt reference material TDB-1 agree with published values (Table 2).

Following digestion and separation of Os from the other HSE, Os fractions were recovered in HBr and further purified by H_2SO_4/H_2CrO_6 micro-distillation (Birck et al., 1997; Nakanishi et al., 2019). One drop of concentrated HBr (0.02 mL) was deposited into the tip of a conical beaker, and 0.01 mL of dichromate solution (H_2SO_4/H_2CrO_6) was added to the Os residue. The beaker was immediately sealed in an inverted position and wrapped in aluminium foil, leaving only a small opening at the top (for details see Birck et al., 1997). It was then heated on a hot plate for at least 3 h to overnight at a surface temperature of ~80 °C. During distillation, the osmium complex ($OsBr_6^{2-}$) was oxidized to OsO_4 by CrO_6^{++}, after which the volatile OsO_4 was transferred in the gas phase to the conical tip, where it was reduced back to $OsBr_6^{2-}$ in the concentrated HBr. After distillation, the beaker was opened and the

HBr was evaporated. Osmium recovery yields for the micro-distillation procedure were evaluated previously by varying operating conditions, including heating time and temperature and the amounts of oxidant and reductant, and are better than > 90%.

Osmium isotope ratios for samples and standards were measured at the Laboratoire G-Time (ULB, Brussels) using a Thermo Scientific Triton Plus thermal ionization mass spectrometer (TIMS) equipped with negative-ion capability and an ion-counter (electron multiplier). High-purity Pt filaments were baked in air to bright red heat prior to loading. Aliquots of the dissolved sample in HBr (1 µL) were loaded onto the filament and covered with 0.3 µL of a saturated $Ba(OH)_2$ solution in NaOH. Samples and the DROsS standard (~200 ng Os) were measured using the electron multiplier in pulse-counting mode. Instrumental mass fractionation was corrected by normalizing $^{192}Os/^{188}Os$ to 3.08271. Spike deconvolution and oxygen correction were applied to calculate Os concentrations and isotope ratios. Oxygen isotope interferences were corrected using Nier's values ($^{17}O/^{16}O$ = 0.00037 and $^{18}O/^{16}O$ = 0.002047; Nier, 1950).

3.2. WP2. Constraining the transfer of material in the early the solar system by studying nucleosynthetic anomalies in carbonaceous and non-carbonaceous meteorites

The methodological strategy of Work Package 2 focused on constraining material transfer processes in the early Solar System through the high-precision isotopic study of meteorites and extraterrestrial particles, in combination with detailed petrographic and geochemical analyses. A comprehensive suite of carbonaceous and non-carbonaceous chondrites, alongside several achondrites and rare meteorite types has been studied primarily from the Belgian Antarctic collection curated at RBINS. Five carbonaceous and five non-carbonaceous chondrites were prepared for bulk chemical analysis (typically ~0.5 g per sample, with larger quantities for achondrites), alongside polished thin and thick sections used for petrographic and mineralogical characterization. Six Antarctic H chondrites covering multiple petrologic subtypes were analysed using large-area LA-ICP-TOF-MS elemental mapping (total mapped area: 45.69 mm^2), complemented by quantitative LA-ICP-MS spot analyses and electron microscopy for phase confirmation. These meteorites were selected to investigate HSE distributions using high-resolution elemental mapping by LA-ICP-TOFMS at Ghent University (Belgium). Elemental maps were acquired using two 193 nm ArF* excimer-based nanosecond laser ablation systems: (i) a customized Teledyne Photon Machines Analyte G2 and (ii) an Iridia LA unit equipped with prototype and commercial versions of the Cobalt ablation chamber, respectively. Both platforms employed low-dispersion tube cell-type ablation cells and were coupled to a TOFWERK icpTOF 2R ICP-TOF-MS equipped with a 1 mm inner-diameter torch injector. Aerosols were transported via a low-dispersion aerosol rapid introduction system developed at Ghent University and commercialized by Teledyne Photon Machines (Van Acker et al., 2021). Further analytical details are provided in Maeda et al. (2023).

Petrographic observations were performed using optical microscopy, SEM-EDS, and BSE imaging. Duplicate thick sections were systematically studied to identify the chondritic components most likely to host nucleosynthetic anomalies and to provide mineralogical context for the isotopic datasets. Several rare meteorite types and samples from terrestrial impact structures were further characterised using petrography, geochemistry, and isotope systematics (e.g., Maeda et al., 2023; Rider-Stokes et al., 2023; Pittarello et al., 2023; Roland et al., 2024; Fischer-Gödde et al., 2024; Kadlag et al., 2024).

Isotopic analyses (Lu-Hf, Sm-Nd and Os) were performed using MC-ICP-MS and TIMS respectively, following protocols established in WP1 for distinguishing pre-late veneer from late-veneer signatures. A new analytical protocol for radiogenic Os isotopes was developed and refined at the Université Libre de Bruxelles specifically for this work package. The dissolved set of Kaapvaal samples was tested under this new protocol for Os isotopic measurements, and the study is ongoing.

In parallel to the meteorite-focused research, WP2 developed and implemented a comprehensive protocol for extracting and analysing extraterrestrial particles from sedimentary archives (Fig. 2) in order to evaluate temporal variations in the flux of extraterrestrial material to Earth. Antarctic sediments collected between 2013 and 2020 by Steven Goderis were processed, yielding more than 100,000 extraterrestrial grains used for training early-career researchers. More recent Antarctic sediments collected during the 2022–2023 field seasons by Vinciane Debaille were further processed using an updated workflow. This led to the recovery of an additional 10,000 micrometeorites.

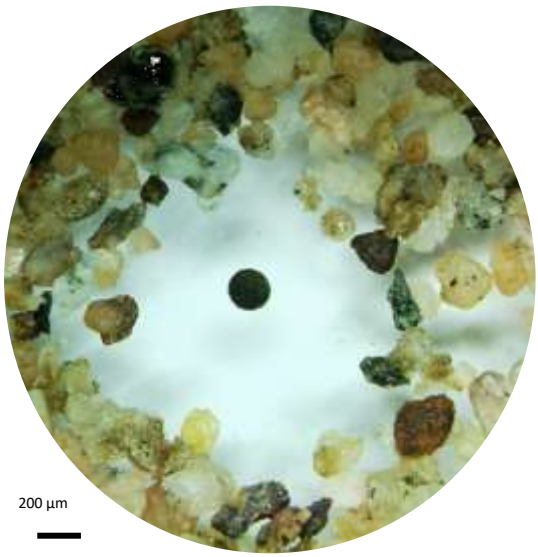

Figure 2.- Micrometeorite in Antarctica sediment observed by optical microscopy.

A selection of particles was analysed using XRF and SEM-EDS to document their chemical composition, mineralogy, textures, and preservation state, and were classified into established micrometeorite types (I-type, G-type, G/I; see Fig. 3 for representative BSE images). Additional sedimentary samples from the Atacama Desert and Greenland provided more than 300 further micrometeorites, analysed in a similar fashion for inter-archive comparison. Together, these archives form the basis for a robust reference dataset designed to quantify temporal fluctuations in the influx of extraterrestrial material and to distinguish true variations in flux from preservation biases.

Finally, WP2 expanded the isotopic investigations to samples from terrestrial impact structures through collaboration with the University of Cologne, applying Ru-isotope systematics to materials formed during hypervelocity impact events. Across all activities, isotopic, petrographic and geochemical datasets were integrated to identify mineralogical carriers of nucleosynthetic anomalies, refine the distinction between carbonaceous and non-carbonaceous reservoirs, and place newly obtained Os and Ru isotope signatures within their broader cosmochemical context.

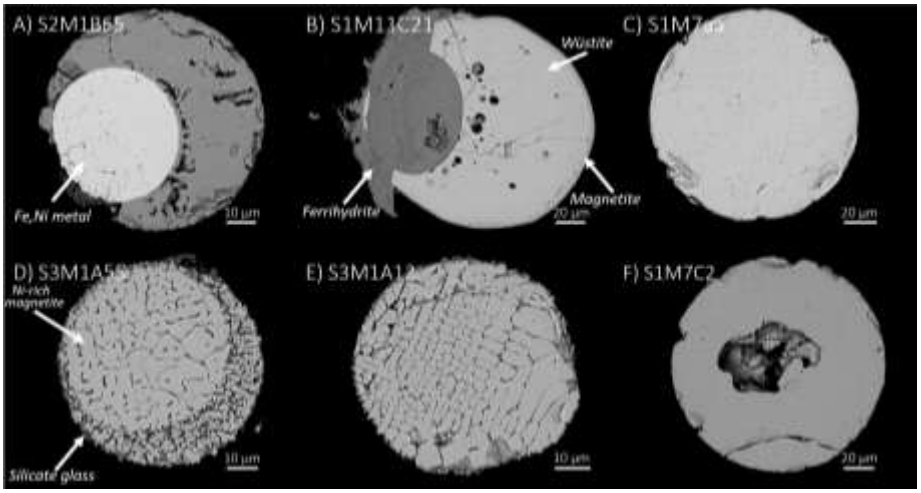

Figure 3. BSE images of extracted fossil I-type and G/I-type cosmic spherule interiors highlighting their mineralogy, texture and alteration features. A) I-type cosmic spherule showing a preserved metal bead; B) I-type cosmic spherule with a metal inclusion altered into ferrihydrite; C) Typical OX I-type cosmic spherule composed of magnetite; D) G/I-type cosmic spherule showing an inner part that is I-type-like and enriched in Ni and an outer rim part that is G-type-like; E) G/I-type cosmic spherule ; F) Typical MET I-type cosmic spherule composed of wüstite and magnetite.

3.3. WP3. Estimating the role of the extraterrestrial influx to mass extinctions based on the Belgian stratigraphic record

For WP3, extensive field sampling was conducted in Upper Devonian carbonate successions in Belgium, with a particular focus on the Devonian-Carboniferous boundary at Chanxhe (Sprimont, Liège), a stratigraphic interval associated with the Hangenberg extinction event. More than 130 kg of carbonate rocks were collected and subdivided into standardized batches to allow systematic extraction and comparison of extraterrestrial particles. The development and implementation of the processing workflow for this material constitute an integral part of the work carried out within WP3 and are therefore presented and discussed in detail in the Results section.

3.4. WP4. Pursuing an efficient curation of Antarctic meteorites at the RBINS and valorizing the Antarctic meteorite collection hosted at RBINS

Work Package 4 establishes an integrated methodological framework to reinforce Belgium's capacity in meteorite recovery, curation, and scientific analysis, while ensuring a continuous and well-documented flow of samples to support the cosmochemical investigations carried out in WP2. The approach combines field-based protocols, laboratory preparation and curation procedures, systematic classification workflows, and digital tools that enhance accessibility, data traceability, and public engagement.

At the field level, WP4 builds on established Belgian-Japanese methodologies for the recovery of meteorites in Antarctica, refined over multiple campaigns such as SAMBA, MICROMETA, and BAMM!. The work package applies systematic search strategies on blue ice areas, moraines, and sediment-rich environments, following standardised procedures that minimise contamination and ensure precise contextual documentation. In addition to recovering macrometeorites, the methodology includes the collection of sediment samples for the extraction of micrometeorites and other extraterrestrial particles. This multi-scale sampling approach allows the acquisition of both large and microscopic extraterrestrial materials, providing complementary datasets for mineralogical, isotopic, and

cosmochemical studies. All material recovered in the field is transported under cold-chain conditions to preserve its pristine character for subsequent analyses.

In parallel, WP4 strengthens the scientific and curatorial infrastructure necessary to prepare, preserve, and manage meteorite samples. Dedicated laboratory workflows ensure that meteorites and micrometeorites are cut, prepared, and stored in accordance with best practices at the international level. Upgrades to preparation facilities and storage environments support the long-term stability, traceability, and scientific reliability of the RBINS meteorite collections. These procedures guarantee that newly recovered materials enter the collection through a robust and well-documented curation pipeline, enabling their use in high-precision petrographic, mineralogical, and isotopic analyses.

A central methodological component of WP4 is the systematic classification of all newly acquired meteorites. The workflow integrates macroscopic and microscopic examination, mineralogical and geochemical characterisation, magnetic susceptibility measurements, and petrographic description. Each sample is then assigned a formal classification following the standards of the Meteoritical Society and is registered in international databases. This ensures global interoperability, facilitates comparative studies, and reinforces Belgium's role within the international meteoritical community.

To broaden access to the collections and facilitate knowledge transfer, WP4 also implements digital methodologies, including the production of high-resolution 3D scans of selected meteorites and the development of online resources to guide amateur collectors in recognising potential meteorites. These tools contribute to improved public engagement, support virtual curation initiatives, and provide new means of visualisation for both research and exhibition purposes.

Finally, WP4 adopts a structured dissemination approach to ensure that the methods, workflows, and scientific outputs generated within the project are shared widely with scientific and non-scientific audiences. This includes contributions to international conferences, preparation for the Meteoritical Society Meeting, and outreach activities aimed at raising public awareness of meteoritics and planetary science. Through this combination of field, laboratory, curatorial, digital, and dissemination methodologies, WP4 ensures that Belgium remains at the forefront of meteorite recovery and research while supporting the broader scientific objectives of DESIRED.

4. SCIENTIFIC RESULTS AND RECOMMENDATIONS

4.1. W1. Unravelling the origin of gold (Au) and the PGE in the Kaapvaal Craton (South Africa)

4.1.1. Brief petrological and mineralogical characterization

A preliminary characterization of the samples was necessary to identify the mineral phases present, to study their textures, and to determine any traces of system perturbation (other than magmatic) that could have induced particular elemental mobilities.

In particular, the komatiite from the Barberton Belt exhibits the typical spinifex texture (Fig. 4a). However, it is mainly composed of minerals from the tremolite-actinolite group and of antigorite–serpentine, which are interpreted as secondary assemblages resulting from the alteration of primary olivine phases (e.g., Robin, 2011). A partial transformation of primary chromite into Cr-rich magnetite is also observed.

The metagabbro from the Dominion Subgroup is rich in hornblende, with subordinate phlogopite, apatite, and Fe and Fe-Cu sulphides (Fig. 4b). The hornblende appears to have formed from the alteration of a presumably primary magmatic amphibole shortly after gabbro emplacement, during late-magmatic autometasomatism (Frimmel et al., 2009).

The Crown lavas and metabasalts of the Ventersdorp Supergroup are strongly altered (Fig. 4c–d). Their original mineralogy has been completely replaced by low-greenschist-facies assemblages composed almost exclusively of chlorite and epidote, with minor calcite and quartz, and still containing relict sulphides (e.g., Armstrong, 1991; Marsh et al., 1992; Humbert et al., 2021).

The Ongeluk basalt is also affected by alteration (Fig. 4e). It consists of a fine-grained chlorite-rich matrix enclosing needles and phenocrysts of clinopyroxene and plagioclase. Secondary minerals such as quartz and epidote are common. In contrast, the mafic rocks of the Bushveld Complex appear largely unaltered, preserving their primary mineralogy. The pyroxenites contain clinoenstatite, augite/diopside, chromite, olivine, and sulphides, with subordinate hornblende and phlogopite, whereas the gabbros and norites display their characteristic mineral assemblages of plagioclase, clinoenstatite, and biotite, associated locally with chromite and/or sulphides (Fig. 4f). Similarly, the carbonatite, pyroxenite, and phoscorite from Phalaborwa exhibit the expected mineralogy: olivine, apatite, and Ti-magnetite in the phoscorite (Fig.4g); calcite, apatite, and magnetite in the carbonatite;

and clinopyroxene, mica, apatite, and magnetite in the pyroxenite. These assemblages are variably associated with Cu sulphides.

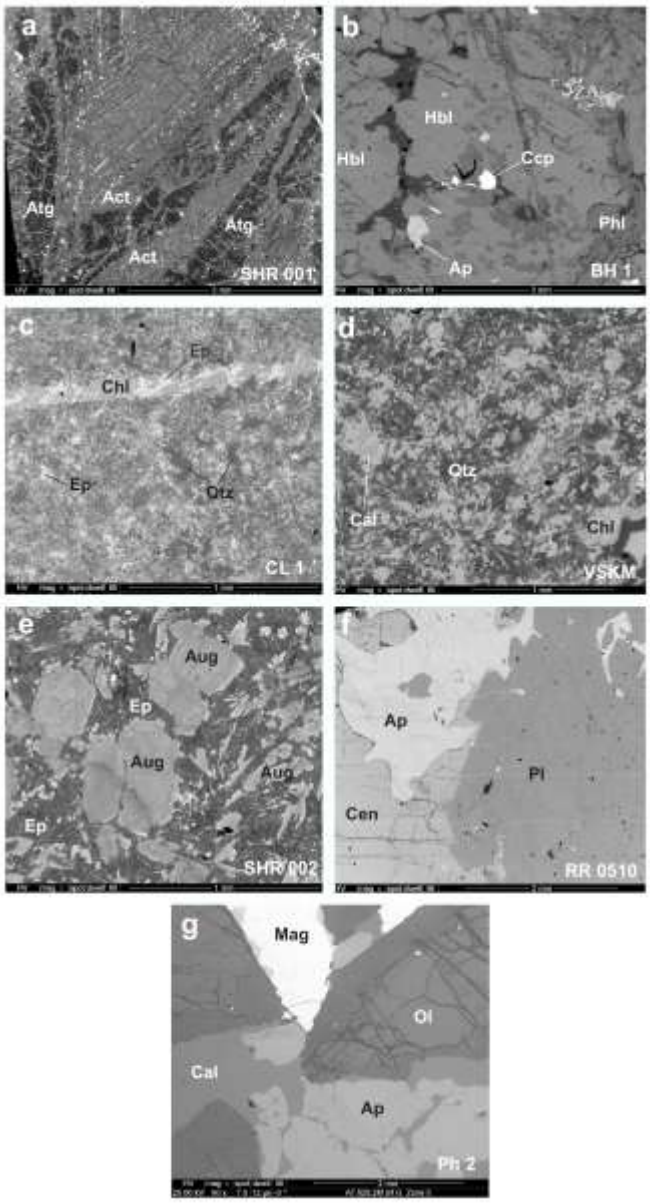

Figure 4. Backscattered electron micrographs. Abbreviations are as follows: Act – actinote-tremolite, Ap – apatite, Atg – antigorite, Aug – augite, Cal - calcite, Ccp – chalcopyrite, Cen – clinoenstatite, Chl – chlorite, Ep – epidote, Hbl – hornblende, Mag – magnetite, Ol – olivine, Phl – phlogopite, Pl – plagioclase, and Qtz – quartz. (a) komatiite that still presents spinifex texture, but with a primary mineralogy relaced by actinolite-tremolite and antigorite. The bright spots are chromite crystals partly replaced by Cr-magnetite, (b) metagabbro of the Dominion SG that is mostly comprised of hornblende, with minor phlogopite and accessory apatite and sulfides, (c) Crown lava and (d) metabasalts of the Ventersdorp Supergroup that are complete replaced by a greenshist facies mineral assemblage, (e) Ongeluk basalt that is made of augite crystals as needles or phenocrysts in a matrix of epidote, (f) norite from the Bushveld that includes clinoenstatite, plagioclase and is also rich in apatite, and (g) phoscorite from Phalaborwa that is mostly made of olivine, spinel (Ti-magnetite) and apatite with minor calcite.

Finally, µXRF imaging clearly reveals the textures of the samples and allows rapid identification of element enrichments and the presence of minerals of particular interest for further investigation—such as apatite, spinels, and sulphides (Fig. 5).

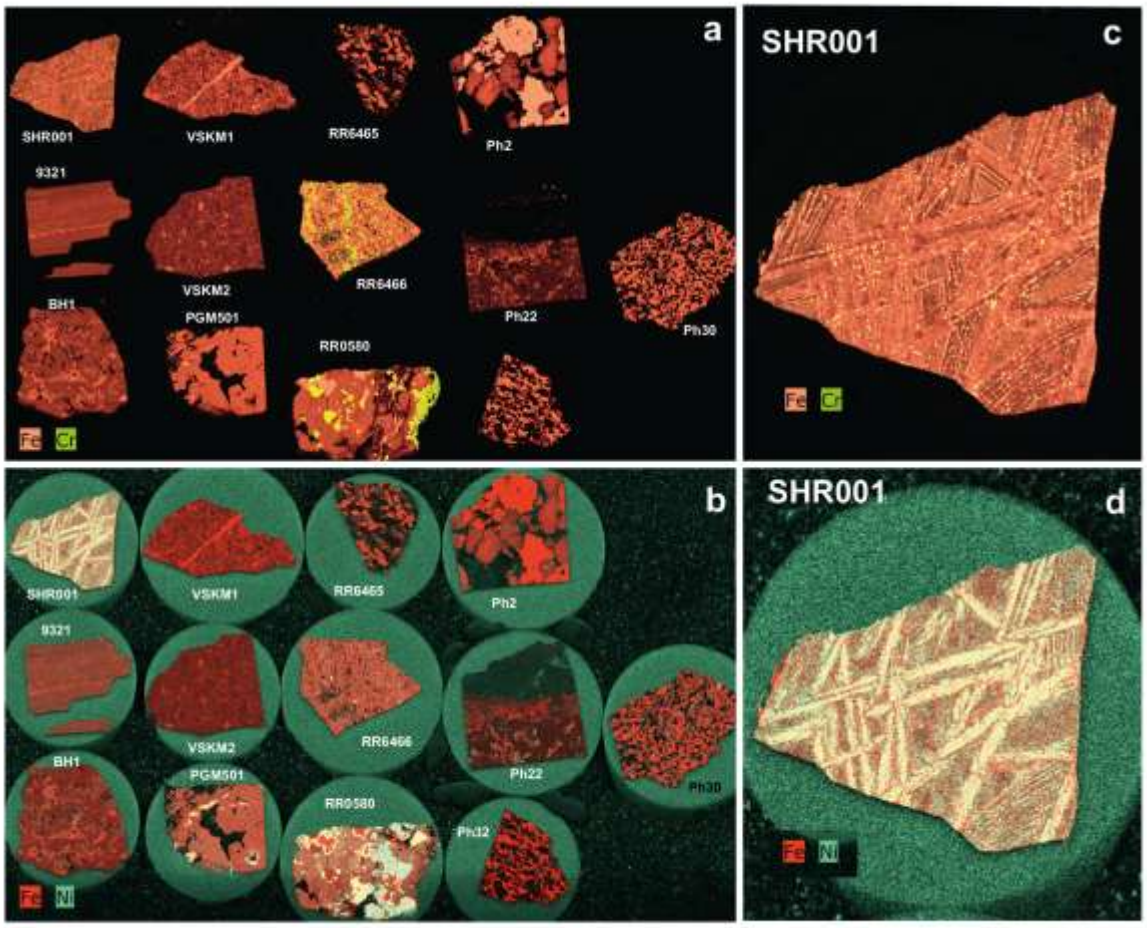

Figure 5. µXRF mapping Fe-Cr (a,c) and Fe-Ni (b,d) of the polished sections representative of the different rocks presented in Table 1 (a,b) with a focus on sample SHR001 (komatiite). The mapping emphasizes the variety of textures encountered in the selected samples and also the enrichments in siderophile elements, and other trace elements of interest.

A detailed mineralogical and geochemical characterization was undertaken to establish a robust interpretative framework for the samples of interest. Electron microprobe analyses (EPMA) were performed to distinguish between mineral species, determine compositional zoning, and identify subtle chemical variations indicative of geological processes. The focus was put on olivine, pyroxene, spinels (chromite and magnetite), sulfides, and apatite. The recalculation of structural formulas was done based on stoichiometric balance and elemental proportions. This recalculation step is essential not only for accurate mineral identification but also for assessing compositional deviations that may reflect post-crystallization processes such as hydrothermal alteration, metamorphism, or weathering.

In this study, olivine from both the Bushveld and Phalaborwa complexes were analyzed. The olivine from the Bushveld Complex sample (PGM501) contains approximately 81.5 mol% Fo, with relatively high NiO (0.45-0.50 wt%) and MnO (~0.18 wt%) contents. These compositions plot close to the Critical Zone field of the Bushveld Complex in the binary diagrams shown in Figure 6. This is consistent with the sample's origin from the Merensky Reef, which belongs to the Critical Zone of the intrusion.

In contrast, olivines from the Phalaborwa Complex display a broader and higher forsterite range, from $Fo_{88.2}$ to $Fo_{95.7}$, but show significantly lower NiO contents (<0.07 wt%) and MnO contents between 0.21 and 0.28 wt%.

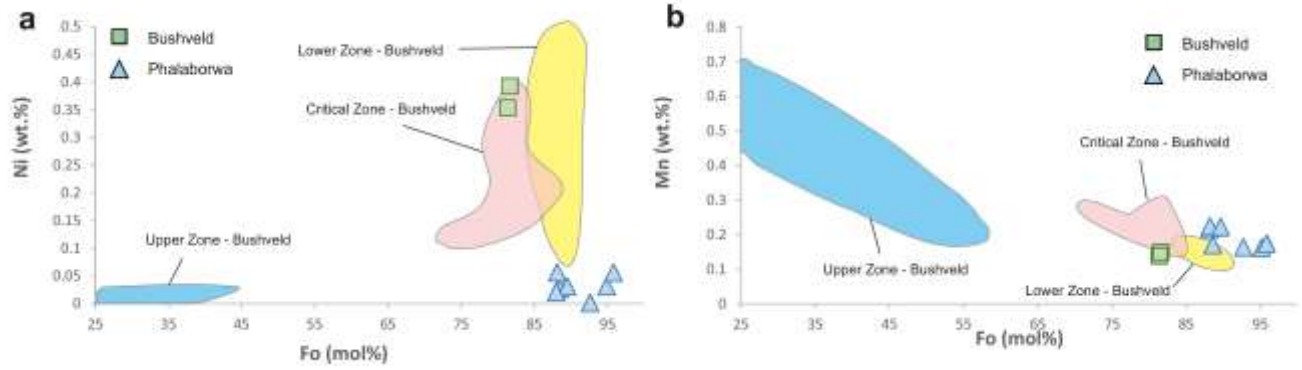

Figure 6. Ni and Mn content vs. Fo content of olivine from the Bushveld and Phalaborwa. Fields for the Bushveld zone are taken from Günter et al. (2018)

In the studied rocks, pyroxenes mainly fall within the clinoenstatite and diopside fields of the Wo-En-Fs ternary diagram (Fig. 7). Specifically, Bushveld pyroxenes plot between clinoenstatite and diopside, those from the Phalaborwa pyroxenites cluster in the diopside field, and those from the Dominion SG metabasalts are primarily augitic.

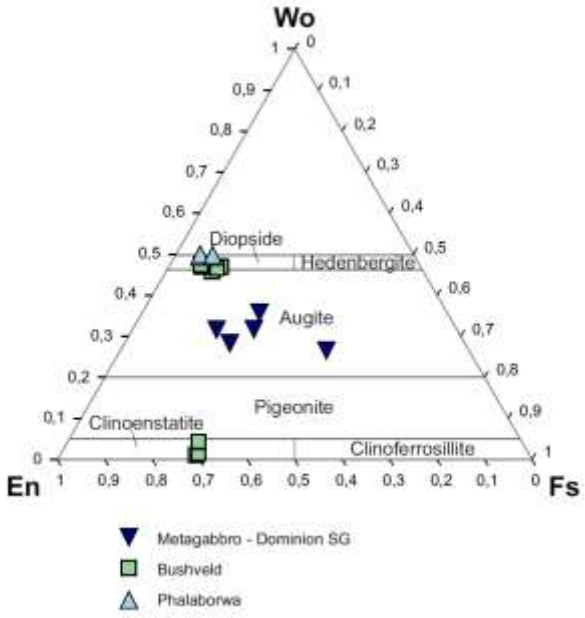

Figure 7. Ternary diagram Wo-En-Fs illustrating the variety of clinopyroxenes encountered in the samples investigated.

Regarding the spinel composition, two distinct types are observed in the komatiite. The first corresponds to primary chromite cores (close to the Cr end-member), whereas the second relates to Cr-rich magnetite rims, indicative of the transformation of primary chromite into Cr-rich magnetite (Fig. 8). This overprinting suggests pervasive alteration under (sub-)oxidizing conditions.

Spinels from the Bushveld Complex show a similar compositional range, from the chromite pole toward Cr-rich magnetite, whereas samples from Phalaborwa contain only Ti-rich magnetite.

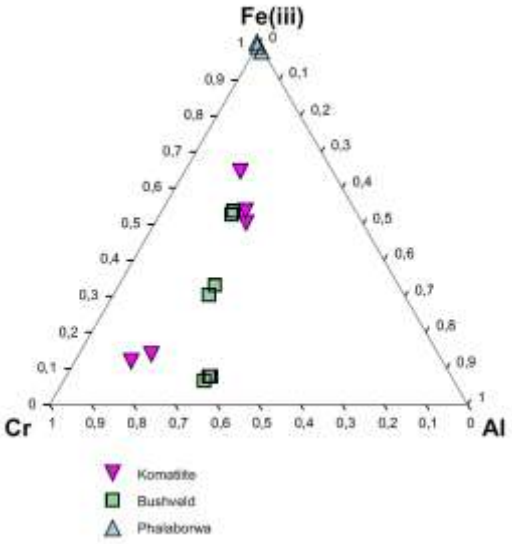

Figure 8. Discrimination diagram for spinels. The Cr end-member represents chromite, whereas the Fe(iii) end-member represents pure magnetite.

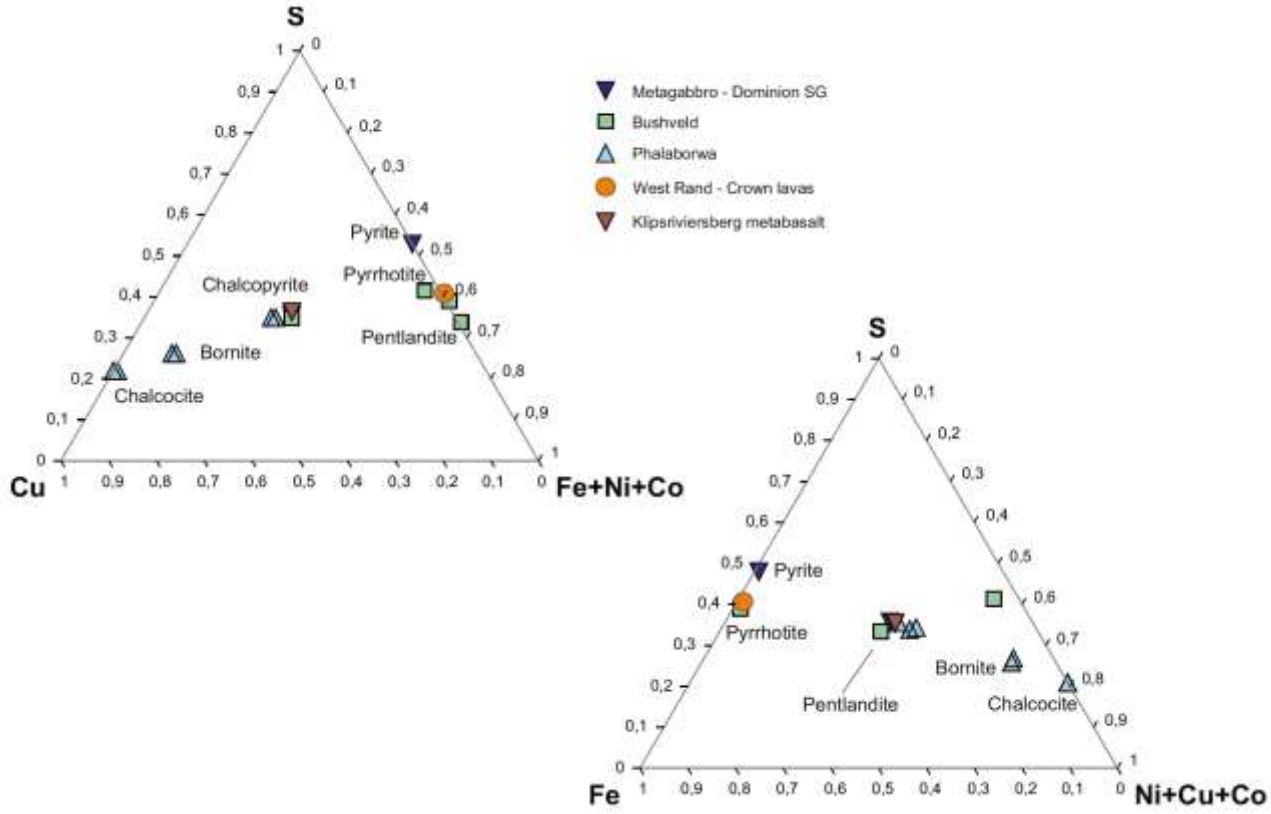

Figure 9. Ternary discrimination diagrams for sulphides.

Ternary discrimination diagrams were also produced for both sulfides and apatite. The sulfide ternary diagrams (Fig. 9) reveal a wide diversity of sulfide phases (pyrite, pyrrhotite, chalcocite, bornite, and chalcopyrite) within mafic rocks of the Kaapvaal Craton dated between ~3.0 and 2.0 Ga. Most of these

sulfides are notably enriched in copper, suggesting distinctive magmatic processes or source characteristics during this extensive time span. Nickel sulfide (pentlandite) is also observed in the Bushveld Complex.

In contrast, the apatite ternary diagram (Fig. 10) shows a much more uniform trend, with most apatite compositions corresponding to fluorapatite. A significant exception occurs in samples from the Bushveld Complex, where apatites exhibit markedly higher chlorine contents, pointing to Cl-rich magmatic or hydrothermal conditions during their crystallization.

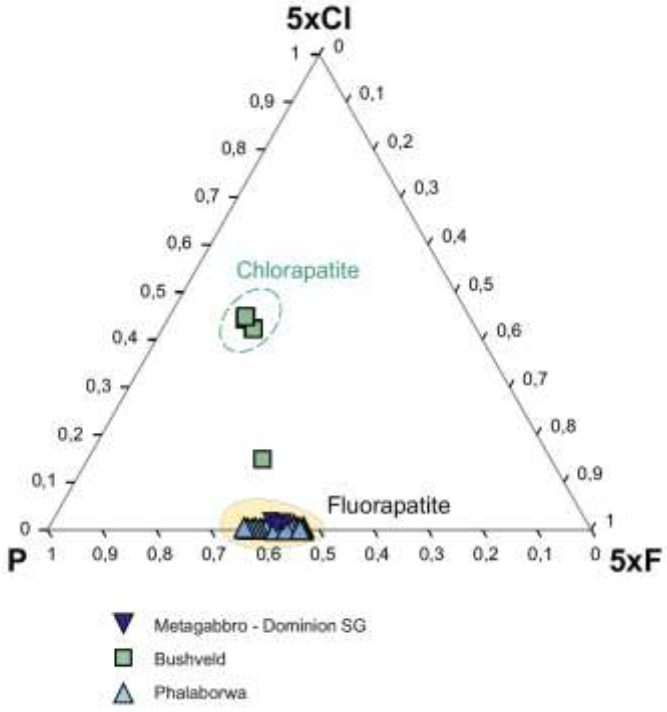

Figure 10. Ternary discrimination diagrams for apatite.

4.1.2. Source and processes deduced from chromite chemistry

The chemical compositions of spinel-group minerals, as shown in the binary and ternary diagrams (Barnes & Roeder, 2001; Yudovskaya & Kinnaird, 2010; Staddon et al., 2021), provide valuable insights into the mantle source characteristics, magmatic affinity, and subsequent evolutionary processes of the parental magmas. Because spinel efficiently incorporates Cr, Al, Ti, and Fe^{3+} in its structure, it acts as a sensitive recorder of both mantle fertility and redox conditions during magmatic differentiation. They allow to define distinct compositional fields corresponding to different magmatic contexts in a set of binary and ternary diagrams, as those presented in Figures I and J.

In the Cr# = Cr/(Cr+Al) vs. Fe# = Fe^{2+}/(Mg+Fe^{2+}) and TiO_2 vs. Fe^{3+}# = Fe^{3+}/(Cr+Al+Fe^{3+}) binary diagrams, as well as in the Fe^{3+}–Cr–Al ternary diagram, the Ti-magnetite from the Phalaborwa carbonatite, phoscorite, and pyroxenite plots within the compositional fields characteristic of alkaline rocks (Fig. Ia,d; Fig. Jb). The spinel from the Bushveld intrusion falls within the field defined for layered mafic intrusions (Fig. Ib,e; Fig. Ja), whereas the chromite from the komatiite plots within the fields typical of chromite cores in such ultramafic rocks (Fig. Ic,f; Fig. Jc). In contrast, the Cr-magnetite, formed through

alteration of primary chromite, plots marginally outside these compositional fields, reflecting secondary (sub-)oxidizing overprints.

Besides classification, these diagrams provide further key insights into both the nature of the mantle source and the magmatic affinity of the system. In the binary diagrams (Fig. 11), chromites from komatiites typically plot at high Cr# values (≈0.60.9) and low Fe^{3+}#, reflecting a highly residual, low-fO_2 harzburgitic mantle source and primitive melts derived from very high degrees of partial melting, a signature fully consistent with the CrAl trend described for mantle-derived and highly primitive magmas (in the ternary diagrams described here below). In contrast, chromites (and magnetites) from layered intrusions (e.g., the Bushveld Complex) display intermediate Cr# (≈0.4-0.6) and higher Fe^{3+}#, marking the effects of low-pressure fractional crystallization and postcumulus reactions with intercumulus liquids that progressively enrich spinels in Fe and Ti during magmatic evolution. This represents the well-established Fe-Ti trend characteristic of differentiated tholeiitic intrusions. Finally, magnetites from alkaline or carbonatitic systems (such as Phalaborwa) are distinguished by very low Cr# (close to 0) and significantly higher TiO_2 contents than those of layered intrusions or komatiitic suites. This position reflects an alkaline/carbonatitic affinity and an enriched mantle source, consistent with the strong partitioning of Ti into ferrian spinels under high oxygen fugacity (fO_2).

These binary relationships are complemented by the Cr^{3+}-Al^{3+}-Fe^{3+} ternary diagram (Fig. 12). The Cr-Al trend corresponds to the mantle trajectory linking Al-rich spinels (from fertile lherzolites) to Cr-rich chromites (from harzburgites and dunites), encoding the degree of partial melting: the higher the melting degree, the higher the Cr content and the lower the Al content. Chromites from komatiites typically align along this trajectory, representing residual mantle or primitive melt compositions. In contrast, the Fe-Ti trend records a magmatic differentiation pathway in which Fe^{3+} and Ti progressively increase, through a combination of low-pressure fractionation, postcumulus reactions, and rising fO_2, driving spinel compositions from chromian spinels toward titanomagnetites. This trajectory is characteristic of layered mafic intrusions (e.g., Bushveld) and differentiated tholeiitic basalts.

4.1.3. Source and processes based on apatite chemistry

Apatite is widely recognized as a robust mineral phase capable of preserving its primary chemical and structural characteristics even after the disintegration of its host rock or exposure to surface weathering (Bouzari et al., 2016). Its crystal structure accommodates a broad range of trace and minor elements through well-documented substitution mechanisms (e.g., Roeder et al., 1987; Fleet & Pan, 1995; Chen et al., 2002; Pan & Fleet, 2002; Waychunas, 2002). Consequently, the geochemical composition of apatite reflects the physicochemical conditions prevailing at the time of crystallization, as well as the chemical nature of the magmatic or hydrothermal system from which it formed. Apatite thus serves as a sensitive recorder of its genetic environment, providing valuable insights into melt evolution, crystallization and differentiation processes, and the extent of fluid–rock interaction associated with the formation of mineralization or its host rocks (e.g., Belousova et al., 2002; Chu et al., 2009; Bouzari et al., 2016; Bruand et al., 2017; Ansberque et al., 2019; O'Sullivan et al., 2020).

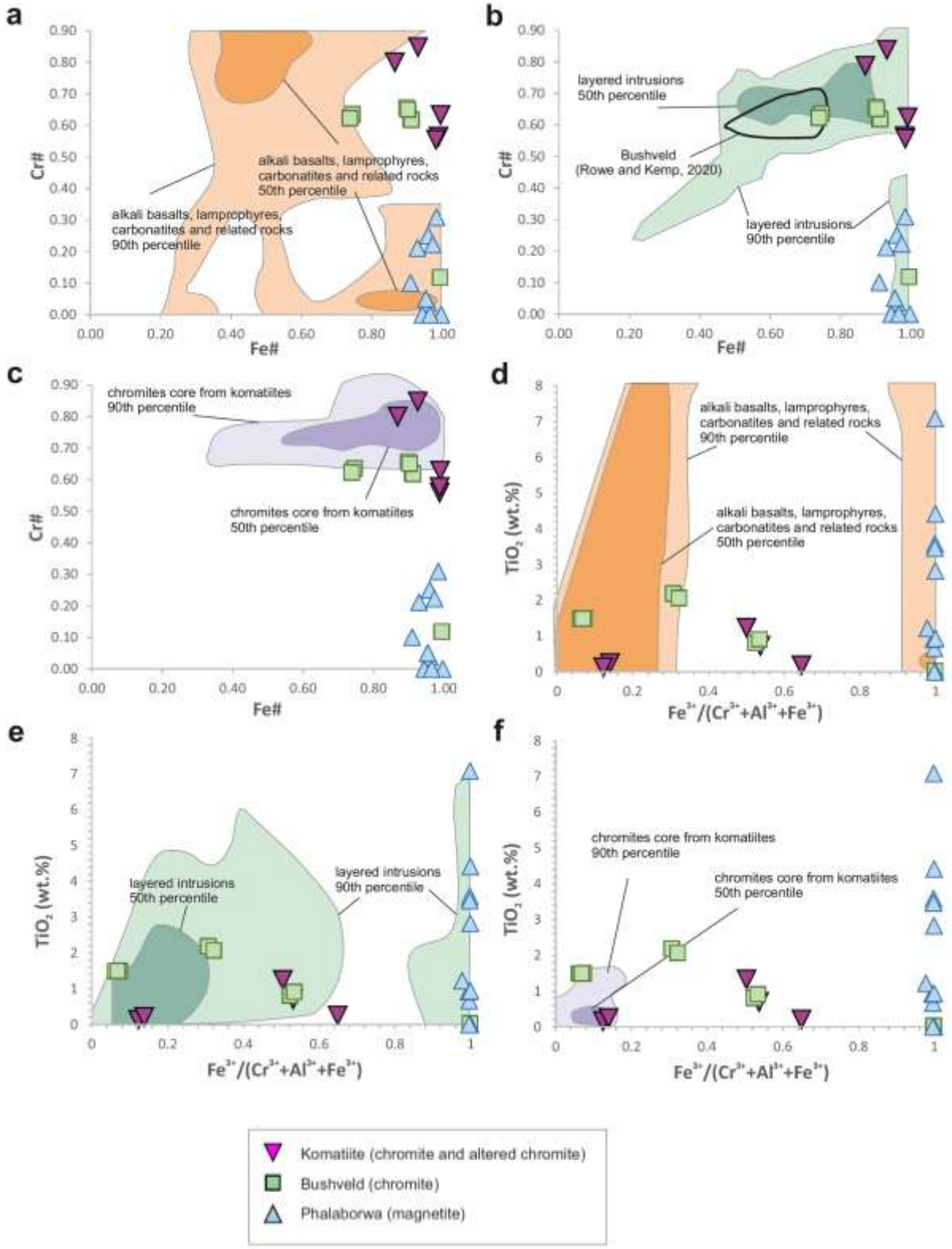

Figure 11. Cr# vs. Fe# (a-c) and TiO_2 vs. Fe/(Cr+Al+Fe) (d-f) binary diagrams (electron microprobe analyses) for the spinels comprised in the komatiite and rocks from Bushveld and Phalaborwa. Fields are taken from Barnes and Roeder (2001) and Staddon et al. (2021), with a focus on alkaline rocks (a,d), layered intrusions (b,e) and komatiites (c,f).

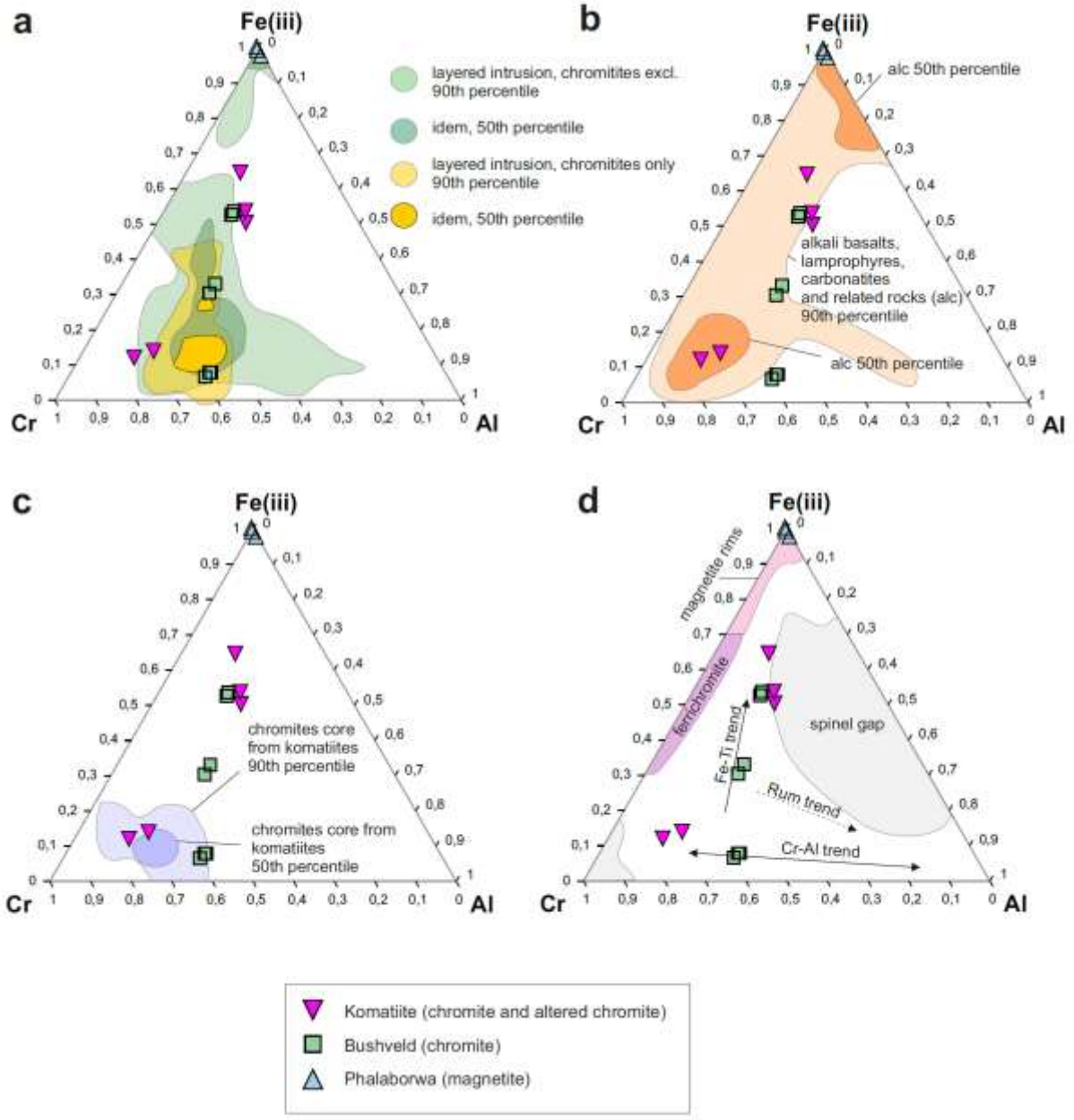

Figure 12. Cr-Al-Fe trivariant plots from Barnes and Roeder (2001) for the spinels (electron microprobe analyses) comprised in the komatiite and rocks from Bushveld and Phalaborwa. The diagrams present the fields defined for layered intrusions (excluding chromitites or chromitites only) (a), alkaline rocks (b), komatiites, and also the main trends/processes encountered in spinels (d).

Beyond its trace-element chemistry, in situ oxygen isotope analyses ($\delta^{18}O$) of apatite obtained by SIMS provide key constraints on mantle sources and the nature of fluids involved in magmatic and hydrothermal systems. Such data enable the distinction between mantle-derived, crustal, and metasomatic components and allow tracing of interactions between magmatic, hydrothermal, or metamorphic reservoirs within mineralizing environments. In situ oxygen isotope analyses ($\delta^{18}O$) of apatite obtained by SIMS (Fig. 13a; data in Table, Annex G) indicate that the phoscorite sample (Ph6) from Phalaborwa displays $\delta^{18}O$ values consistent with those previously reported using the same

technique (Decrée et al., 2020). This similarity suggests derivation from the same magmatic source, namely a metasomatized, enriched lithospheric mantle (Wu et al., 2011). In contrast, the sample representing a carbonatite crosscutting a pyroxenite (Ph2) exhibits lighter $\delta^{18}O$ values, comparable to those recorded in syenite and trachyte from Phalaborwa. Such depleted compositions may reflect the involvement of ^{18}O-poor meteoric water at moderate temperatures (above 200 °C; Deines, 1989), the assimilation of crustal material previously altered by meteoric fluids (Riishuus et al., 2006), or enhanced fluid–rock interaction during the cooling of a CO_2-rich deuteric fluid (Broom-Fendley et al., 2016a). Overall, these results suggest that the carbonatite cutting the pyroxenite may have originated from a slightly different process or magmatic evolution than the primary Phalaborwa rocks.

Apatite from the metagabbro of the Dominion Subgroup plots within the compositional field of primary igneous apatite as defined by Broom-Fendley et al. (2016). In contrast, apatite from the Bushveld Complex exhibits markedly lower $\delta^{18}O$ values, questioning its purely magmatic origin. Several zones of the Bushveld Complex, particularly the Critical Zone, did not remain closed magmatic systems after crystallization but were subsequently affected by hydrothermal and late-magmatic alteration. Circulation of volatile-rich fluids, either exsolved from the residual magma or introduced externally through fractures, induced widespread metasomatism that modified both silicate and oxide mineral assemblages (Hulbert & Von Gruenewaldt, 1985; Naldrett, 2004; Van der Merwe et al., 2005). These fluids promoted recrystallization and re-equilibration of primary minerals, oxidation of Fe-Ti oxides and chromites, and mobilization or redistribution of base metals and platinum-group elements (PGE) along microfractures and grain boundaries. Hydrothermal alteration is typically expressed by the formation of serpentine, chlorite, amphibole, epidote, and carbonate assemblages, and by localized sulfide remobilization or PGE enrichment/depletion near chromitite and sulfide reefs, such as the Merensky and UG2 horizons (Hulbert & Von Gruenewaldt, 1985; Naldrett, 2004; Van der Merwe et al., 2005).

In situ SIMS $\delta^{18}O$ analyses support the involvement of low-temperature fluids of crustal or meteoric origin. The observed decrease in $\delta^{18}O$ values can be attributed to interaction with high-temperature meteoric fluids that percolated through the crystallized cumulates, thereby superimposing a secondary isotopic signature on the original magmatic record (Demény et al., 2004; Broom-Fendley et al., 2016). These hydrothermal overprints—though unevenly distributed across the complex—exert a major influence on the mineralogical, geochemical, and isotopic evolution, playing a key role in the post-magmatic redistribution of metals.

One manifestation of this redistribution is seen in the rare earth element (REE) patterns: apatite from the Bushveld Complex shows a pronounced enrichment in light REE (LREE) relative to other analyzed apatite samples (Fig. 13b). Moreover, these apatite grains exhibit a distinctive chemistry, being notably enriched in Cl (Fig. H). The co-enrichment in LREE and Cl is consistent with metasomatic or hydrothermal processes, as Cl acts as an effective complexing agent in such fluid systems (Engvik et al., 2009; Harlov, 2011).

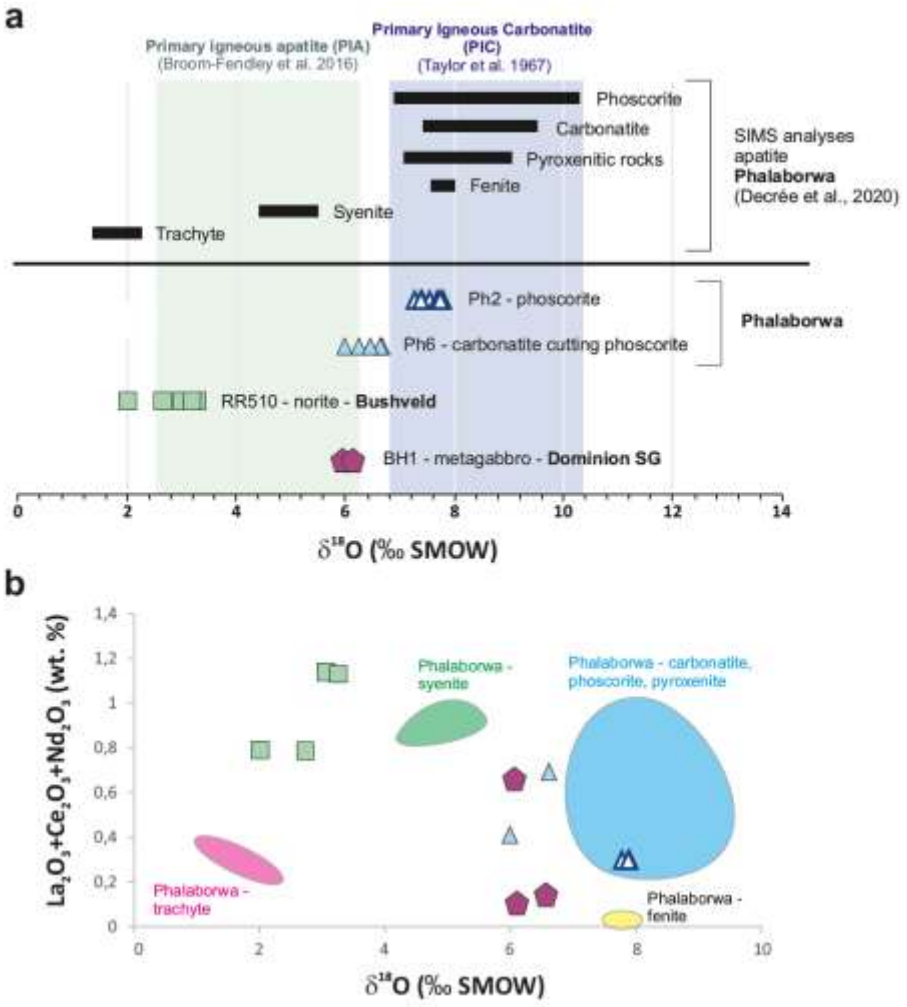

***Figure 13**. (a) In-situ $\delta^{18}O$ for apatite (SIMS analyses) hosted in the metagabbro of the Dominion SG, the norite of the Bushveld and 2 rocks of Phalaborwa (phoscorite and carbonatite cutting a pyroxenite). Data from the literature are given for comparison: Taylor et al. (1967) for the primary igneous carbonatite, Broom-Fendley et al. (2016) for the primary igneous apatite, and Decrée et al. (2020) for analyses obtained on apatite from Phalaborwa; (b) La_2O_3+Ce_2O_3+Nd_2O_3 vs. $\delta^{18}O$ for apatite from the same rocks (electron microprobe and SIMS analyses). The fields of the main Phalaborwa facies (redrawn from the data provided in Decrée et al. (2020)) are given for comparison.*

4.1.4. Preliminary conclusions regarding the nature (primary vs. altered) character of the Kaapvaal rock investigated

The mineralogical and geochemical characterization of the studied samples highlight contrasting alteration histories among the investigated Kaapvaal lithologies. Several rock types, notably the Archean komatiites from the Barberton Belt and the Crown lavas and metabasalts of the Ventersdorp Supergroup, have undergone pervasive alteration and metamorphic overprinting. In these units, primary igneous minerals are almost entirely replaced by secondary tremolite-actinolite, antigorite-serpentine, chlorite, and epidote assemblages. The transformation of primary chromite into Cr-rich magnetite under (sub-)oxidizing conditions further attests to intense post-magmatic alteration. Such mineralogical re-equilibration reflects open-system behavior and is likely to have affected elemental mobility, thereby complicating the interpretation of primary geochemical and isotopic signatures.

In contrast, the metagabbro of the Dominion Subgroup, the Ongeluk metabasalt, and the mafic–ultramafic rocks of both the Bushveld and Phalaborwa complexes (gabbros, norites, pyroxenites, carbonatites, and phoscorites) preserve largely unaltered primary mineral assemblages. Their petrographic and microchemical characteristics indicate limited metamorphic or hydrothermal disturbance, making them suitable for reconstructing mantle-derived compositions and primary magmatic processes. In particular, the presence of fresh olivine, pyroxene, and spinel in these rocks supports their use as reference lithologies for isotopic investigations.

Nevertheless, localized hydrothermal overprints are documented in some Bushveld samples, particularly within the Critical Zone, where circulation of volatile-rich fluids and late-magmatic metasomatism have modified mineral assemblages and isotopic compositions. These processes, reflected by Cl- and LREE-enriched apatite and by depleted $\delta^{18}O$ values, suggest partial interaction with externally derived fluids of crustal or meteoric origin.

Taken together, these observations indicate that while several Archean units (e.g., komatiites, Ventersdorp lavas) are strongly altered and unsuitable for preserving pristine isotopic records, the younger mafic–ultramafic intrusions of the Bushveld and Phalaborwa complexes, as well as the metagabbro of the Dominion Subgroup, retain their primary magmatic character. These latter lithologies thus provide a robust basis for subsequent isotopic investigations aimed at constraining mantle sources, magmatic differentiation, and fluid–rock interaction histories across the Kaapvaal Craton.

4.1.5. Insights from whole rock chemistry (trace elements and HSE)

4.1.5.1. Trace elements

Particular attention was devoted to the evaluation of siderophile isotope systems relevant to the project objectives. Refractory elements such as W, Ru, Cr, and Mo, as well as transitional elements such as Fe, were identified as key tracers. A major constraint identified at this stage is the low and highly variable abundance of refractory elements across the investigated lithologies, ranging from shales to komatiites.

The primitive mantle-normalized REE and incompatible trace element diagrams presented in Figures 14 to 16 are primarily used as a geochemical screening tool rather than for detailed genetic interpretations. At this stage, they provide a first-order assessment of the compositional variability of the investigated lithologies and allow evaluation of the diversity of source reservoirs, ranging from mantle-derived to crustal-influenced materials. In particular, these diagrams make it possible to quantify the degree of enrichment in incompatible and refractory elements, to identify the lithologies most promising for subsequent siderophile isotope investigations (Ru, W, Mo, Cr), and to recognize the potential imprint of secondary processes such as alteration, metasomatism, or crustal recycling.

In Figure 14, most of the whole-rock samples from the Bushveld Complex display enrichments in LREE and incompatible trace elements, contrasting with the comparatively simpler and less fractionated pattern of the komatiite sample (SHR001). Negative Nb anomalies and variability in Th–U ratios in several Bushveld samples point to variable degrees of crustal or lithospheric influence. In contrast, the komatiite exhibits a more mantle-like signature, making it a valuable reference material for distinguishing inherited mantle signatures from secondary or crustal-overprinted geochemical signals.

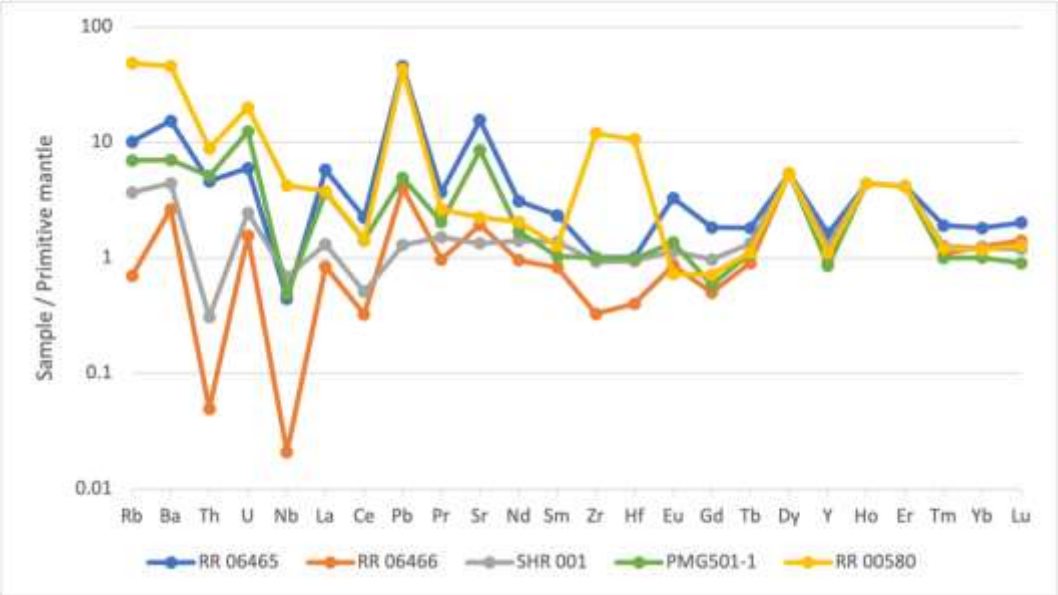

Figure 14. Primitive mantle-normalized REE and incompatible trace element patterns for whole-rock from the Bushveld complex and a komatiite (SHR 001). Normalizing values after McDonough & Sun (1989).

The samples presented in Figure 15, including the Crown Lavas, associated basalts, and mantle-derived rocks from the Phalaborwa Complex, overall show internally coherent REE and trace element patterns within each lithological group, albeit with significant dispersion in large-ion lithophile elements (Rb, Ba, Th, U). The mantle-derived rocks from the Phalaborwa Complex are characterized by particularly high enrichments in incompatible elements, consistent with low-degree partial melting and/or mantle metasomatic processes. These geochemical features highlight their potential as prime candidates for PGE concentration measurements, provided that absolute abundances are sufficient. The basaltic samples exhibit smoother and less extreme patterns, representing intermediate compositions between primitive mantle-derived melts and more enriched mantle reservoirs.

Figure 16 illustrates the geochemical characteristics of shales from the Barberton Greenstone Belt and the Witwatersrand Basin. These samples display enriched and relatively homogeneous REE and incompatible element patterns, typical of integrated crustal reservoirs. As such, they represent effective recorders of regional-scale geochemical fluxes. Their sedimentary nature raises the issue of potential dilution or overprinting of primary mantle-derived signals, which must be carefully considered in subsequent isotopic interpretations.

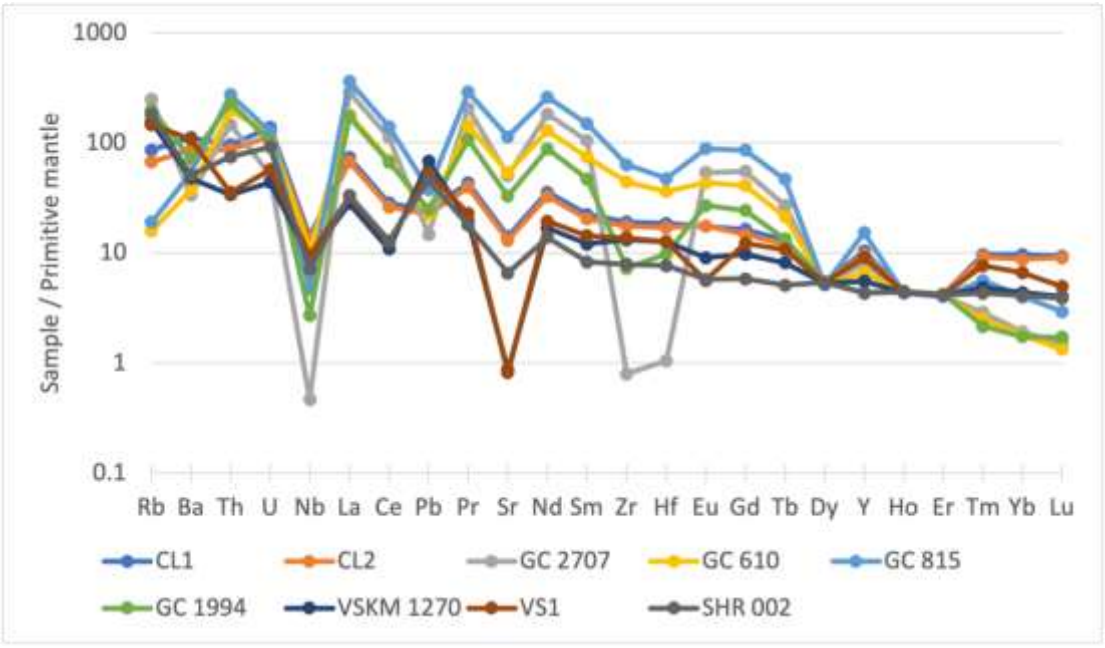

Figure 15. Primitive mantle-normalized REE and incompatible trace element patterns for the Crown Lavas, the Klipsriviersberg basalt, the Ongeluk basalt, and the mantle-derived rocks from the Phalaborwa Complex. Normalizing values after McDonough & Sun (1989).

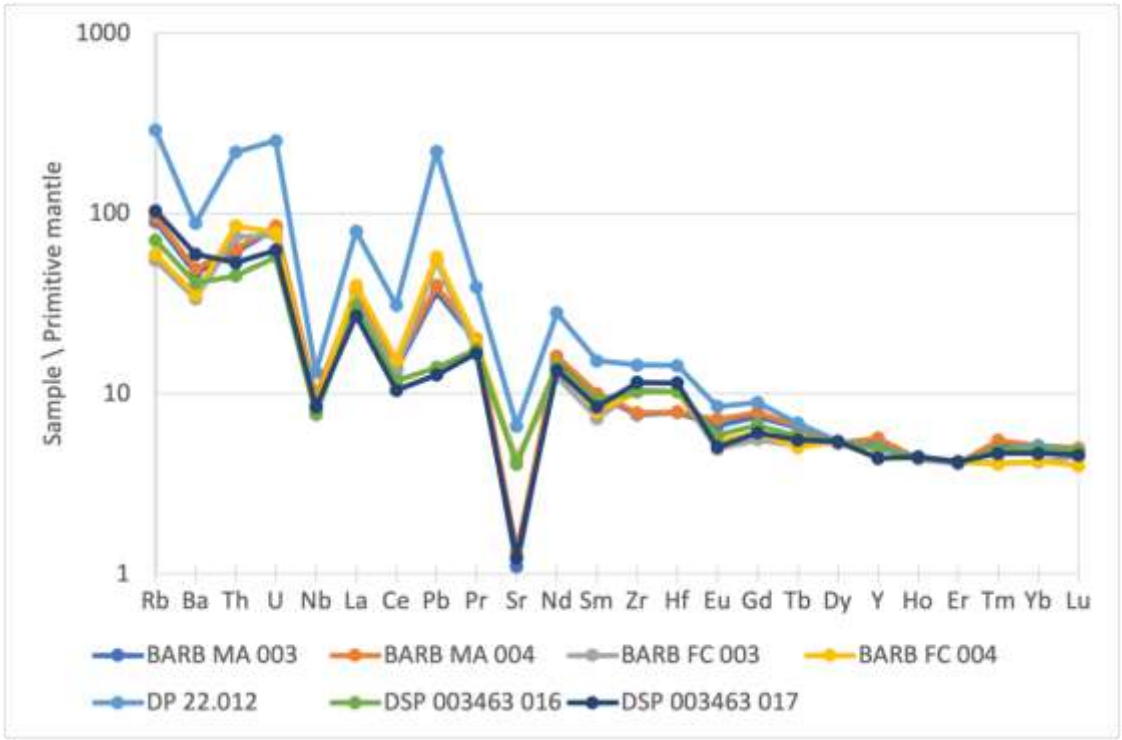

Figure 16. Primitive mantle-normalized REE and incompatible trace element patterns for the Barberton and Witwatersrand shales. Normalizing values after McDonough & Sun (1989).

4.1.6.2. High siderophile elements

The Kaapvaal craton lithologies define CI-normalized HSE (PGE and Re) patterns that broadly overlap with previously reported datasets (Schulz et al., 2017; Siebert et al., 2005; Ozdemir et al., 2019). Several samples show a systematic rise from the more refractory IPGE (Ir-Ru) toward the more incompatible PPGE (Pt-Pd), followed by a decrease toward Re (Fig. 17). This relative PPGE enrichment is consistent with strong control by mantle melting processes and, in particular, by sulfide saturation/segregation, whereas IPGE are more commonly retained in high-temperature phases and melt residues or hosted in refractory alloys and spinel-group minerals.

Komatiite and one gabbro sample display the most pronounced Pt-Pd peaks, while basalt and shale remain comparatively depleted and exhibit flatter patterns (Fig. 17). In contrast, gabbro and pyroxenite show the greatest internal variability, pointing to substantial small-scale heterogeneity, likely reflecting an uneven distribution of sulfide- and PGE-bearing phases within these units. Finally, Re is commonly decoupled from the PGEs in several samples, indicating that its distribution is not solely governed by the same processes controlling PGE fractionation and may instead reflect additional (potentially secondary) controls

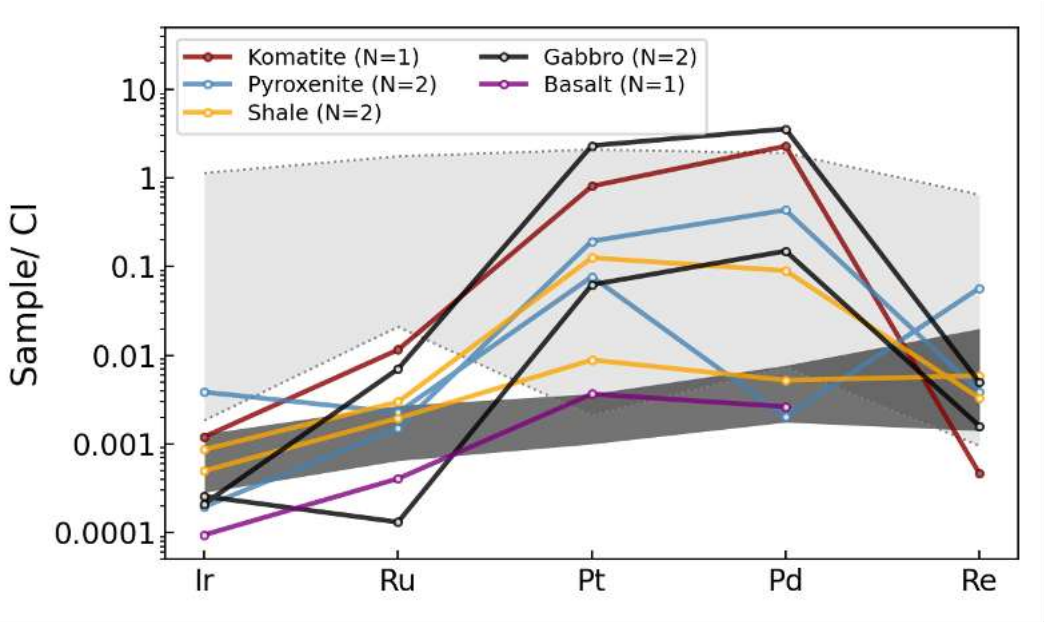

Figure 17. highly siderophile element patterns for the Kaapvaal craton samples normalized to CI-chondritic composition (Lodders, 2010). The color lines show individual samples grouped by lithology. The dark grey area represents Fig Tree Group sediments from the BGB (Siebert et al., 2005) and the light gray area presents BARB5 spherule samples (Schulz et al., 2017). Y-axes are shown on logarithmic scale.

Across the 2.0-3.5 Ga age range spanned by the Kaapvaal samples, absolute HSE abundances (Table 2) vary by several orders of magnitude and appear to be controlled by lithology rather than by age (Fig. 18). The oldest sample (komatiite, ~3.5 Ga) is characterized by elevated Ru, Pt, and Pd concentrations but comparatively low Re, whereas the youngest lithologies (~2.0 Ga pyroxenites and gabbro) show a wider variation with moderate to high HSE contents. Platinum and Pd display the largest variability (from ~1 ppb to ~2000 ppb), consistent with a dominant influence of sulfide saturation/segregation and the heterogeneous distribution of PGE-bearing phases in the rocks (Barnes

et al., 2015). In contrast, Re varies over a narrower range and does not covary systematically with Pt-Pd, implying partial decoupling from the PGE budget and the involvement of additional processes controlling its final abundance.

Within individual lithologies, the data highlight pronounced heterogeneity among samples of similar age. At ~2.0 Ga, the gabbro exhibits elevated Pt, Pd, and Ru abundances, whereas the pyroxenites contain lower but still variable HSE concentrations (Fig. 18). The ~2.7 Ga basalt is uniformly depleted in most HSEs, consistent with overall low HSE contents and a relatively flat CI-normalized pattern compared to the intrusive and ultramafic rocks (Fig. 17). Shales at ~3.2 Ga show intermediate concentrations for most elements but comparatively higher Re than the komatiite, supporting mobilization of Re probably influenced by redistribution during alteration and/or sedimentary processes.

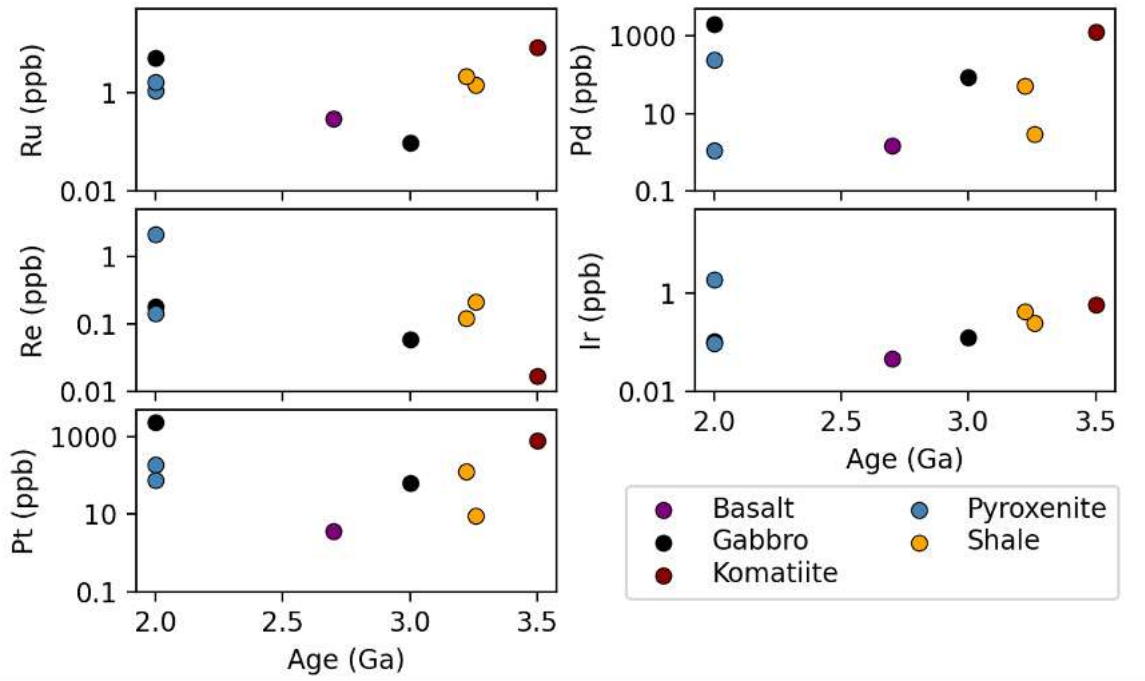

Figure 18. Absolute HSE concentrations (Ru, Pd, Re, Ir, and Pt) in ppb vs sample age (Ga) for the same Kaapvaal craton lithologies shown in Fig. 4. The colour dots show different lithologies (basalt, gabbro, komatiite, pyroxenite, and shale). Y-axes are shown on logarithmic scales. Data from this study, Frimmel et al. (2009), and Wu et al. (2011).

A subset of lithologies suggests an age-related trend in Ir, with higher Ir concentrations generally associated with older samples (Fig. 18). However, the small number of analyses within each lithology prevents a robust statistical evaluation. The absence of a consistent, monotonic age-HSE trend across all elements indicates that primary petrogenetic controls such as sulfide saturation/segregation, HSE host-phase mineralogy, and small-scale heterogeneity dominate the observed variability.

Table 2. Highly siderophile element concentrations (Ir, Ru, Pt, Pd, and Re) measured in the eight Kaapvaal samples and the international reference material TDB-1 analyzed in this study, compared with the certified values of Govindaraju (1994) and the recommended values of Meisel and Moser (2004).

Sample	Lithology	Ir [ng/g]	Ru [ng/g]	Pt [ng/g]	Pd [ng/g]	Re [ng/g]
SHR001	Komatiite	0.579	8.23	802.8	1286	0.017
BARB fc3	Shales	0.240	1.39	8.79	2.94	0.214
BARB MA3	Shales	0.416	2.12	124.9	50.51	0.121
BH1	Gabbro	0.123	0.093	62.1	84.12	0.058
RR 06465	Gabbro	0.102	5.01	2299	2008	0.181
GC 2707	Pyroxenite	0.094	1.08	192.6	244.12	0.141
VS1	Basalt	0.045	0.289	3.62	1.47	bdl
RR580	Pyroxenite	1.85	1.61	76.50	1.13	2.09
TDB-1 (reference material)	this study	0.035	0.238	7.13	18.78	1.82
TDB-1 (certified)	Govindaraju (1994)	0.15	0.3	5.8 (±1.1)	22.4 (±1.4)	-
TDB-1 (Recommended N=7)	Meisel and Moser (2004)	0.075	0.179	5.01	24.3	0.794

4.1.6. Osmium isotopes

WP1 and WP2 are linked through the development and implementation of a new protocol for high-precision Os isotope measurements by TIMS at ULB. The workflow comprises (i) isolating Os by micro-distillation to minimize procedural blanks and reduce matrix-related effects, (ii) converting Os to a volatile oxide species appropriate for TIMS analysis, and (iii) applying routine corrections for baseline/background, procedural blanks, potential isobaric interferences, and instrumental mass fractionation during data reduction. Method performance was assessed using the DROsS standard, a widely adopted reference material for Os isotopic analysis (e.g., Luguet et al., 2008). Using Faraday cup detection, replicate analyses produced $^{187}Os/^{188}Os$ ratios consistent with published DROsS compositions (differences <0.007; Fig. 19), demonstrating accurate and reproducible results across analytical sessions and confirming the robustness of both filament loading and instrument tuning.

To extend the protocol to natural samples characterized by low Os concentrations (e.g., Kaapvaal Craton samples), we also evaluated electron multiplier (EM) detection, which offers higher sensitivity at low signal intensities. In contrast to the Faraday measurements, repeated EM analyses of DROsS standards and natural samples were difficult to reproduce, with ratios showing temporal drift and decreased stability (Fig. 20). We are pursuing our efforts to offer a better analytical reproducibility for low Os concentration sample measurements.

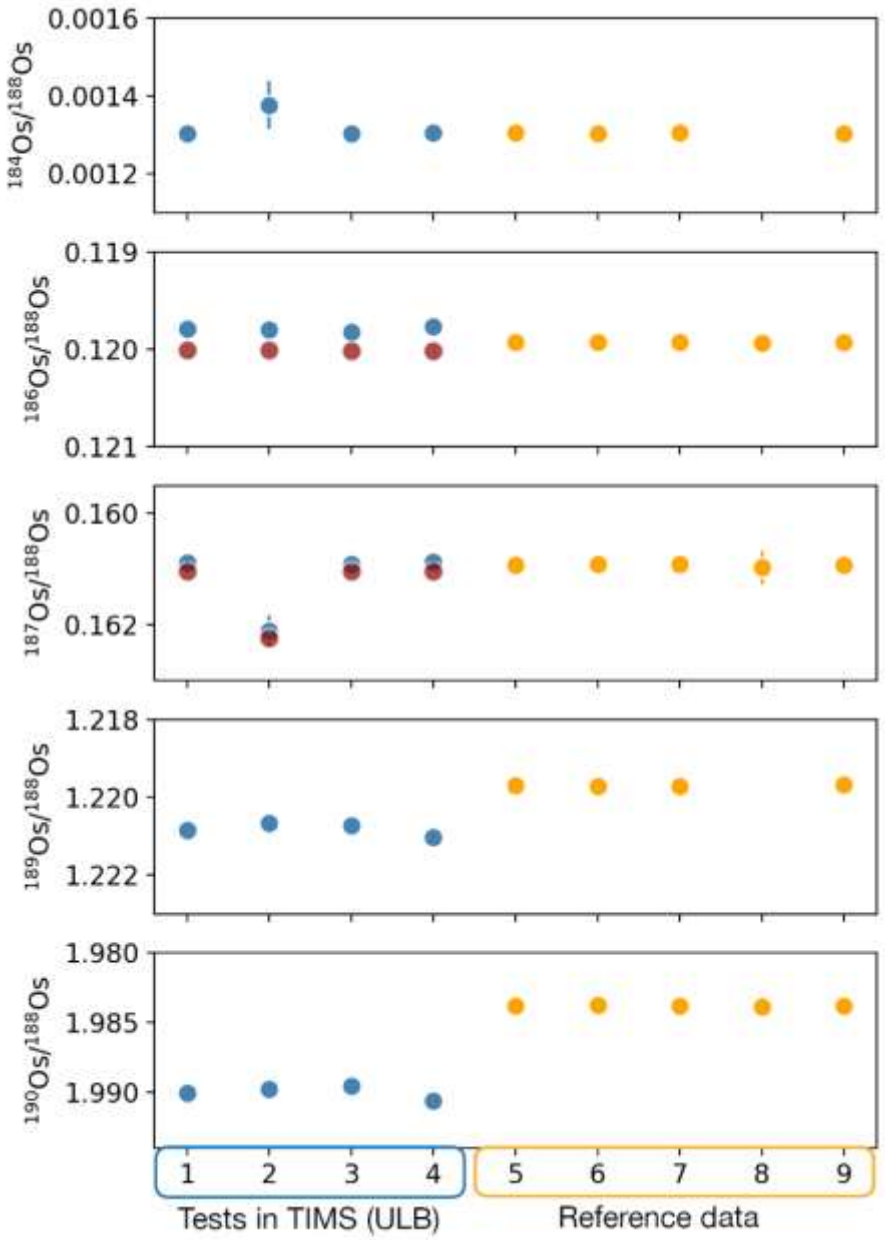

Figure 19. Os isotope ratio of the DROsS standard comparing the results obtained using the developed method at ULB (blue dots) with reference data (orange dots). The tests conducted at ULB utilized the DROsS standard with Os loads of 200 ng. Test number 2 employed a cycle of 180 individual measurements, while Tests 1, 3, and 4 used a cycle of 280 individual measurements. The red dots in the $^{186}Os/^{188}Os$ and $^{187}Os/^{188}Os$ plots represent corrections made using the natural ratio for $^{192}Os/^{188}Os$ (3.083). The reported values for the DRsSS standard are sourced from [5] Luguet et al. (2008); [6] Coggon et al. (2013); [7] Chatterjee and Lassiter (2015); [8] Reisberg and Zimmerman (2021) and [9] Waterton et al. (2023). Error bars are smaller than dot sizes.

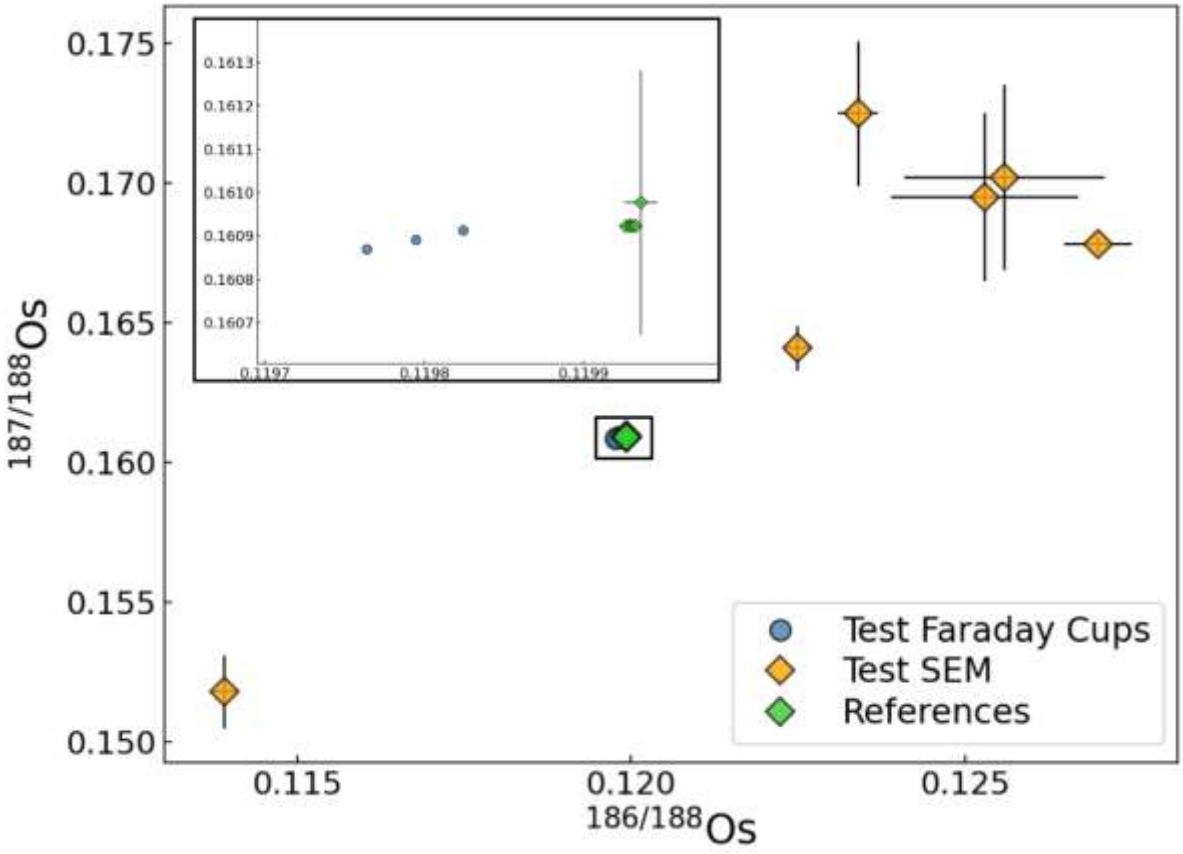

Figure 20. Three-isotope plot of $^{187}Os/^{188}Os$ vs $^{186}Os/^{188}Os$ for the DROsS standard measured by TIMS using Faraday cups (blue circles) and the electron multiplier (EM) (orange diamonds), compared with published reference values (green diamonds). Error bars represent analytical uncertainties. The inset shows a zoom of the Faraday-cup results and reference data. EM analyses display greater scatter and offsets relative to Faraday and reference values.

4.1.7. Side study: tracing the source of the PGE in the ore of the Niutitang Formation (China) using apatite chemistry and in-situ isotopes

In relation to the use of apatite as a tool to constrain the sources of PGE in highly mineralized systems, we investigated a unique PGE-Ni deposit in China (the Mo-Ni-PGE-rich sulphidic black shales of the Niutitang Formation), which represents one of the most metal-enriched sedimentary horizons known worldwide. The origin of the Ni and PGE enrichment in this bed remains debated, with hypotheses invoking either a mafic-hydrothermal contribution or direct seawater input. We proposed that, in such a context, the geochemical and isotopic signatures of apatite could be used to identify a mafic component, thereby providing an explanation for the exceptionally high Ni-PGE contents observed in these Chinese shales. This approach can be directly applied to the rocks of the Kaapvaal Craton, where similar questions regarding the sources and redistribution of PGE persist.

The study demonstrates that apatite, owing to its ability to incorporate and retain a wide range of trace elements (REE, Sr, Y, Th, U, Mn, Fe, etc.) and its resistance to post-depositional alteration, constitutes an excellent geochemical and isotopic archive. In the Niutitang case study, the combination of trace-element compositions and in situ Sr isotopic analyses (and, by extension, O isotope compositions) revealed a hybrid signal involving both mafic–hydrothermal and seawater-derived components. This mixed geochemical fingerprint allowed us to distinguish between mantle-

derived and crustal fluid inputs, to quantify the metal sources (Ni, Mo, PGE), and to reconstruct the redox evolution of the system during ore formation. This work was published in *Ore Geology Reviews* (Decrée et al., 2022).

4.2. WP2. Constraining the transfer of material in the early the solar system by studying nucleosynthetic anomalies in carbonaceous and non-carbonaceous meteorites

4.2.1. Os isotopes

Initial results of the DROsS standard for Os isotope analysis have been successfully obtained, demonstrating consistency with previously reported data. This indicates that the developed method for Os isotope analysis using TIMS is largely operational and reliable for analysing the first set of meteorite samples.

4.2.1. High siderophile elements distribution in unequilibrated chondrites

To better constrain the enrichment of HSE in the terrestrial mantle associated with the late veneer, it is essential to first identify the dominant carrier phases of these elements across materials from the inner and outer Solar System. With this motivation, we investigated the principal host phases and spatial distribution of high siderophile elements (HSE: Re, Au, and the platinum-group elements) in unequilibrated ordinary chondrites (OCs) agglomerated in the inner part of the solar system. Ordinary chondrites are largely devoid of calcium-aluminium-rich inclusions (CAIs), however can exhibit bulk HSE abundances comparable to carbonaceous chondrites, implying that their HSE budget is concentrated in components other than CAIs.

Our combined LA-ICP-TOF-MS elemental mapping, quantitative LA-ICP-MS spot analyses, and electron microscopy show that the most refractory HSE are hosted predominantly in Fe-Ni metal (taenite and kamacite), with only minor contributions from sulfides (Fig. 21). HSE-enriched areas represent ~0.48 to 2.84% of the mapped areas across the different samples and occur mainly in the matrix and along chondrule margins. No HSE-rich metal was identified within chondrules. The HSE patterns of these metal-rich domains do not follow a simple nebular condensation signature (e.g., they lack a pronounced Pd depletion that would be expected as Pd is slightly more volatile than other PGE). The PGE pattern is instead consistent with HSE concentration during quenching of a silicate melt under reducing conditions, rather than direct condensation from the solar nebula (Schwander et al., 2015). This would imply that metal-silicate segregation actually took place during chondrule evolution, a mechanism that would also solve the conundrum of compositional differences between chondrules and matrix (Palme et al., 2015). With increasing metamorphic grade, refractory HSE-rich grains become larger (from ~19.4 ± 7.1 µm in H3.3 to ~49.4 ± 30.6 µm in H3.9), and Pd- and Au-bearing grains become more abundant. Finally, in the highly weathered H3.9 meteorite ALH-78084, secondary oxides display elevated and more homogeneous HSE patterns, indicating potential HSE mobilization and/or selective alteration of HSE-rich metal phases (e.g., tetrataenite)

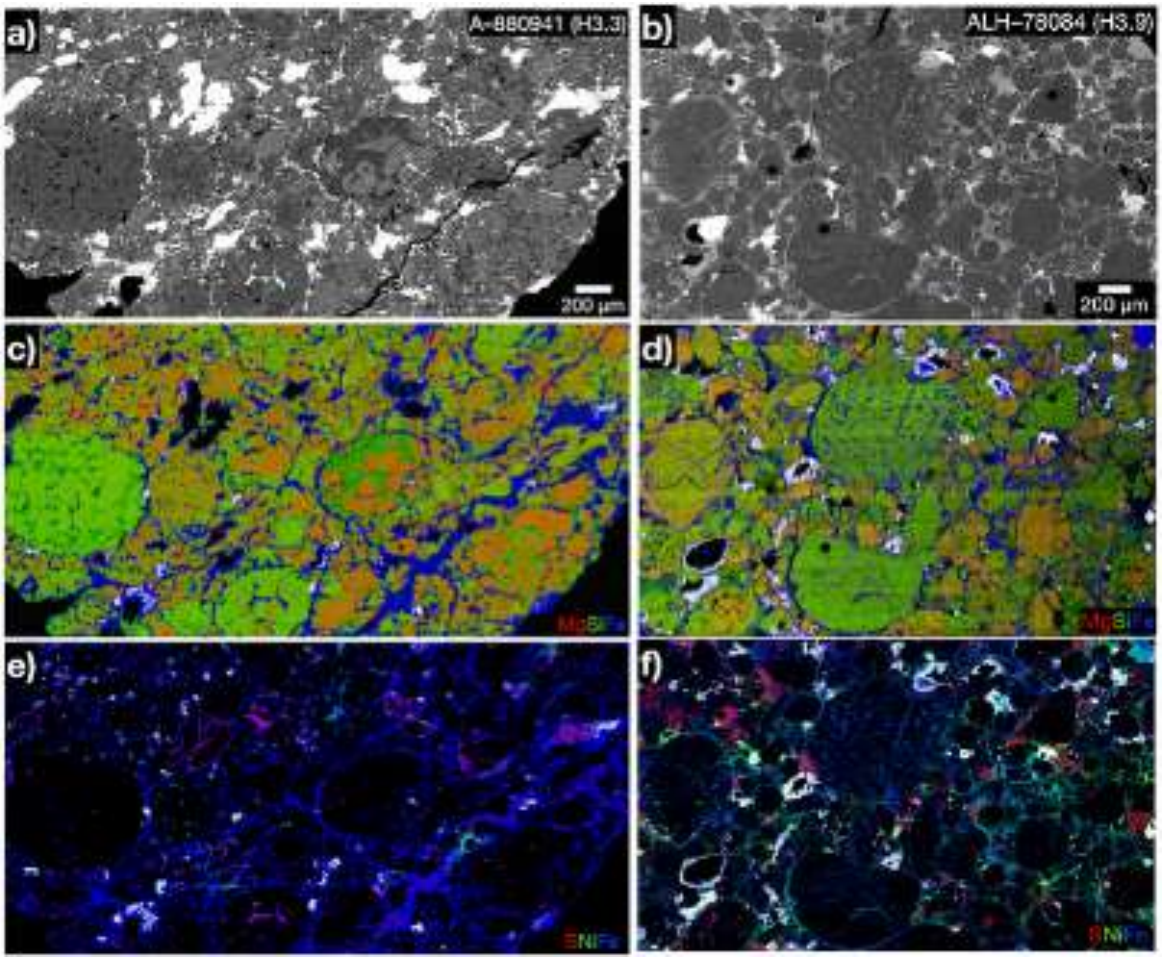

Figure 21. Analyzed areas on A-880941 (H3.3) and ALH-78084 (H3.9). In (a,b) backscattered electron images, (c,d) X-ray compositional mapping of Mg, Si, and Fe (RGB), and (e,f) S, Ni, and Fe (RGB). White regions in compositional maps spotlight areas enriched in refractory HSE, which include Os, Ir, Ru, Rh, and Pt.

4.2.2. Petrographic description

The 3D analysis of Asuka 12236 (CM2.8), illustrated in Figure 22, provides a powerful complement to traditional petrographic observations of carbonaceous-rich material. By revealing the internal architecture of the sample in three dimensions, this dataset enables a far more comprehensive petrographic description than 2D sections alone. In particular, the 3D reconstruction allows precise quantification of the distribution, connectivity, and volumetric abundances of metallic phases-parameters that are often underestimated or overlooked in conventional thin-section studies. Furthermore, it can be useful for future exhibitions and analysis.

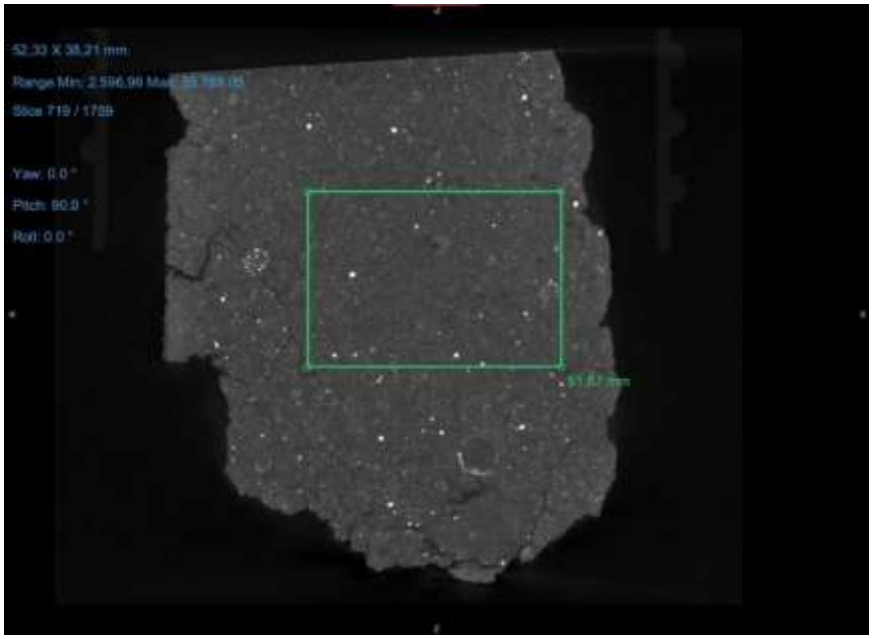

Figure 22. Selected 3D slice from the X-ray microtomography analysis of Asuka 12236 (CM~2.8) from the RBINS meteorite collection. The highlighted green square indicates an area of particular interest for detailed analysis. The voxel resolution of the data is 24 µm³.

4.2.3 Additional analyses

Considerable new data, among which Ga isotopes and Ga and Ce contents or distribution (Fig. 23), have been obtained in the framework of work package 2. During the course of the project, we also investigated volatile loss in Antarctic meteorites, notably in terms of moderately siderophile element budget (Roland et al., 2024). For that, we examined how impact shock and thermal processes could affect moderately siderophile volatile elements in equilibrated H6 ordinary chondrites from Antarctica, hosted at the RBINS. Fifteen meteorites spanning a range of shock (S2-S5) and weathering grades were analyzed for bulk elemental abundances and for Zn, Ga, Cu, and Fe isotope compositions using the MC-ICP-MS Nu-Plasma 2 at ULB, chosen for their progressively higher condensation temperatures. Zinc shows the largest isotopic variability, followed by gallium, copper, and iron, consistent with their relative volatilities. However, neither elemental depletions nor isotopic fractionations correlate with shock stage or weathering grade, indicating that impact-related shock heating is not the primary driver of the observed isotope variations.

We concluded that while minor evaporative loss during parent-body thermal metamorphism may explain some Zn and Ga fractionation, this process was limited. Copper and iron isotopes remain essentially unfractionated, pointing instead to inherited nebular heterogeneity or mixing of distinct components as dominant controls, especially for Cu. Overall, the results suggest that volatile element isotope signatures in ordinary chondrites largely predate impact processing and instead reflect early Solar System condensation, accretion, and metamorphic histories.

We also reported the first systematic measurements of stable cerium (Ce) isotopic compositions (δ^{142}Ce) in non-carbonaceous chondrites to evaluate whether nebular conditions, parent-body processes, or terrestrial alteration fractionated Ce isotopes in the early Solar System (Pourkhorsandi et al., 2024). We analyzed 18 well-characterized meteorites, including enstatite (EH, EL), ordinary (H,

L, LL), and one Rumuruti chondrite, spanning a wide range of oxidation states, thermal metamorphic grades, and weathering conditions for their Ce isotope compositions, using the MC-ICP-MS Nu-Plasma 2 at ULB. All samples display remarkably homogeneous δ^{142}Ce values, with a global mean of 0.01 ± 0.30‰ (2SD), and no systematic differences between chondrite classes, oxidation environments, or petrologic types.

The lack of resolvable Ce isotope fractionation indicates that Ce stable isotopes were largely insensitive to nebular physicochemical variables such as oxygen fugacity, as well as to parent-body thermal metamorphism and terrestrial weathering. Given Ce's refractory and lithophile behavior, these results suggest efficient mixing of Ce isotopes in the solar nebula and minimal modification during subsequent geological processing. Consequently, the average Ce isotopic composition of non-carbonaceous chondrites is inferred to be representative of the Bulk Silicate Earth. We highlight the cosmochemical significance of this isotopic homogeneity and recommend extending stable isotope studies of Ce and other rare earth elements to additional chondrite groups and individual chondritic components to further constrain early Solar System processes.

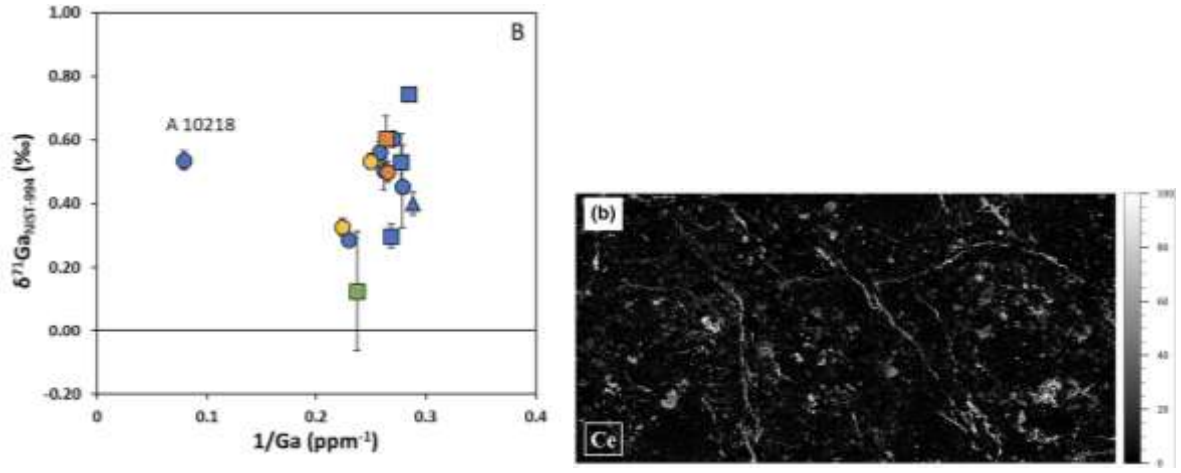

Figure 23. (left) Isotope data for Ga plotted against their reciprocal respective concentration in the studied samples, ordered by shock stage (color code) and weathering grade (shape code). Errors bars are represented as 2σ. From Roland et al. (2024). (right) Cerium distribution map based on LA-ICP-MS highlighting the state of alteration in Antarctic meteorites as the result of fluid flow (Maeda et al. 2023).

4.3. WP3. Estimating the role of the extraterrestrial influx to mass extinctions based on the Belgian stratigraphic record

Over the reporting period, the project has also focused on quantifying the flux of extraterrestrial material to Earth across critical intervals of the Belgian stratigraphic record, with particular emphasis on the Devonian–Carboniferous boundary and the Hangenberg Event. By combining the development of a novel extraction methodology, the construction of an unprecedented fossil micrometeorite (MM) dataset, and multi-proxy geochemical analyses, the project aims to assess the potential role of extraterrestrial influx variations in paleoenvironmental change and mass extinction processes.

4.3.1. Development and validation of a novel fossil micrometeorite extraction protocol

Fossil micrometeorites are extremely rare and have historically been recovered using heterogeneous, non-standardized extraction techniques, limiting recovery efficiency and preventing robust inter-study comparisons. During this project, a new extraction protocol was developed, validated, and systematically applied. This method minimizes lithological bias and enables the recovery of all major micrometeorite types (I-, S-, and G-types), including fragile silicate particles that are typically underrepresented in fossil collections.

The protocol is based on partial dissolution of carbonate rocks using 15% hydrochloric acid until a fine sand-sized residue remains. The residue is subsequently sieved into grain-size fractions and processed using a two-step extraction strategy combining wet magnetic separation and optical picking under a binocular microscope. Compared to earlier approaches (e.g., ~20 micrometeorites recovered from 137 kg of carbonate), this method represents a major shift in efficiency and preservation. To date, this approach has yielded approximately 2000 fossil micrometeorites from ~50 kg of Late Devonian carbonates from the Chanxhe section, making this one of the largest fossil micrometeorite collections worldwide. This protocol is now routinely used at AMGC-VUB and provides a robust methodological foundation for future fossil micrometeorite studies. This method will be submitted as a paper in *Metoritical and Planetary Science* in early 2026.

4.3.2. Fossil micrometeorite diversity and classification

A comprehensive paper describing the Chanxhe fossil micrometeorite collection has been published in *Geochimica et Cosmochimica Acta* (September 2025). The fossil micrometeorites recovered during the project reveal a broader range of textures, mineralogies, and alteration features than captured by conventional classification schemes. In particular, G-type micrometeorites, intermediate between I- and S-types, display significant textural diversity, including variable magnetite dendrite morphologies, glass contents, and secondary alteration features that are commonly overlooked. Based on systematic observations, a new G/I-type subgroup was defined to better capture the continuum between I-type iron-dominated and G-type silicate-bearing micrometeorites. This refined classification highlights the complexity of extraterrestrial dust inputs and underscores the importance of fossil micrometeorites for sampling parent bodies that are poorly represented in meteorite collections.

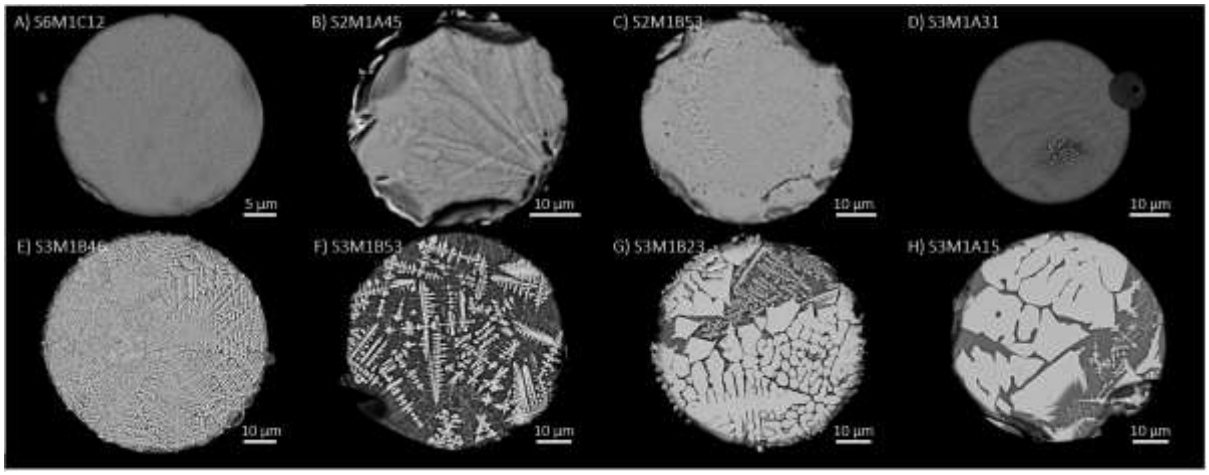

Figure 24. BSE images of extracted fossil G-type and S-type cosmic spherule interiors highlighting their mineralogy, texture and alteration features. A-D) S-types display V-, and CC- type textures; E-H) G-types spherules with textures going from fine to bulky magnetite. All particles from Chanxhe, Liège (Krämer Ruggiu et al., 2025, GCA).

4.3.3. Analytical characterization of extraterrestrial particles

More than 450 micrometeorites were mounted in epoxy, polished into sections, and characterized by scanning electron microscopy (SEM) at the Vrije Universiteit Brussel to determine mineralogy, textures, and major-element chemistry. Electron microprobe analyses (EMPA) were carried out on over 100 micrometeorites in collaboration with the Museum für Naturkunde in Berlin (October 2023), providing high-precision major and minor element data. Trace element compositions of ~30 micrometeorites were determined by LA-ICP-MS at VUB in March 2025. Triple oxygen isotope measurements were conducted at CRPG Nancy (February 2024 and February 2025) to constrain parent body affinities and assess isotopic modification during atmospheric entry and post-depositional alteration (see section 4.3.4). The development of a new method for in-situ iron isotope measurements using a femtosecond laser (fs-LA) coupled to a multicollector inductively coupled plasma mass spectrometer (MC-ICP-MS) was done at the Laboratoire Géosciences Environnement Toulouse (GET) in France. The in-situ iron isotope compositions of 13 particles (November 2022) and 35 particles (July 2025) from Chanxhe were measured. The in-situ Fe isotope measurements were performed at high spatial resolution, using raster analysis with spot sizes that are 7 µm wide and between 70 and 100 µm long (see Fig. 25), and high precision with uncertainties of about 0.1‰ for δ^{56}Fe. The micrometeorites display positive δ^{56}Fe signatures ranging from 11.99 ± 0.03 ‰ to -0.31 ±0.1. Fe isotope ratios may thus be used to identify cosmic particles when preserved under excellent conditions. Those combined analyses allow to assess the degree of pristinity using a combination of textural criteria (primary versus secondary recrystallization), Mn/Fe ratios, Raman spectroscopy, and oxygen and iron isotopes. This integrated approach allows selection of the least altered particles for potential future paleoenvironmental reconstruction.

Figure 25. I-type micrometeorite (M7) during fs-LA MC-ICP-MS measurements using raster analysis (7x98 mm) at the Laboratoire Géosciences Environnement Toulouse (France).

4.3.4. Oxygen isotope constraints on parent bodies and atmospheric interaction

Triple oxygen isotopes provide powerful tracers of micrometeorite parent bodies, as distinct meteorite groups occupy well-defined isotopic fields. Modern micrometeorites preserve these fingerprints despite atmospheric entry and weathering, with approximately 21% originating from inner-belt asteroids, more than 60% from carbonaceous chondrite-like bodies, and minor cometary contributions. Late Devonian micrometeorites extracted during the project retain both extraterrestrial and atmospheric oxygen isotope signatures, demonstrating the feasibility of dual isotopic interpretation. This confirms that fossil micrometeorites can be used not only to trace parent body reservoirs but also to probe atmospheric composition at the time of deposition.

4.3.5. Reconstruction of extraterrestrial flux

A key objective of the project is to reconstruct temporal variations in extraterrestrial flux across the Chanxhe section in the Late Devonian. Using 13 stratigraphically constrained samples and their fossil micrometeorite content, a first quantitative flux profile was established. The data reveal significant variability, with flux changes of up to a factor of two and a pronounced peak occurring in the middle of the section, immediately preceding the Hangenberg Event.

To evaluate potential preservation biases and better constrain the causes of flux variation, conventional geochemical proxies are being measured on the host sediments, including osmium isotopic ratios, iridium and platinum-group element concentrations, and ^{3}He contents. These complementary datasets will help distinguish between true increases in extraterrestrial input and sedimentological or diagenetic effects. Preliminary results were presented at Goldschmidt 2025 in Prague and EPSC 2025 in Helsinki.

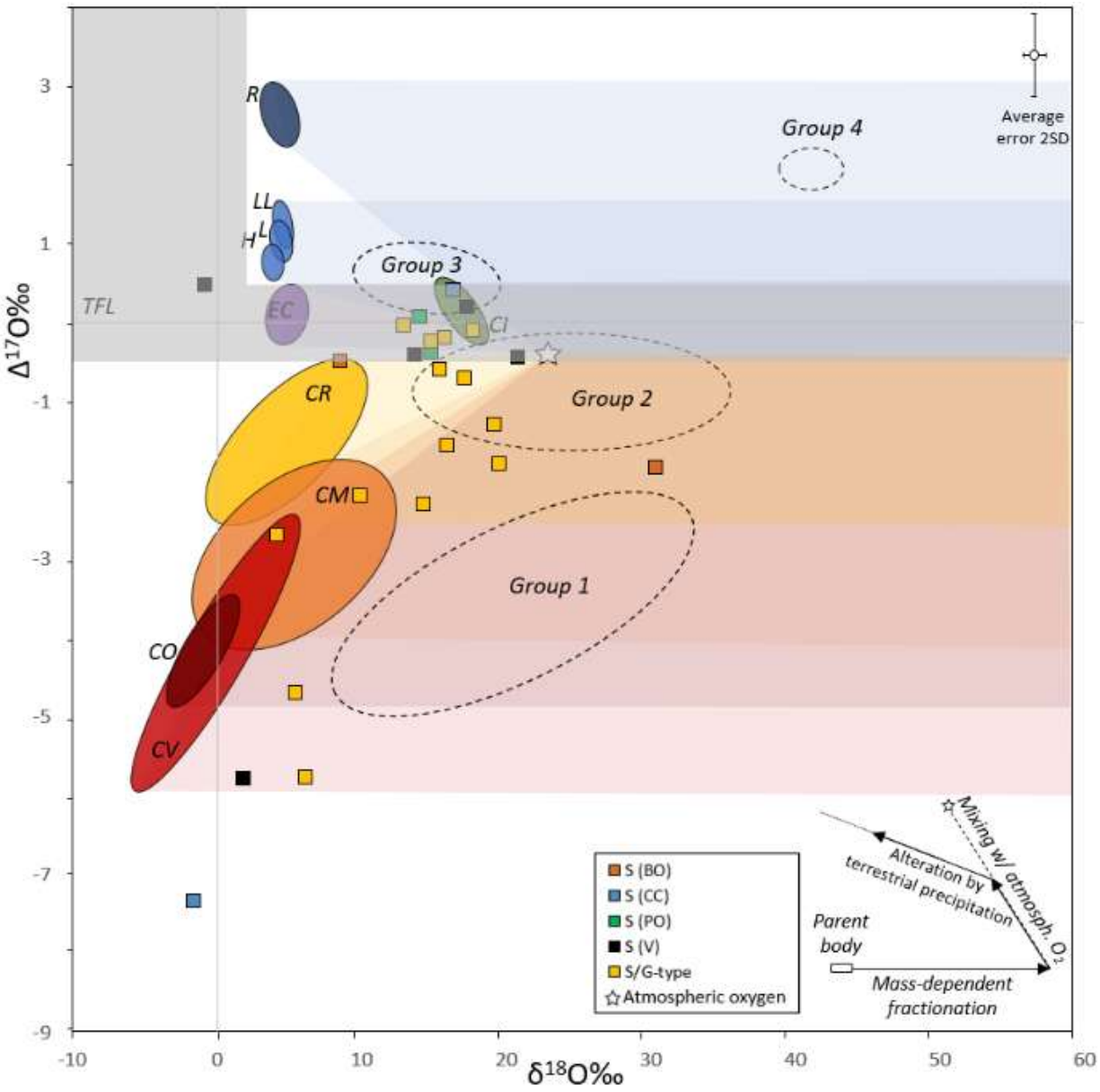

Figure 26. Triple oxygen SIMS-analyses data of the extracted fossil S-type cosmic spherules represented in $\delta^{18}O$ (horizontal) versus $\Delta^{17}O$ (vertical) in ‰ (Kr. The solid line represents the terrestrial fractionation line TFL (~ $\delta^{17}O = 0.52 \times \delta^{18}O$). The star represents the present average isotopic composition of oxygen around the transition from the stratosphere to the mesosphere ($\delta^{18}O$ ~ 23.5‰ and $\delta^{17}O$ ~ 11.8‰; Thiemens et al., 1995). The plots are adapted after Suavet et al. (2010) and Cordier and Folco (2014): colored domains represent potential meteoritical parent bodies (Clayton et al., 1991; Schulze et al., 1994; Clayton and Mayeda, 1999; Newton et al., 2000) and shaded areas designate the range of possible values for micrometeorites derived from the particular parent body. The outlines of the 4 groups originally identified by Suavet et al. (2010) are represented using dotted lines. Dashed arrows reflect the direction of possible shifts due to the atmospheric entry and formation of alteration products in equilibrium with terrestrial precipitation. Analytical uncertainties for SIMS measurements are ± 0.4 ‰ for $\delta^{18}O$ and ± 0.5‰ for $\Delta^{17}O$ (2σ). With standard deviation being on average $\delta^{18}O$ ± 0.4 ‰ and $\Delta^{17}O$ ± 0.5 ‰, grey zones represent data that could have extensive hydration from terrestrial precipitation (positive $\Delta^{17}O$ and $\delta^{18}O$ < 0.2‰) and potential TFL overprint ($\Delta^{17}O$ between -0.5 and 0.5‰).

4.4. WP4. Pursuing an efficient curation of Antarctic meteorites at the RBINS and valorizing the meteorite collection hosted at RBINS

The activities carried out during the reporting period reflect the continued growth and strengthening of the meteorite research programme at the RBINS. They encompass field-based recovery in Antarctica, the expansion and scientific enhancement of the national meteorite collection, improvements in public-facing digital resources, and progress in the classification and characterization of newly recovered samples.

4.4.1. Antarctic campaign 2024-2025

A meteorite recovery expedition to the Belgica Mountains, Queen Maud Land, East Antarctica, took place during the BELARE 2024-2025 field season. The field mission had several objectives: collecting meteorites and ice samples from blue ice field areas (BIA), collecting sampling sediments for the recovery of micrometeorites, collecting extracting soils and water samples for organic analysis (eDNA and lipids distribution) for the potential detection of microorganism communities and recovering geological samples for dating the formation age range of different geological units and rock weathering investigations. Systematic searches were performed in moraines and on BIAs, and resulted in the recovery of a total of 115 possible meteorites. The small size of the meteorite samples, with all but two of the meteorites weighting less than the 200 g wind displacement threshold, strongly suggests that after the meteorites are brought back to the surface by ice movement, wind serves as the primary mechanism for meteorite accumulation in the main meteorite accumulation zone near Mount Notre-Dame de Lorette. We hereby propose to distinguish between the primary and secondary mechanisms of meteorite accumulation in BIAs. Preliminary classification was performed on site using magnetic susceptibility and tentatively indicated the presence of a pallasite, achondrites, and carbonaceous chondrite. The recovered meteorites were transported in frozen state to the Royal Belgian Institute of Natural Sciences in Brussels and have been thawed in under vacuum conditions to be further classified based on their mineralogy (Fig. 27).

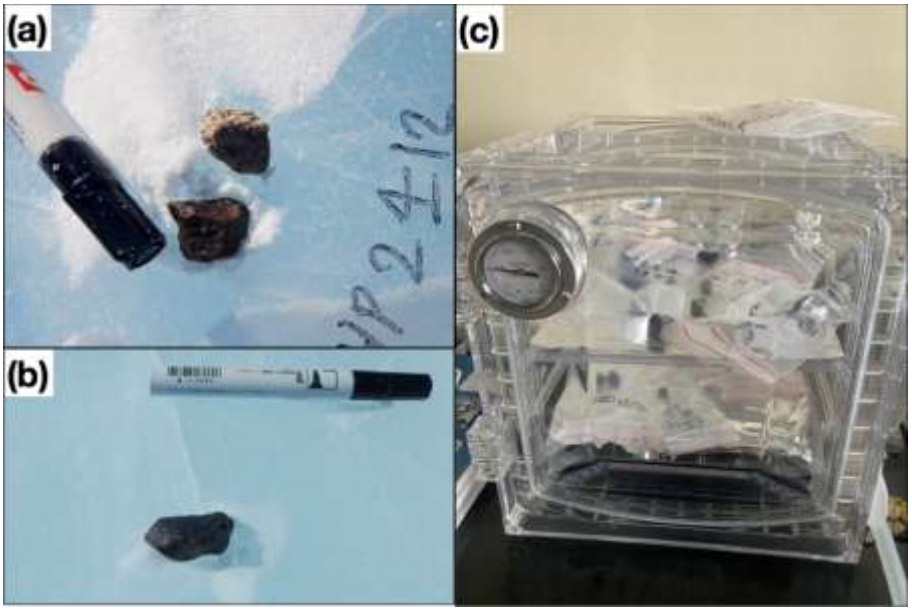

Figure 27. Pictures illustrating meteorite recovery and curation. (a-b) Two meteorite fragments immediately after collection, shown with a marker for scale. (c) Desiccator used to defrost the meteorites under vacuum prior to further handling and subsampling for classification.

4.4.2. Increase of the collection

Overview of New Meteorite Acquisitions 2018–2025:

Antarctic Meteorites: 55 specimens with a total weight of 11,251.44 grams

Achondrites:

- Eucrite: 2 specimens, 70.72 g

Chondrites:

- Enstatite: 4 specimens, 625.9 g
- Carbonaceous: 3 specimens, 146.79 g
- LL: 7 specimens, 488.29 g
- L: 23 specimens, 2,016.82 g
- H: 16 specimens, 7,903.35 g

Non-Antarctic Meteorites: 47 specimens with a total weight of 2,955.414 grams

- 7 fragments of Belgian meteorites from two different falls (Tintigny and Lesves)
- 3 Martian fragments totalling 22.45 g
- 2 Lunar fragments totalling 6.624 g

Achondrites:

- 2 Diogenite specimens totalling 22.94 g
- 2 Ureilite specimens totalling 78.71 g
- 2 Eucrite specimens totalling 210.6 g
- 1 Pallasite, 32.86 g
- 10 iron meteorites totalling 962.85 g

Chondrites:

- 14 Ordinary chondrites totalling 97.33 g
- 1 Mesosiderite 8 g
- 4 R chondrites totalling 46.77 g
- 4 Carbonaceous chondrites totalling 430.14 g
- 2 pieces classified as “Unknown, not yet defined” totalling 1,036.14 g

4.4.3. Update of the webpages dedicated to meteorites

All newly acquired meteorites were photographed using a photo-stacking technique (Fig. 28). This method allows details to be captured clearly and makes it possible to view the meteorite without physically removing it from storage.

Figure 28. Photographs of samples using the photo-stacking technique

For 16 specimens, a 3D scan was also made (Fig. 29). This way, the meteorite can be examined from all angles via digital view. An example can be found at https://sketchfab.com/3d-models/meteorite-tintigny-bde52e8f3aed4f1fb3ef9fb5e2acb77c

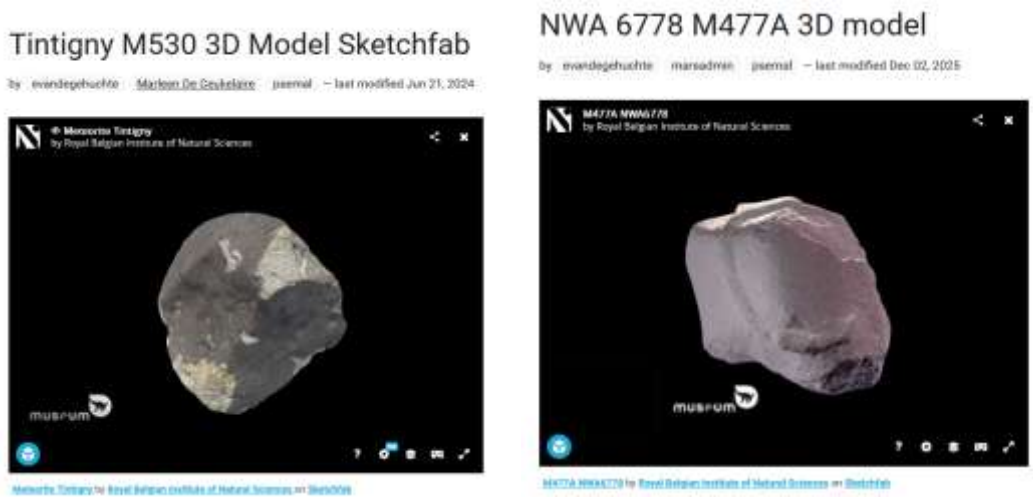

Figure 29. 3D scans of meteorites

Images were also prepared with a µCT scanner (Fig. 30), but the results were unfortunately not sufficiently detailed. Four of them are added to the database.

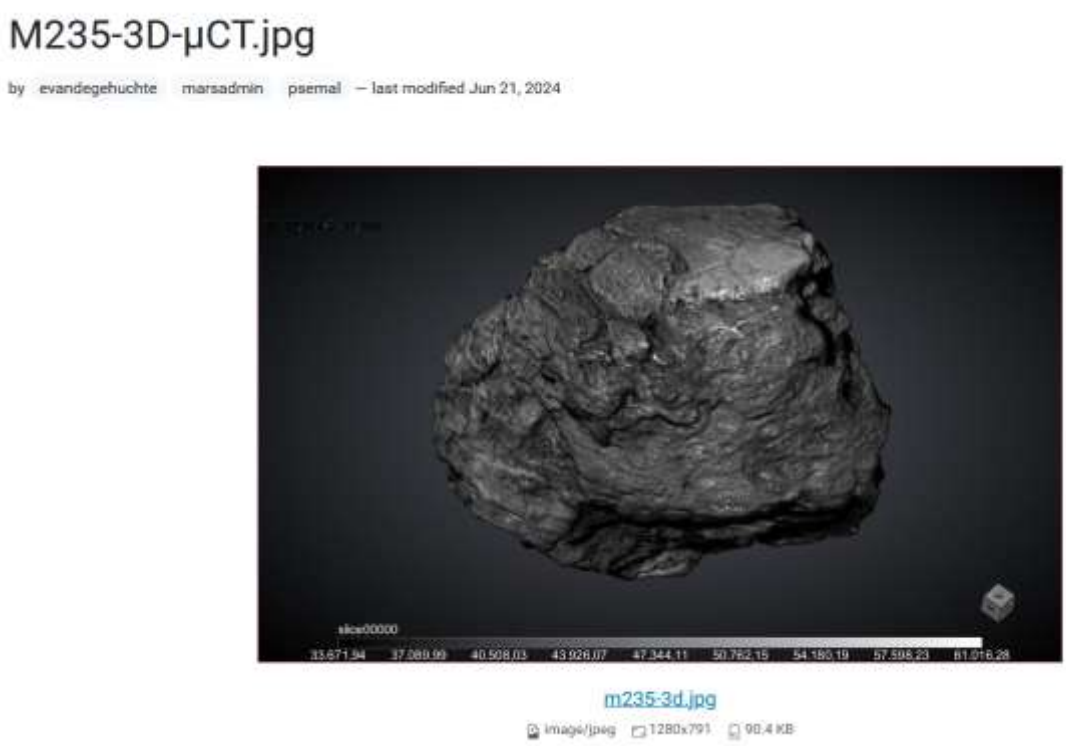

Figure 30. Picture obtained using the µCT scan.

Finally, a dedicated guidance page on the RBINS website to assist the public in identifying potential meteorites (and similar materials) and in contacting the appropriate experts is under development.

4.4.4. Meteorite classification

Work focused first on the preparation and classification of the meteorites recovered during the 2022-2023 Antarctic Recovery Expedition (Debaille et al., 2023). In parallel, detailed characterization of selected specimens from the RBINS collection was conducted to assess their state of preservation and to establish links with specific parent bodies. This included petrographic, mineralogical, and geochemical investigations carried out within the framework of ongoing collaborations (e.g., Rider-Stokes et al., 2023; Maeda et al., 2023; Pittarello et al., 2023; Chernonozhkin et al., 2024, 2025; McKibbin et al., 2025).

Related to the recently collected meteorites in the Belgica Mountains (expedition 2024-2025), thick polished sections are currently being prepared at RBINS for each sample (>100). We initiated SEM-EDS characterization of these polished sections in November 2025 as the first step toward the formal classification workflow, establishing initial petrographic and chemical composition to support the subsequent submission for official classification.

4.5. Prospects

The geochemical results obtained to date will continue to be exploited beyond 2026, with the goal of producing a publication that synthesizes the most significant findings on the Kaapvaal rocks. This manuscript will integrate the petrographic observations, the mineral-scale geochemical data acquired by LA-ICP-MS, and the isotopic results. In addition, the meteorite and micrometeorite work will lead to additional high-impact scientific publications. Furthermore, the meteorite classification work will continue as a daily task at the RBINS.

Finally, two new BELSPO projects have been secured, representing a direct continuation of the DESIRED project:

Understanding the Landscape, Tectonics, Ice, and Meteorite Origins in Antarctica

The ULTIMO project (January 2023 - May 2027) represents the continuation and expansion of a 15 year-long Belgian-Japanese scientific collaboration between VUB-ULB-RBINS-NIPR, focused on understanding the coupled evolution of rocks, ice, and extraterrestrial materials in Antarctica. Building on the exceptional results obtained around the Princess Elisabeth Antarctica (PEA) station in the Sør Rondane Mountains, where more than 1,300 meteorites and nearly 100,000 micrometeorites and other cosmic particles have been recovered, ULTIMO extends this interdisciplinary research to the Belgica Mountains, one of the least explored yet most promising meteorite accumulation areas on the Antarctic continent.

The Belgica Mountains, an isolated chain about 16 km long and located ~100 km east-southeast of the Sør Rondane Mountains, were first discovered during the Belgian Antarctic Expedition (1957-1958) led by Gaston de Gerlache. Only a short reconnaissance mission by the Japanese Antarctic Research Expedition (JARE) in 1998 revisited the area, recovering 37 meteorites in just three days, confirming its exceptional potential. ULTIMO returned to this site to conduct a systematic and multidisciplinary investigation.

The project pursues four main objectives:

1. Validate machine-learning models predicting meteorite concentration zones in Antarctic blue ice fields, through targeted field collection and characterization of newly recovered meteorites.

2. Expand the inventory of extraterrestrial materials (micrometeorites, impact debris, airburst particles) by sampling sedimentary deposits in the Belgica Mountains, and compare their chemical, isotopic, and mineralogical features with existing Antarctic collections to infer the early evolution of the Solar System.

3. Assess the potential of Belgica Mountain blue ice fields to host ancient ice, by combining $\delta^{18}O$–δD stable isotope mapping, direct surface ice dating, and ice-flow modelling to reconstruct the spatiotemporal dynamics of the local ice sheet.

4. Reconstruct the geological and exposure history of the Belgica Mountains' bedrock and moraines through geomorphological mapping and cosmogenic nuclide analyses.

By integrating geology, glaciology, meteoritics, and planetary science, ULTIMO explores how extraterrestrial material arriving on Earth records the earliest stages of Solar System evolution and

how Antarctic ice archives preserve this cosmic history. The project's results refine models of tectonic and glacial evolution, constrain extraterrestrial flux variations over the past few million years, and enhance understanding of ice–rock interaction processes in polar environments. Ultimately, ULTIMO consolidates Belgium's leading role in Antarctic science and planetary research, positioning the VUB-ULB-RBINS-NIPR consortium at the forefront of efforts to link Earth's geological record with the broader cosmic context of planetary formation.

Blue ice and mEteorites Recovered from the Yamato (Queen Fabiola) Mountains

The BERYL project (September 2025 - December 2029) is another chapter in the major Belgian-Japanese scientific initiative coordinated by VUB–ULB–RBINS in collaboration with the National Institute of Polar Research (NIPR, Japan). It aims to explore and sample the Yamato (Queen Fabiola) Mountains in East Antarctica, the most productive regions on Earth for meteorite recovery. Building upon more than a decade of successful Belgian-led Antarctic missions (SAMBA, BAMM!, DESIRED, ULTIMO), BERYL will expand the scope of research to this iconic region located east of the Belgica Mountains, first discovered by the Belgian Antarctic Expedition of 1958. Through a highly interdisciplinary approach bridging meteoritics, glaciology, planetary science, geochemistry, and astrobiology, BERYL seeks to:

1. Collect and characterise new meteorites from the blue ice areas surrounding the Yamato Mountains and compare them to existing specimens in the Royal Belgian Institute of Natural Sciences (RBINS) collection.

2. Expand the inventory of extraterrestrial particles, including micrometeorites, airburst debris, and impact ejecta, to reconstruct variations in the extraterrestrial flux to Earth over the last few million years.

3. Map the isotope composition ($\delta^{18}O$, δD) of blue ice fields to assess their potential to preserve ancient ice, thereby refining regional paleoenvironmental and glaciological models.

4. Investigate rock-ice-life interactions to address key astrobiological questions regarding the colonisation of meteorites by Antarctic microorganisms and the implications for extraterrestrial life detection.

5. Engage the public through outreach, including citizen science initiatives, exhibitions at the RBINS and Brussels Planetarium, and artistic collaborations centred on space materials.

Methodologically, BERYL combines state-of-the-art analytical facilities (FEG-SEM, LA-ICP-MS, MC-ICP-MS, Raman, EBSD, XRD, and DNA sequencing) with machine-learning algorithms that predict meteorite concentrations on the Antarctic ice sheet. Field validation of these models in the Yamato blue ice areas will advance the understanding of meteorite accumulation processes and ice dynamics.

By integrating geological, isotopic, and biological perspectives, BERYL will shed new light on the formation and evolution of the Solar System, the stability of the East Antarctic Ice Sheet, and the potential for life in extreme environments. It will also reinforce Belgium's leading role in Antarctic research, planetary science, and international curation of meteorites, ensuring that the RBINS remains Europe's largest Antarctic meteorite repository and a key partner for future ESA sample-return missions.

5. DISSEMINATION AND VALORISATION

Significant work was done regarding the diffusion and the valorisation of the scientific results.

First, the peer-reviewed papers and conference abstracts listed in the "6. Publications" section of this report testify for the valorisation of the research led for DESIRED.

Second, the 2024-2025 expedition attracted major media attention. For instance, in the new meteorites that entered the collection were advertised in Bruzz (interview Marleen De Ceukelaire; Fig. 31). Links to interviews are provided here below.

Figure 31. Images taken from the interview done by Bruzz

https://actus.ulb.be/fr/actus/recherche/de-retour-dantarctique-avec-une-impressionnante-recolte-de-meteorite

https://press.vub.ac.be/belgian-led-team-of-researchers-brings-back-impressive-haul-of-meteorites-during-antarctic-research-expedition#

https://dailyscience.be/19/02/2025/recolte-de-meteorites-perilleuse-mais-fructueuse-sur-les-pentes-des-montagnes-belgica/?print-posts=print

https://www.brusselstimes.com/1399383/belgian-led-research-team-returns-from-antarctica-with-meteorites

https://www.rtbf.be/article/des-chercheurs-de-l-ulb-et-de-la-vub-recoltent-plus-de-100-meteorites-en-antarctique-11490490

https://www.vrt.be/vrtnws/nl/2025/01/17/belgische-onderzoekers-vinden-115-meteorieten-op-antarctica/

https://www.rtl.be/actu/environnement/levolution-de-la-vie-plus-de-100-meteorites-decouvertes-par-des-chercheurs/2025-01-18/article/735990

https://www.sudinfo.be/id939304/article/2025-01-16/des-chercheurs-de-lulb-et-de-la-vub-recoltent-plus-de-100-meteorites-en

https://civis.eu/en/get-informed/news/impressive-haul-of-meteorites-brought-back-by-belgian-led-team-of-researchers

https://www.hln.be/weer-en-wetenschap/belgische-wetenschappers-vinden-zeldzame-meteorieten-op-expeditie-in-antarctica-essentieel-stukje-van-onze-puzzel~a3b7c1273/

https://www.demorgen.be/snelnieuws/onderzoeksteam-onder-belgische-leiding-vindt-zeldzame-meteorieten-op-antarctica~b5ea9763/?referrer=https%3A%2F%2Fwww.bing.com%2F

https://togethermag.eu/belgian-scientists-make-exciting-antarctic-discovery/

https://www.jpost.com/science/science-around-the-world/article-838175

Another major event during this project was the organization of the 86th Annual Meeting of the Meteoritical Society & Workshop about curation at the Institute of Natural Sciences (July 27-August 2 2024): The 86th Annual Meeting of the Meteoritical Society (MetSoc 24) was held from July 28 to August 2 2024 at the Palace of the Academies in Brussels, Belgium (Figs. 32-35). This was the first MetSoc meeting in Belgium, and also the first since the pandemic to be in-person only. The organization was a joint effort between the Vrije Universiteit Brussel, Université libre de Bruxelles, and the Belgian Institute of Natural Sciences. In total, 505 participants from 33 different countries attended the conference, including 329 professionals (scientists + exhibitors), 137 student participants, and 39 guests. A total of 470 abstracts were accepted for 314 oral, 150 poster and 6 print-only presentations. Oral presentations were scheduled in three parallel sessions from Monday (29 July) to Friday (2 August) while two poster sessions took place on Tuesday and Thursday in the late afternoon. The conference program and abstract volume can be accessed on the website of the Lunar and Planetary Institute: https://www.hou.usra.edu/meetings/metsoc2024/technical_program/.

Figure 32. Logo designed for the MetSoc meeting 2024 Brussels.

The conference kicked off on Saturday 27 July and Sunday 28 July with the pre-conference workshop chaired by Aurore Hutzler (ESA) and Tomohiro Usui (JAXA) at the Belgian Institute for Natural Sciences in Brussels, dedicated to the advanced curation of extra-terrestrial samples in an increasing international community. Around 100 participants attended the workshop. A digital view in the depository was shown (https://www.youtube.com/watch?v=cX8T9b94HU0), but also a real visit was on the program.

Figure 33. Image taken from the movie dedicated to the repository at RBINS that was shown during pre-conference workshop.

On Sunday, this was followed by the welcome reception that took place at the city hall of Brussels. The Barringer lecture was presented on Monday evening by Véronique Dehant of the Royal Observatory of Belgium in the Plaza Hotel in Brussels. Her talk, entitled "Does the Red Planet have a heart? Results from the Mars InSight mission" was dedicated to the deep interior of Mars. The talk was attended by a large audience.

Figure 34. Pictures of the pre-conference workshop.

On Wednesday morning, the presentation of Society Awards and distinguished lectures occurred. Monica Grady, recipient of the Leonard Medal, gave a lecture about "A Voyage in Space and Time". John Spray, recipient of the Barringer Medal, presented on "Bulk Versus Discrete Deformation in Rocks: A Question of Scale?". Richard Greenwood received the Service Award, while Elishevah van Kooten was awarded the Nier Prize. Wednesday afternoon was dedicated to cultural activities in and around Brussels. The conference banquet took place on Wednesday evening at the Museum of Natural Sciences. The conference was concluded on Friday mid-afternoon, when around 130 remaining attendees said goodbyes during a farewell party.

A full report on the meeting has been published in the December 2024 issue of the scientific journal Elements:

https://pubs.geoscienceworld.org/msa/elements/article-pdf/20/6/420/7061871/gselements-20-6-420.pdf

Figure 35. Picture of the attendees at the Palais des Académies.

In May 2025, the meteorites were in the spotlight for three days during the Nerdland Festival (Fig. 36), a big festival for nerds with sciencetopics, in Wachtebeke. The public, composed of both children and adults, was encouraged to discover the different types of meteorites and their characteristics.

Figure 36. Meteorite exhibition at Nerdland 2025.

Finally, in the frame of the Metsoc in Brussels in 2024, we initiated discussions to build a temporary meteorite exhibition at the Planetarium of Brussels. Due to the lack of funds and time, we could not launch the exhibit in 2024, but discussions have been ongoing since, and a small funding for this exhibit has been secured through the BERYL project. We now hope being able to launch this exhibit in 2026-2027.

6. PUBLICATIONS

6.1. Peer-reviewed papers (see Annex H)

Krämer Ruggiu L., Villeneuve J., Da Silva A.-C., **Debaille V.**, **Decrée S.**, Hecht L., Kaufmann F. E. D., and **Goderis S.** 2025. Diversity among fossil micrometeorites in the late Devonian. Geochimica et Cosmochimica Acta, accepted. (2024 IF: 5.0, 7/100 in Geochemistry & Geophysics, Q1)

Del Rio M., Folco L., Mugnaiola E., **Goderis S.**, and Masotta M. 2025. Loss and accretion of moderately volatile elements K and Na in Australasian microtektites from Antarctica. Geochimica et Cosmochimica Acta 395, 212-228. doi.org/10.1016/j.gca.2025.03.005 (2024 IF: 5.0, 7/100 in Geochemistry & Geophysics, Q1)

Chernonozhkin S. M., Pittarello L., Hublet G., Weyer S., Horn I., Claeys Ph., **Debaille V.**, Vanhaecke F., and **Goderis S.** 2025. Metal differentiation on asteroids recorded in Zn and Fe isotopic signatures of ureilites. Geochemical Perspectives Letters 33, 38-43. doi.org/10.7185/geochemlet.2501 (2024 IF: 3.7, 15/100 in Geochemistry & Geophysics, Q1)

McKibbin S. J., Ávila J. N., Ireland T. R., Van Ginneken M., Soens B., Van Maldeghem F., Huber M., Baeza L., Patkar A., Vanhaecke F., **Debaille V.**, Claeys Ph., and **Goderis S.** 2025. Triple-oxygen isotopes of stony micrometeorites by Secondary Ion Mass Spectrometry (SIMS): Olivine, glass, and iron oxide matrix effects for Sensitive High-mass Resolution Ion Micro-Probe – Stable Isotope (SHRIMP-SI). Rapid Communications in Mass Spectrometry 39, e9921. doi.org/10.1002/rcm.9921 (2024 IF: 1.7, 78/111 in Chemistry, Analytical, Q3)

Chernonozhkin S. M., Pittarello L., Hublet G., Claeys Ph., **Debaille V.**, Vanhaecke F., and **Goderis S.** 2024. Fe, Zn, and Mg stable isotope systematics of acapulcoite lodranite clan meteorites. Meteoritics & Planetary Science 59, 2956-2980. doi: 10.1111/maps.14258 (2024 IF: 2.4, 41/100 in Geochemistry & Geophysics, Q2)

Fischer-Gödde M., Tusch J., **Goderis S.**, Bragnani A., Mohr-Westheid T., Messling N., Elfers B.-M., Schmitz B., Reimold W. U., Maier W. D., Claeys Ph., Koeberl C., Tissot F. L. H., Bizzarro M., and Münker C. 2024. Ruthenium isotopes show the Chicxulub impactor was a carbonaceous-type chondrite. Science 385, 752-756. doi.org/10.1126/science.adk4868 (2024 IF: 45.8, 3/135 in Multidisciplinary Sciences, Q1)

Van Maldeghem F., Maeda R., Soens B., Suttle M. D., Krämer Ruggiu L., Cordier C., Yamaguchi A., Schmitz B., Claeys Ph., Folco L., and **Goderis S.** 2024. Chrome-rich spinels in micrometeorites from modern Antarctic sedimentary deposits. Earth and Planetary Science Letters 641, 118837. doi.org/10.1016/j.epsl.2024.118837 (2024 IF: 5.1, 6/100 in Geochemistry & Geophysics, Q1)

Kadlag Y., Anand A., Fischer-Gödde M., Mezger K., Szilas K., **Goderis S.**, and Leya I. 2024. Identification of Earth's late accretion by large impactors through mass independent Cr isotopes. Icarus 418, 116143. doi.org/10.1016/j.icarus.2024.116143 (2024 IF: 3.0, 27/84 in Astronomy & Astrophysics, Q2)

Tollenaar V., Zekollari H., Kittel C., Farinotti D., Lhermitte S., **Debaille V**., **Goderis S.**, Claeys Ph., Joy K. H., and Pattyn F. 2024. Antarctic meteorites threatened by climate warming. Nature Climate Change 14, 340–343. doi.org/10.1038/s41558-024-01954-y (2024 IF: 27.1, 3/374 in Environmental Sciences, Q1)

Roland J., **Debaille V.**, Pourkhorsandi H., and **Goderis S.** 2024. Moderately volatile elemental and isotopic variations in variably shocked equilibrated chondrites from Antarctica. Icarus 412, 115983. doi.org/10.1016/j.icarus.2024.115983 (2022 IF: 3.2, 26/69 in Astronomy & Astrophysics, Q2)

Jonker G., Van Maldeghem F., van Ginneken M., **Krämer Ruggiu L.**, and **Goderis S.** 2024. Oxygen isotopic compositions of fresh rooftop micrometeorites from the Budel collection – Insights into the contemporary cosmic dust flux. Meteoritics & Planetary Science, accepted. (2022 IF: 2.2, 48/87 in Geochemistry & Geophysics, Q3)

van Ginneken M., Wozniakiewicz P., Brownlee D. E., **Debaille V.**, Della Corte V., Delauche L., Duprat J., Engrand C., Folco L., Fries M., Gattacceca J., Genge M. J., **Goderis S.**, Gounelle M., Harvey R. P., Jonker G., K**rämer Ruggiu L.**, Larsen J., Lever J. H., Noguchi T., Peterson S., Rochette P., Rotundi A., Rudraswami N. G., Suttle M. D., Taylor S., Van Maldeghem F., and Zolensky M. 2024. Micrometeorite collections: a review, and their current status. Philosophical Transactions of the Royal Society A 382, 10230195. doi.org/10.1098/rsta.2023.0195 (2024 IF: 3.7, 28/135 in Multidisciplinary Sciences, Q1)

van Ginneken M., Harvey R. P., **Goderis S.**, Artemieva N., Boslough M., Maeda R., Gattacceca J., Folco L., Yamaguchi A., Sonzogni C., and Wozniakiewicz P. 2024. Earth and Planetary Science Letters 627, 118562. doi.org/10.1016/j.epsl.2023.118562 (2022 IF: 5.3, 7/87 in Geochemistry & Geophysics, Q1)

Debaille V., Schönbächler M., Valdes M., Maeda R., Poudelet M., **Goderis S.**, Heck Ph. R., Tollenaar V., Zekollari H., and Claeys Ph. 2023. Comprehensive report of the BELARE 2022-2023 meteorite reconnaissance expedition in the Sør Rondane area, East Antarctica. Antarctic Record 67, 12-27.

Pittarello L., Ferrière L., Chernonozhkin S., Vanhaecke F., and **Goderis S.** 2023. The vesiculated layer in the anomalous diogenite Northwest Africa 12973. Meteoritics & Planetary Science 58, 1677-1690. doi.org/10.1111/maps.14091 (2022 IF: 2.2, 48/87 in Geochemistry & Geophysics, Q3)

Serra C., Vinogradoff V., Poinot P., Blancart Remaury Q., Duvernay F., Le Sergeant d'Hendecourt L., Danger G., Claeys Ph., **Goderis S.**, and Schmitt-Kopplin Ph. 2023. Assessing the Effect of Aqueous Alteration on Soluble Organic Matter in Primitive Carbonaceous Chondrites: The Case of Asuka 12236. ACS Earth Space Chemistry 7, 1980-1991. doi.org/10.1021/acsearthspacechem.3c00106 (2022 IF: 3.4, 83/178 in Chemistry, Multidisciplinary, Q2)

Maeda R., **Goderis S.**, Yamaguchi A., Van Acker T., Vanhaecke F., **Debaille V.**, and Claeys Ph. 2023. Fluid mobilization of rare earth elements (REEs), Th, and U during the terrestrial alteration of chondrites. Meteoritics & Planetary Science 58, 1018-1038. doi.org/10.1111/maps.14034 (2022 IF: 2.2, 48/87 in Geochemistry & Geophysics, Q3)

Pourkhorsandi, H., Debaille, V., Armytage, R.M.G and de Jong, J. 2024. Cerium Stable Isotopic Composition of Non-Carbonaceous Chondrites.ACS Earth and Space Chemistry **2024** *8* (12), 2452-2462. DOI: 10.1021/acsearthspacechem.4c00206

Roland J., **Debaille V.**, de Jong J., and **Goderis S.** 2023. Comparison of two gallium purification procedures for isotopic measurements by MC-ICP-MS in a set of silicate reference materials. Talanta 263, 124714. doi.org/10.1016/j.talanta.2023.124714 (2022 IF: 6.1, 9/86 in Chemistry, Analytical, Q1)

Rider-Stokes B. G., Greenwood R. C., Anand M., White L. F., Franchi I. A., **Debaille V.**, **Goderis S.**, Pittarello L., Yamaguchi A., Mikouchi T., and Claeys Ph. 2023. Impact mixing among rocky

planetesimals in the early Solar System from angrite oxygen isotopes. Nature Astronomy 7, 836-842. 10.1038/s41550-023-01968-0 (2022 IF: 14.1, 5/69 in Astronomy & Astrophysics, Q1)

Maeda R., Van Acker T., Vanhaecke F., Yamaguchi A., **Debaille V.**, Claeys Ph., and **Goderis S.** 2023. Quantitative elemental mapping of chondritic meteorites using laser ablation-inductively coupled plasma-time of flight-mass spectrometry (LA-ICP-TOF-MS). Journal of Analytical Atomic Spectrometry 38, 369-381. doi.org/10.1039/d2ja00317a (2022 IF: 3.4, 29/86 in Chemistry, Analytical, Q2)

Decrée, S., Pašava, J., Baele, J. M., Mercadier, J., Rösel, D., & Frimmel, H. (2022). In-situ trace element and Sr isotope signature of apatite: A new key to unravelling the genesis of polymetallic mineralisation in black shales of the Early Cambrian Niutitang Formation, Southern China. Ore Geology Reviews, 150, 105130.

6.2. Participation to national and international conferences

Abstracts have been presented at the Meteoritical Society Annual Meeting, EGU Annual Meeting, NIPR Symposium, LPSC, and Goldschmidt:

Krämer Ruggiu L., Villeneuve J., Da Silva A.-C., **Debaille V.**, **Decrée S.**, Hecht L., Kaufmann F. E. D. and **Goderis S.** (2025) Tracing variations in the Flux of Extraterrestrial Material in the late Devonian. Goldschmidt conference [Abstract].

Pinto G. A., Maeda R., **Debaille V.**, Van Acker T., Vanhaecke F. and **Goderis S.** (2025) Primary Carrier Phase of High Siderophile Elements in Ordinary Chondrites: Insights from In Situ LA-ICP-TOF-MS Analysis. Goldschmidt conference [Abstract].

Feignon J.-G., **Goderis S.**, Fischer-Gödde M., Hibiya Y., McDonald I., Schmitt R. -T., Schmitz B., Spray J., Tagle R., Vanhaecke F. and Claeys Ph. (2025). Multi-parameter approach to constrain projectile types and origins in impactites: relation between the Ordovician impact spike and the L-chondrite parent body (LCPB) breakup. Goldschmidt conference [Abstract].

Dumas F., **Debaille V.**, and **Goderis S.** (2025) Revisiting the systematic classification of iron meteorites. Goldschmidt conference [Abstract].

Pinto G.A., **Debaille V.**, Locatelli C., Leduc, T., De Ceukelaire, M., **Goderis, S.,** and **Decree, S.** (2024). Forensic classification of meteorites: The case of an oriented specimen from the Belgian Antarctic collection. *86th Annual Meeting of The Meteoritical Society*, Brussels, Belgium.

Tollenaar V., Zekollari H., Kittel C., Farinotti D., Lhermitte S., **Debaille V.**, **Goderis S.**, Claeys Ph., Joy K. H., and Pattyn F. 2024. The impact of climate change on meteorite finds in East Antarctica. EGU Annual Meeting [Abstract EGU24-1488].

Debaille V. Schönbächler M, Valdes M., Maeda R., Poudelet M., **Goderis S.**, Heck Ph., Tollenaar V., Zekollari H., and Claeys Ph. 2024. In search of new meteorite dense collection area in the Sor Rondane Mountains. NIPR Symposium [Abstract].

Maeda R., **Goderis S.**, Yamaguchi A., **Debaille V.**, and Claeys Ph. 2024. The effect of fluid alteration in Antarctic chondrites. NIPR Symposium [Abstract].

Serra C., Vinogradoff V., Poinot P., Blancart Remaury Q., Duvernay F., Le Sergeant d'Hendecourt L., Danger G., Claeys Ph., **Goderis S.**, Schmitt-Kopplin. 2024. Unveiling the relationship between aqueous alteration and soluble organic matter in primitive carbonaceous chondrites: lessons from Asuka 12236. LPSC conference [Abstract 2990].

Krämer Ruggiu L., **Goderis S.**, **Debaille V.**, Da Silva A.-C., Percival L. 2023. Tracing variations in the Flux of Extraterrestrial Material through time. In Goldschmidt conference. [Abstract #16540].

Rabin S., **Goderis S.,** Krämer Ruggiu L., Smit J. and **Debaille V.** 2023. Iron isotope signatures of distal impact spherules from the Cretaceous-Paleogene boundary. Goldschmidt 2023 [Abstract #20408].

Roland J., Debaille V., and **Goderis S.** 2023. Moderately volatile elements in CB and CH chondrites. Goldschmidt 2023 [Abstract].

Fischer-Gödde M., Tusch J., **Goderis S.**, Bragagni A., Mohr-Westheide T., Messling N., Elfers B.-M., Schmitz B., Reimold W. U., Tissot F. L. H., Koeberl C., Claeys Ph., Maier W., Münker C. 2023. Ruthenium isotope composition of the K-Pg impactor and terrestrial impact structures. Goldschmidt 2023 [Abstract].

Chernonozhkin S. M., **Goderis S.**, Hublet G. C., Weyer S., Horn I., Pittarello L., Claeys Ph., **Debaille V.**, and Vanhaecke F. 2023. Fe, Zn and Mg stable isotope records of early differentiation and core formation of the ureilite parent body. Goldschmidt 2023 [Abstract].

7. ACKNOWLEDGEMENTS

All sample providers from the Kaapvaal Craton are gratefully acknowledged for their valuable contributions to this project. In particular, we warmly thank Hartwig Frimmel and Glen Nwaila for their key role in helping to gather and facilitate access to these samples.

8. REFERENCES

Ansberque, C., Mark, C., Caulfield, J. T., & Chew, D. M. (2019). Combined in-situ determination of halogen (F, Cl) content in igneous and detrital apatite by SEM-EDS and LA-Q-ICPMS: A potential new provenance tool. Chemical Geology, 524, 406-420. DOI: 10.1016/j.chemgeo.2019.07.012

Armstrong, R. A., Compston, W., Retief, E. A., Williams, I. T., & Welke, H. J. (1991). Zircon ion microprobe studies bearing on the age and evolution of the Witwatersrand triad. Precambrian Research, 53(3-4), 243-266.

Barnes, S. J., & Roeder, P. L. (2001). The range of spinel compositions in terrestrial mafic and ultramafic rocks. *Journal of petrology*, *42*(12), 2279-2302.

Barnes, S. J., Mungall, J. E., & Maier, W. D. (2015). Platinum group elements in mantle melts and mantle samples. *Lithos*, *232*, 395-417.

Becker, H., Horan, M. F., Walker, R. J., Gao, S., Lorand, J. P. & Rudnick, R. L. (2006). Highly siderophile element composition of the Earth's primitive upper mantle: Constraints from new data on peridotite massifs and xenoliths. *Geochimica et Cosmochimica Acta*, 70, 4528–4550.

Belousova EA, Griffin WL, O'Reilly SY, Fisher NI (2002) Apatite as an indicator mineral for mineral exploration: trace-element compositions and their relationship to host rock type. J Geochem Explor 76, 45-69

Birck, J. L., Barman, M. R., & Capmas, F. (1997). Re-Os isotopic measurements at the femtomole level in natural samples. *Geostandards newsletter*, *21*(1), 19-27.

Bouzari, F., Hart, C. J., Bissig, T., & Barker, S. (2016). Hydrothermal alteration revealed by apatite luminescence and chemistry: a potential indicator mineral for exploring covered porphyry copper deposits. Economic Geology, 111(6), 1397-1410. DOI: 10.2113/econgeo.111.6.1397

Bruand, E., Fowler, M., Storey, C., & Darling, J. (2017). Apatite trace element and isotope applications to petrogenesis and provenance. American Mineralogist, 102(1), 75-84. DOI: 10.2138/am-2017-5744

Budde, G., Kleine, T., Kruijer, T. S. & Burkhardt, C. (2016). Tungsten isotopic evidence for rapid accretion and differentiation in the early solar system. *Nature Geoscience*, 9, 722–727. Budde, G., Kruijer, T. S. & Kleine, T. (2019). Heterogeneous accretion of the Earth inferred from molybdenum isotopes. *Nature Geoscience*, 12, 674–678.

Burkhardt, C., Budde, G., Fischer-Gödde, M., Kruijer, T. S. & Kleine, T. (2019). Nucleosynthetic isotope variations among inner solar system materials. *Geochimica et Cosmochimica Acta*, 261, 145–170.

Cawthorn, R. G., & Walraven, F. (1998). Emplacement and crystallization time for the Bushveld Complex. Journal of Petrology, 39(9), 1669-1687.

Chen, N., Pan, Y., & Weil, J. A. (2002). Electron paramagnetic resonance spectroscopic study of synthetic fluorapatite: Part I. Local structural environment and substitution mechanism of Gd3+ at the Ca2 site. American Mineralogist, 87(1), 37-46.

Chen J, Shen SZ, Li XH, Xu YG, Joachimski MM, Bowring SA et al. (2016) High-resolution SIMS oxygen isotope analysis on conodont apatite from South China and implications for the end-Permian mass extinction. Palaeogeogr Palaeoclimatol Palaeoecol 448:26–38

Chou, C. L. (1978). Fractionation of siderophile elements in the Earth's upper mantle. *Proceedings of the 9th Lunar and Planetary Science Conference*, 219–230.

Chu MF, Wang KL, Griffin WL, et al. (2009) Apatite composition: tracing petrogenetic processes in Transhimalayan granitoids. J Petrol 50: 1829-1855

Clayton, R. N., Mayeda, T. K., Goswami, J. N. & Olsen, E. J. (1991). Oxygen isotopic studies of ordinary chondrites. *Geochimica et Cosmochimica Acta*, **55**, 2317–2337.

Clayton, R. N. & Mayeda, T. K. (1999). Oxygen isotope studies of carbonaceous chondrites. *Geochimica et Cosmochimica Acta*, **63**, 2089–2104.

Cordier, C. & Folco, L. (2014). Oxygen isotopes in cosmic spherules: Constraints on their precursors and formation processes. *Geochimica et Cosmochimica Acta*, **146**, 18–34.

Dauphas, N. (2017). The isotopic nature of the Earth's accreting material and the origin of volatiles. *Nature*, 541, 521–524.
Dauphas, N., Teng, F. Z. & Arndt, N. T. (2014). Analytical advances in isotope geochemistry. *Treatise on Geochemistry*, 2nd ed., Elsevier.
Day, J. M. D., Pearson, D. G. & Taylor, L. A. (2016). Highly siderophile element constraints on Earth accretion and core formation. *Earth and Planetary Science Letters*, 451, 266–276.

Decrée, S., Cawthorn, G., Deloule, E., Mercadier, J., Frimmel, H., & Baele, J. M. (2020). Unravelling the processes controlling apatite formation in the Phalaborwa Complex (South Africa) based on combined cathodoluminescence, LA-ICPMS and in-situ O and Sr isotope analyses. Contributions to Mineralogy and Petrology, 175(4), 34.

Deines P (1989) Stable isotope variations in carbonatite. In: Bell K (ed) Carbonatites: Genesis and Evolution, Unwin Hyman, London

de La Parra, F., Jaramillo, C., Kaskes, P., Goderis, S., Claeys, P., Villasante-Marcos, V., ... & Caballero, D. (2022). Unraveling the record of a tropical continental Cretaceous-Paleogene boundary in northern Colombia, South America. *Journal of South American Earth Sciences*, *114*, 103717.

de Winter, N.J. and Claeys, P. (2017), Micro X-ray fluorescence (µXRF) line scanning on Cretaceous rudist bivalves: A new method for reproducible trace element profiles in bivalve calcite. Sedimentology, 64: 231-251. https://doi.org/10.1111/sed.12299

Edwards, C. T., Jones, C. M., Quinton, P. C., & Fike, D. A. (2022). Oxygen isotope (δ18O) trends measured from Ordovician conodont apatite using secondary ion mass spectrometry (SIMS): Implications for paleo-thermometry studies. Bulletin, 134(1-2), 261-274.

Fischer-Gödde, M. & Kleine, T. (2017). Ruthenium isotopic evidence for an inner solar system origin of the late veneer. *Nature*, 541, 525–527.

Fischer-Gödde, M., Burkhardt, C., Kruijer, T. S. & Kleine, T. (2020). Ru isotope heterogeneity in the solar nebula: Implications for Earth's late accretion. *Geochimica et Cosmochimica Acta*, 275, 128–144.

Fleet, M. E., & Pan, Y. (1995). Site preference of rare earth elements in fluorapatite. American Mineralogist, 80(3-4), 329-335.

Frimmel, H. E. (2005). The Witwatersrand gold deposit and its formation. *Earth-Science Reviews*, 74, 1–51.

Frimmel, H. E., Zeh, A., Lehrmann, B., Hallbauer, D., & Frank, W. (2009). Geochemical and geochronological constraints on the nature of the immediate basement next to the Mesoarchaean auriferous Witwatersrand Basin, South Africa. Journal of Petrology, 50(12), 2187-2220.

Goderis, S., Debaille, V., Van Ginneken, M., et al. (2019). The Belgian Antarctic meteorite collection: A decade of fieldwork and research. *Polar Science*, 19, 1–12.
Govindaraju, K. (1994). 1994 compilation of working values and sample description for 383 geostandards. *Geostandards newsletter*, *18*, 1-158.

Günther, T., Haase, K. M., Junge, M., Oberthür, T., Woelki, D., & Krumm, S. (2018). Oxygen isotope and trace element compositions of platiniferous dunite pipes of the Bushveld Complex, South Africa–Signals from a recycled mantle component?. Lithos, 310, 332-341.

Hopp, T., Dauphas, N., Abe, Y., Aléon, J., O'D. Alexander, C. M., Amari, S., ... & Yurimoto, H. (2022). Ryugu's nucleosynthetic heritage from the outskirts of the Solar System. Science advances, 8(46), eadd8141.

Humbert, F., Hofmann, A., Kock, M. D., Agangi, A., Chou, Y. M., & Mambane, P. W. (2021). A geochemical study of the Crown Formation and Bird Member lavas of the Mesoarchaean Witwatersrand Supergroup, South Africa. South African Journal of Geology 2021, 124(3), 663-684.

Jones, J. H. & Drake, M. J. (1986). Geochemical constraints on core formation in the Earth. *Nature*, 322, 221–228.

Kaskes, P., Déhais, T., de Graaff, S.J., Goderis, S., Claeys, P. (2021). Micro–X-ray fluorescence (µXRF) analysis of proximal impactites: High-resolution element mapping, digital image analysis, and quantifications, Large Meteorite Impacts and Planetary Evolution VI, Wolf Uwe Reimold, Christian Koeberl

Kimura, K., Lewis, R. S. & Anders, E. (1974). Distribution of gold and rhenium between nickel–iron and silicate melts. *Geochimica et Cosmochimica Acta*, 38, 683–701.

Kleine, T., Münker, C., Mezger, K. & Palme, H. (2005). Rapid accretion and early core formation on asteroids and the terrestrial planets from Hf–W chronometry. *Geochimica et Cosmochimica Acta*, 69, 5805–5818.

Kruijer, T. S., Burkhardt, C., Budde, G. & Kleine, T. (2017). Age of Jupiter inferred from the distinct genetics and formation times of meteorites. *Proceedings of the National Academy of Sciences*, 114, 6712–6716.

Lowe, D. R., & Byerly, G. R. (1999). Stratigraphy of the west-central part of the Barberton Greenstone Belt, South Africa.

Maier, W. D., Barnes, S. J. & Groves, D. I. (2013). The Bushveld Complex, South Africa: Formation of platinum-group element deposits. Mineralium Deposita, 48, 1–56.

Marsh, J. S., Bowen, M. P., Rogers, N. W., & Bowen, T. B. (1992). Petrogenesis of late Archaean flood-type basic lavas from the Klipriviersberg Group, Ventersdorp Supergroup, South Africa. Journal of Petrology, 33(4), 817-847.

McDonough, W. F. & Sun, S.-S. (1995). The composition of the Earth. *Chemical Geology*, 120, 223–253.

Meisel, T., & Moser, J. (2004). Platinum-group element and rhenium concentrations in low abundance reference materials. *Geostandards and Geoanalytical Research*, *28*(2), 233-250.

Nakanishi, N., Yokoyama, T., & Ishikawa, A. (2019). Refinement of the Micro-Distillation Technique for Isotopic Analysis of Geological Samples with pg-Level Osmium Contents. *Geostandards and Geoanalytical Research*, *43*(2), 231-243.

Newton, J., Franchi, I. A. & Pillinger, C. T. (2000). Oxygen isotope variations in stony meteorites. *Meteoritics & Planetary Science*, **35**, 689–698.

Nier, A. O. (1950). A redetermination of the relative abundances of the isotopes of carbon, nitrogen, oxygen, argon, and potassium. *Physical Review*, *77*(6), 789.

O'Sullivan, G., Chew, D., Kenny, G., Henrichs, I., & Mulligan, D. (2020). The trace element composition of apatite and its application to detrital provenance studies. Earth-Science Reviews, 201, 103044. DOI: 10.1016/j.earscirev.2019.103044

Ozdemir, S., Schulz, T., van Acken, D., Luguet, A., Reimold, W. U., & Koeberl, C. (2019). Meteoritic highly siderophile element and Re-Os isotope signatures of Archean spherule layers from the CT 3 drill core, Barberton Greenstone Belt, South Africa. *Meteoritics & Planetary Science*, *54*(10), 2203-2216.

Pan Y, Fleet ME (2002). Compositions of the apatite-group minerals: Substitution mechanisms and controlling factors. Rev Miner Geochem 48: 13-49

Palme H., Hezel D.C., Ebel, D.S. (2015). The origin of chondrules: Constraints from matrix composition and matrix-chondrule complementarity. Earth and Planetary Science Letters, 411, 11-19.

Peucker-Ehrenbrink, B. (2013). Accretion of extraterrestrial matter during the Phanerozoic. *Elements*, 9, 53–60.
Pourkhorsandi, H., Debaille, V., Armytage, R.M.G., de Jong, J. (2024). Cerium Stable Isotopic Composition of Non-Carbonaceous Chondrites ACS Earth and Space Chemistry *8* (12), 2452-2462.

Righter, K., Pando, K. M. & Danielson, L. (2015). Partitioning of Mo, W, P, and other siderophile elements among metal, silicate, and sulfide: Implications for core formation. *Geochimica et Cosmochimica Acta*, 166, 241–259.
Roeder, P. L., MacArthur, D., Ma, X. P., Palmer, G. R., & Mariano, A. N. (1987). Cathodoluminescence and microprobe study of rare-earth elements in apatite. American mineralogist, 72(7-8), 801-811.

Roland, J., Debaille, V., Pourkhorsandi, H., Goderis, S. (2024). Moderately volatile elemental and isotopic variations in variably shocked equilibrated ordinary chondrites from Antarctica, Icarus, Volume 412.

Schmitz, B., Peucker-Ehrenbrink, B., Lindström, M. & Tassinari, M. (2001). Accretion rates of meteorites and cosmic dust in the early Ordovician. *Science*, 294, 1693–1696.
Schmitz, B., Häggström, T. & Tassinari, M. (2003). Sediment-dispersed extraterrestrial chromite traces a major asteroid disruption event. *Science*, 300, 961–964.

Schulze, H., Bischoff, A., Palme, H., Spettel, B., Dreibus, G. & Otto, J. (1994). Mineralogy and chemistry of carbonaceous chondrites: Oxygen isotopic constraints. *Geochimica et Cosmochimica Acta*, **58**, 3725–3739.

Schulz, T., Koeberl, C., Luguet, A., van Acken, D., Mohr-Westheide, T., Ozdemir, S., & Reimold, W. U. (2017). New constraints on the Paleoarchean meteorite bombardment of the Earth–Geochemistry and Re-Os isotope signatures of spherule layers in the BARB5 ICDP drill core from the Barberton Greenstone Belt, South Africa. *Geochimica et Cosmochimica Acta*, *211*, 322-340.

Schwander, D., Kööp, L., Berg, T., Schönhense, G., Heck, P. R., Davis, A. M., & Ott, U. (2015). Formation of refractory metal nuggets and their link to the history of CAIs. *Geochimica et Cosmochimica Acta*, *168*, 70-87.

Siebert C., Kramers J. D., Meisel T., Morel P., and Nägler T. F.2005. PGE, Re-Os, and Mo isotope systematics in Archean and early Proterozoic sedimentary systems as proxies for redox conditions of the early Earth. *Geochimica et Cosmochimica Acta*69: 1787–1801.

Staddon, L. G., Parkinson, I. J., Cavosie, A. J., Elliott, T., Valley, J. W., Fournelle, J., ... & Shirey, S. B. (2021). Detrital chromite from Jack Hills, Western Australia: signatures of metamorphism and constraints on provenance. *Journal of Petrology*, *62*(12), egab052.

Suavet, C., Cordier, C., Rochette, P., Folco, L., Gattacceca, J., Sonzogni, C. & Harutyunyan, A. (2010). Classification of modern micrometeorites based on oxygen isotopic compositions. *Earth and Planetary Science Letters*, **293**, 313–320.

Sun Y, Wiedenbeck M, Joachimski MM, Beier C, Kemner F, Weinzierl C (2016) Chemical and oxygen isotope composition of gem-quality apatites: implications for oxygen isotope reference materials for secondary ion mass spectrometry (SIMS). Chem Geol 440: 164-178

Touboul, M., Puchtel, I. S. & Walker, R. J. (2012). W isotope evidence for an early Moon-forming giant impact. *Nature*, 477, 395–398.

Thiemens, M. H., Jackson, T., Zipf, E. C., Erdman, P. W. & Van Egmond, C. (1995). Carbon dioxide and oxygen isotope anomalies in the mesosphere and stratosphere. *Science*, **270**, 969–972.

Trinquier, A., Birck, J. L. & Allègre, C. J. (2009). The nature of the Earth's building blocks as revealed by Mo isotopes. *Earth and Planetary Science Letters*, 266, 97–103.
Trotter JA, Williams IS, Barnes CR., Lécuyer C, Nicoll RS (2008) Did cooling oceans trigger Ordovician biodiversification? Evidence from conodont thermometry. Science 321, 550-554

Van Acker, T., Van Malderen, S. J., Van Helden, T., Stremtan, C., Šala, M., van Elteren, J. T., & Vanhaecke, F. (2021). Analytical figures of merit of a low-dispersion aerosol transport system for high-throughput LA-ICP-MS analysis. *Journal of Analytical Atomic Spectrometry*, *36*(6), 1201-1209.

Walker, R. J. (2009). Highly siderophile elements in the Earth, Moon and Mars: Update and implications for planetary accretion and differentiation. *Chemie der Erde – Geochemistry*, 69, 101–125.
Warren, P. H. (2011). Stable isotopes and the non-carbonaceous–carbonaceous meteorite dichotomy. *Earth and Planetary Science Letters*, 311, 93–100.
Wood, B. J., Walter, M. J. & Wade, J. (2006). Accretion of the Earth and segregation of its core. *Nature*, 441, 825–833.

Waychunas GA (2002) Apatite luminescence. In: Kohn MJ, Rakovan J, Hughes JM (eds) Reviews in Mineralogy and Geochemistry Volume 48 – Phosphates. Mineralogical Society of America, Washington DC, pp 701-742

Wood, B. J., Walter, M. J. & Wade, J. (2006). Accretion of the Earth and segregation of its core. *Nature*, 441, 825–833.

Wotte, T., Skovsted, C.B., Whitehouse, M.J. and Kouchinsky, A. (2019) Isotopic evidence for temperate oceans during the Cambrian Explosion. Nature Sci. Rep., 9(1), 1-9.

Yang, Q., Xia, X. P., Zhang, L., Zhang, W., Zhang, Y., Chen, L. et al. (2020) Oxygen isotope homogeneity assessment for apatite U-Th-Pb geochronology reference materials. Surf. Interf. Anal., 52(5), 197-213.

Yudovskaya, M. A., & Kinnaird, J. A. (2010). Chromite in the Platreef (Bushveld Complex, South Africa): occurrence and evolution of its chemical composition. *Mineralium Deposita*, *45*(4), 369-391.

Zeng LP, Zhao XF, Li XC, Hu H, McFarlane C (2016). In situ elemental and isotopic analysis of fluorapatite from the Taocun magnetite-apatite deposit, Eastern China: Constraints on fluid metasomatism. Am Miner 101: 2468-2483

Zigaitė Z, Whitehouse M (2014) Stable oxygen isotopes of dental biomineral: differentiation at the intra-and inter-tissue level of modern shark teeth. GFF 136: 337-340

ANNEXES

Annex A. Mineralogical identification of the Kaapvaal samples using the SEM-EDS.

Sample	Description	More descriptions	Mineral assemblages - preliminary SEM-EDS identification
SHR 001	Komatiite		actinolite-tremolite, antigorite, chromite, Cr-magnetite
BH1 - 33.35-33.50m	metagabbro < basement	Dominion SG	hornblende, phlogopite, apatite, Fe and Fe-Cu sulphides
CL 1	Crown lavas sample	West Rand?	chlorite, epidote, calcite, quartz
CL 2	Crown lavas sample	West Rand?	chlorite, pyrrhotite, calcite, quartz
VSKM-1270m (à 1 m du précédent)	Klipsriviersberg metabasalt	Ventersdorp SG/Klipriversberg G.	clinochlore, Fe-Cu sulphides, calcite, quartz
VS 1			clinochlore, Fe-Cu sulphides, calcite, quartz
SHR 002	Ongeluk basalt	Flood basalt in Pretoria G./Transvaal SG	augite, epidote
PGM501-1	Bushveld Complex	pyroxenite above anothosite, no chromite	olivine, clinoenstatite, augite, chromite
RR06465	Bushveld Complex	gabbro	clinoenstatite, augite, plagioclase, phlogopite
RR06466	Bushveld Complex	Porphyric pyroxenite from the critical zone	clinoenstatite, augite, chromite
RR00580	Bushveld Complex	pyroxenite with pyrrhotite	clinoenstatite, hornblende, phlogopite, chromite, Fe, Fe-Ni, Fe-Cu sulphides
RR00510	Bushveld Complex	norite	clinoenstatite, plagio, biotite, apatite, chromite,Fe-Ni sulphides
GC 610//Ph2	Phalaborwa Complex	phoscorite	apatite, olivine, magnetite, ilmenite, Cu sulphides
GC 813// Ph6	Phalaborwa Complex	carbonatites cutting phoscorite	apatite, magnetite, calcite
GC 815//Ph8	Phalaborwa Complex	phoscorite	apatite, olivine, Cu sulphides
GC 1994//Ph22	Phalaborwa Complex	banded carbonatite cutting pyroxenite	cpx, mica, apatite, ilmenite, Cr-magnetite, calcite
GC 2707//Ph30	Phalaborwa Complex	apatite-mica-cpx rock with fragments of mica	apatite, mica, augite, magnetite

Annex B. Electron microprobe analyses of apatite.

Analysis spot	BH1_1	BH1_2	BH1_3	RR510_1	RR510_2	RR510_3	RR510_4	PH2_1	PH2_2	PH8_1	PH8_2	PH6_1	PH6_2	PH22_1	PH22_2	PH22_3	PH22_4	PH22_5	PH30_1	PH30_2	PH30_3	PH30_4
F	3,47	3,13	3,36	2,7	1,46	1,78	1,5	2,84	3,36	3,18	3,29	3,54	3,41	3,28	3,68	3,49	3,79	3,23	3,75	3,41	3,4	3,22
Cl	0,15	0,16	0,1	1,25	4,61	4,5	4,79	0,01	0	0,03	0,03	0,05	0,06	0,1	0,04	0,06	0,08	0,09	0,02	0	0,02	0,01
SO3	0,12	0,27	0,19	0,11	0,8	0,17	0,1	0,03	0,03	0,01	0	0	0,02	0,03	0,04	0,03	0,01	0,04	0,01	0,02	0,05	0,02
SiO2	0,21	0,24	0,15	0,48	0,33	0,63	0,45	0,19	0,08	0,13	0,15	0,12	0,07	0,42	0,29	0,24	0,12	0,36	0,4	0,15	0,72	0,52
P2O5	40,17	40,37	41,1	39,59	38,27	38,71	38,96	40,8	41,3	40,3	40,97	41,03	40,68	40,08	40,07	40,66	40,47	39,48	40,63	41,05	39,14	40,48
FeO	0,03	0,01	0,07	0,03	0,2	0,2	0,05	0	0	0,03	0,04	0,02	0,01	0,01	0,07	0,02	0,01	0,05	0,08	0,02	0,04	0,01
MnO	0,12	0,04	0,01	0,02	0,03	0	0,01	0,08	0,02	0	0,04	0	0	0,02	0,01	0,02	0,03	0,05	0,01	0,04	0,03	0,02
MgO	0,05	0,02	0,06	0,02	0,06	0,07	0,08	0,11	0,13	0,09	0,06	0,03	0,01	0,03	0,08	0,06	0,05	0,07	0,04	0,02	0,08	0,04
Na2O																						
La2O3		0,15	0,03	0,3	0,23	0,32	0,26	0,06	0,05	0,08	0,07	0,14	0,13	0,26	0,23	0,16	0,16	0,21	0,2	0,1	0,33	0,22
Ce2O3	0,14	0,18	0,07	0,02	0,46	0,66	0,52	0,12	0,19	0,13	0,18	0,27	0,25	0,58	0,51	0,45	0,31	0,45	0,56	0,19	0,69	0,45
Nd2O3		0,33		0,21	0,1	0,16	0,1	0,05	0,34			0,26		0,22	0,55	0,2	0,19	0,06	0,04	0,29	0,57	0,27
BaO	0,05	0,04	0,06	0,05	0,01		0,08	0,06	0,08			0,18	0,04	0,07		0,05		0,03		0		0,11
SrO	0,01		0,11	0	0,17	0,07	0,03	0,41	0,5	0,47	0,39	0,63	0,62	0,6	0,52	0,5	0,61	0,46	0,7	0,81	0,72	0,53
CaO	55,73	55,86	55,86	55,16	54,23	53,46	54,07	55,45	55,44	55,3	55,99	55	55,16	54,91	54,73	55,71	55,5	55,69	55,32	55,45	54,48	54,69
Total	100,25	100,78	101,15	100,44	100,9	100,71	100,9	100,28	101,15	100,17	101,21	101,23	100,44	100,61	100,92	101,61	101,31	99,59	101,74	101,51	100,27	100,57
Cations pour 12,5 oxygenes																						
F	0,90	0,81	0,86	0,71	0,39	0,48	0,40	0,73	0,86	0,83	0,85	0,92	0,89	0,86	1,02	0,90	0,99	0,85	0,97	0,88	0,90	0,84
Cl	0,02	0,02	0,01	0,18	0,69	0,67	0,72	0,00	0,00	0,00	0,00	0,01	0,01	0,01	0,01	0,01	0,01	0,01	0,00	0,00	0,00	0,00
SO3	0,01	0,02	0,01	0,01	0,05	0,01	0,01	0,00	0,00	0,00	0,00	0,00	0,00	0,00	0,00	0,00	0,00	0,00	0,00	0,00	0,00	0,00
SiO2	0,02	0,02	0,01	0,04	0,03	0,05	0,04	0,02	0,01	0,01	0,01	0,01	0,01	0,04	0,03	0,02	0,01	0,03	0,03	0,01	0,06	0,04
P2O5	2,92	2,91	2,94	2,90	2,85	2,90	2,91	2,94	2,90	2,93	2,94	2,96	2,95	2,92	2,93	2,93	2,93	2,90	2,93	2,95	2,88	2,94
FeO	0,00	0,00	0,00	0,00	0,01	0,01	0,00	0,00	0,00	0,00	0,00	0,00	0,00	0,00	0,01	0,00	0,00	0,00	0,01	0,00	0,00	0,00
MnO	0,01	0,00	0,00	0,00	0,00	0,00	0,00	0,01	0,00	0,00	0,00	0,00	0,00	0,00	0,00	0,00	0,00	0,00	0,00	0,00	0,00	0,00
MgO	0,01	0,00	0,01	0,00	0,01	0,01	0,01	0,01	0,02	0,01	0,01	0,00	0,00	0,00	0,01	0,01	0,01	0,01	0,01	0,00	0,01	0,01
Na2O	0,00	0,00	0,00	0,00	0,00	0,00	0,00	0,00	0,00	0,00	0,00	0,00	0,00	0,00	0,00	0,00	0,00	0,00	0,00	0,00	0,00	0,00
La2O3	0,00	0,00	0,00	0,01	0,01	0,01	0,01	0,00	0,00	0,00	0,00	0,00	0,00	0,01	0,01	0,01	0,01	0,01	0,01	0,00	0,01	0,01
Ce2O3	0,00	0,00	0,00	0,00	0,01	0,02	0,02	0,00	0,01	0,00	0,01	0,01	0,01	0,02	0,02	0,01	0,01	0,01	0,02	0,01	0,02	0,01
Nd2O3	0,00	0,01	0,00	0,01	0,00	0,01	0,00	0,00	0,00	0,01	0,00	0,01	0,00	0,01	0,02	0,01	0,01	0,00	0,00	0,01	0,02	0,01
BaO	0,00	0,00	0,00	0,00	0,00	0,00	0,00	0,00	0,00	0,00	0,00	0,01	0,00	0,00	0,00	0,00	0,00	0,00	0,00	0,00	0,00	0,00
SrO	0,00	0,00	0,01	0,00	0,01	0,00	0,00	0,02	0,02	0,02	0,02	0,03	0,03	0,03	0,03	0,02	0,03	0,02	0,03	0,04	0,04	0,03
CaO	5,12	5,10	5,06	5,12	5,11	5,07	5,10	5,06	5,03	5,09	5,09	5,02	5,07	5,06	5,07	5,08	5,09	5,13	5,05	5,04	5,08	5,02
Site F	0,93	0,83	0,88	0,89	1,08	1,15	1,12	0,74	0,86	0,83	0,85	0,92	0,90	0,87	1,02	0,91	1,00	0,86	0,97	0,88	0,90	0,84
Site P	2,94	2,95	2,97	2,95	2,93	2,96	2,95	2,96	2,97	2,95	2,95	2,97	2,96	2,96	2,95	2,95	2,95	2,94	2,96	2,96	2,95	2,96
Site Ca	5,14	5,11	5,08	5,12	5,14	5,09	5,12	5,10	5,07	5,13	5,12	5,06	5,10	5,10	5,11	5,11	5,13	5,16	5,10	5,09	5,13	5,05

Annex C. Electron microprobe analyses of olivine.

	PGM501b_1	PGM501b_2	PH6_4	PH6_5	PH2_4	PH2_5	PH2_6	PH8_4	PH8_5
SiO2	40,14	39,95	38,63	37,66	41,28	41,92	41,63	37,81	42,39
TiO2	0	0	0,27	0,01	0,02	0	0	1,71	0
Al2O3	0	0,01	0,01	0,03	0	0,03	0	0,01	0
Cr2O3	0,02	0	0	0	0,01	0	0	0,01	0
FeO	17,32	17,18	4,07	4,93	11,03	11,45	11,35	6,92	9,8
MnO	0,19	0,18	0,23	0,21	0,22	0,28	0,29	0,21	0,28
MgO	43,79	42,54	55,92	55,36	49,06	49,15	48,97	51,19	48,82
CaO	0	0	0	0,02	0,02	0,02	0,04	0,02	0
Na2O	0,02	0,01	0,02	0,01	0	0	0	0	0
F	0,05	0	0	0	0	0,07	0,02		0,2
P2O5	0	0	0	0	0	0,02	0	0	0
Cl	0	0	0	0	0	0	0	0,01	0,01
K2O	0	0,01	0,01	0	0	0	0,01	0	0
V2O3	0,03	0	0	0,02	0,01	0	0,01	0	0,02
CoO	0,09	0,11	0	0,02	0,09	0,08	0	0,04	0
NiO	0,5	0,45	0,07	0,04	0,03	0,03	0,07	0	0,04
CuO	0,04	0,01	0,04	0,02	0,04	0	0,03	0,08	0
ZnO	0,01	0,01	0	0	0,01	0,04	0,08	0,07	0
Total									
cations	atoms								
Si	1,00	1,02	0,92	0,91	1,00	1,01	1,00	0,93	1,03
Ti	0,00	0,00	0,00	0,00	0,00	0,00	0,00	0,03	0,00
Al	0,00	0,00	0,00	0,00	0,00	0,00	0,00	0,00	0,00
Cr	0,00	0,00	0,00	0,00	0,00	0,00	0,00	0,00	0,00
Fe3	0,00	0,00	0,15	0,18	0,00	0,00	0,00	0,07	0,00
Fe2	0,36	0,37	-0,07	-0,09	0,22	0,23	0,23	0,08	0,20
Mn	0,00	0,00	0,00	0,00	0,00	0,01	0,01	0,00	0,01
Mg	1,63	1,61	1,99	1,99	1,77	1,76	1,76	1,89	1,77
Ca	0,00	0,00	0,00	0,00	0,00	0,00	0,00	0,00	0,00
tot. cat.	3,00	3,00	3,00	3,00	3,00	3,00	3,00	3,00	3,00
tot. oxy.	4,00	4,02	4,00	4,00	4,00	4,01	4,00	4,00	4,03
	0,36	0,37	0,08	0,10	0,22	0,23	0,23	0,14	0,20
end member	mole %'								
Te	0,201	0,196	0,224	0,205	0,226	0,285	0,297	0,216	0,292
Fo	81,676	81,370	95,862	95,023	88,577	88,167	88,186	92,726	89,616
Fa	18,122	18,435	3,914	4,747	11,172	11,522	11,466	7,032	10,092

Annex D. Electron microprobe analyses of pyroxene.

	SHR002_2	SHR002_4	SHR002_J SHR002_(SHR002_7	PGM501_8 RR510_3	RR510_4	RR6466_J RR6466_(RR6465_1	RR6465_J RR6465_(RR6465_5	RR6465_(PH30_1	PH30_2	PH22_4	PH22_5
SiO2	52,63	48,06	53,31 52,06	43,56 53,86	54,25	54,3 53,95	54,13 53,5	54,72 53,45	54,72 53,62	54,75	55,2 54,99	54,49
TiO2	0,02	0,96	0,26 0,03	0,04 0,28	0,15	0,11 0,31	0,37 0,31	0,21 0,51	0,19 0,24	0,15	0,17 0	0,12
Al2O3	1,79	1,97	1,46 1,87	7,14 1,71	0,84	1,08 1,53	1,51 1,51	0,8 1,73	0,83 1,47	0,17	0,11 0,07	0,16
Cr2O3+TiO2	0,29	0,98	0,3 0,39	0,33 0,94	0,23	0,3 0,95	0,99 0,54	0,3 0,77	0,3 0,48	0,16	0,2 0,15	0,52
Cr2O3	0,27	0,02	0,04 0,36	0,29 0,66	0,08	0,19 0,64	0,62 0,23	0,09 0,26	0,11 0,24	0,01	0,03 0,15	0,4
FeO	14,55	26,51	14,01 14,11	16,27 4,72	6,4	18,66 4,36	4,07 6,72	18,68 6,91	17,76 6,68	3,39	3,3 5,77	6,17
MnO	0,27	0,49	0,28 0,3	0,32 0,13	0,14	0,42 0,04	0,12 0,19	0,48 0,16	0,33 0,21	0,06	0,13 0,17	0,25
MgO	13,67	9,64	17,55 12,67	14,19 16,13	15,82	25,46 16,37	16,29 15,15	25,19 14,75	24,64 15,15	16,39	16,24 14,98	14,8
CaO	14,13	11,84	13,96 15,93	12,34 23,09	22,64	0,55 23,17	23,38 22,96	0,81 23	2,19 22,86	24,85	25,09 24,24	24,22
Na2O	0,28	0,12	0,1 0,35	0,4 0,28	0,32	0 0,25	0,21 0,26	0,01 0,31	0,04 0,28	0,23	0,27 0,59	0,58
K2O	0,06	0,04	0 0,03	0 0,01	0,01	0 0,01	0 0,01	0 0	0,01 0,01	0	0,02 0	0,02
F	0,11	0,18	0,08 0,14	0,32 0,33	0,57	0,27 0	0,06 0,24	0,4 0,42	0 0,06	0,28	0,19 0,06	0
P2O5	0,16	0,1	0,18 0,29	0,06 0,31	0,25	0,02 0,32	0,32 0,29	0,04 0,33	0,04 0,28	0,28	0,27 0,24	0,32
Cl	0	0	0,01 0,01	0,01 0	0	0 0	0 0,01	0 0	0 0,01	0,01	0,01 0	0,01
V2O3	0,02	0,11	0,06 0,02	0,02 0,28	0,32	0,03 0,02	0,04 0,03	0,02 0,04	0,03 0,05	0,02	0,02 0,02	0,03
CoO	0,05	0,01	0,12 0,04	0,06 0	0,08	0 0,01	0,02 0,01	0,04 0	0,05 0,03	0,01	0,07 0,03	0,02
NiO	0,01	0,02	0,03 0,04	0 0,16	0,03	0,03 0,14	0,05 0,06	0,07 0,04	0,06 0,01	0,07	0,04 0,03	0,02
CuO	0,03	0,02	0,03 0,05	0,01 0,01	0,01	0,07 0,05	0,02 0,04	0,02 0,04	0,02 0,02	0,06	0 0,02	0,04
ZnO	0,1	0,02	0,04 0,05	0 0,01	0,08	0,01 0,02	0,01 0	0,02 0,03	0 0,08	0,07	0,02 0	0
Total	98,35	100,06	101,44 98,24	95,03 101,35	101,04	101,2 99,95	101,18 101,24	101,14 101,95	100,98 101,29	100,39	100,95 101,37	101,65
atoms												
cations												
Si	2,04	1,90	1,96 2,02	1,72 1,96	1,98	1,97 1,96	1,97 1,96	1,98 1,96	1,89 1,97	2,00	2,01 2,01	1,99
Ti	0,00	0,03	0,01 0,00	0,00 0,01	0,00	0,00 0,01	0,01 0,01	0,01 0,01	0,01 0,01	0,00	0,00 0,00	0,00
Al	0,08	0,09	0,06 0,09	0,33 0,07	0,04	0,05 0,07	0,06 0,07	0,03 0,07	0,04 0,06	0,01	0,00 0,00	0,01
Fe+3	0,00	0,06	0,00 0,00	0,24 0,00	0,01	0,01 0,00	0,00 0,01	0,00 0,00	0,00 0,01	0,00	0,00 0,02	0,04
Cr+3	0,01	0,00	0,00 0,01	0,01 0,02	0,00	0,01 0,02	0,02 0,01	0,00 0,01	0,00 0,01	0,00	0,00 0,00	0,01
Fe+2	0,47	0,82	0,43 0,46	0,29 0,14	0,19	0,56 0,13	0,12 0,20	0,57 0,21	0,54 0,20	0,10	0,10 0,15	0,15
Mn	0,01	0,02	0,01 0,01	0,01 0,00	0,00	0,01 0,00	0,00 0,01	0,01 0,00	0,01 0,01	0,00	0,00 0,01	0,01
Mg	0,79	0,57	0,98 0,73	0,84 0,87	0,86	1,37 0,89	0,88 0,83	1,36 0,81	1,33 0,83	0,89	0,88 0,82	0,81
Ca	0,58	0,50	0,55 0,66	0,52 0,90	0,89	0,02 0,90	0,91 0,90	0,03 0,90	0,09 0,90	0,97	0,96 0,95	0,95
Na	0,02	0,01	0,01 0,03	0,03 0,02	0,02	0,00 0,02	0,01 0,02	0,00 0,00	0,00 0,02	0,02	0,02 0,04	0,04
K	0,00	0,00	0,00 0,00	0,00 0,00	0,00	0,00 0,00	0,00 0,00	0,00 0,00	0,00 0,00	0,00	0,00 0,00	0,00
H												
Ortho and Calcic CPX												
Wo	31,75	26,54	28,31 35,74	31,64 46,92	45,79	1,09 46,95	47,50 46,82	1,61 47,02	4,35	46,64	49,40 49,92	49,42 49,64
En	42,73	30,07	49,52 39,55	50,62 45,60	44,52	70,25 46,15	46,05 42,99	69,49 41,95	68,11	43,01	45,34 44,96	42,50 42,37
Fs	25,52	43,40	22,18 24,71	17,74 7,49	9,69	28,66 6,90	6,45 10,19	28,91 11,03	27,54	10,35	5,26 5,12	8,08 7,79

Annex E. Electron microprobe analyses of oxides.

	SHR001_1 chromite	SHR001_3 chromite	SHR001_3 chromite	SHR001_4 chromite	SHR001_5 chromite	PGM501_1 chromite	PGM501_3 chromite	RR6466_1 chromite	RR6466_2 chromite	RR6466_3 chromite	RR6466_6 chromite	RR6466_7 chromite	PGM501_4 magnetite	PH01_1 magnetite	PH01_2 magnetite	PH0_3 magnetite	PH8_1 magnetite	PH8_2 magnetite	PH8_3 magnetite	PH2_1 magnetite	PH2_2 magnetite	PH2_3 magnetite
SiO2	0.02	1.63	0.09	0.08	0	0	0	0	0	0.06	0	0.06	0.84	0.02	0.03	0.06	0	0	0.02	0	0.05	0.02
TiO2	1.33	0.32	0.73	0.21	0.28	0.91	1.5	1.49	1.49	1.49	2.19	2.07	0.03	0	0.67	0.92	1.22	4.42	3.59	3.47	2.83	7.09	0.94
Al2O3	9.49	7.66	8.77	6.07	5.71	8.37	8.21	16.91	16.51	17.1	10.6	10.7	0.05	0.04	0.02	0.17	0.25	1	0.07	0.1	0.05	0.06	0.03
Cr2O3	18.49	43.68	17.65	50.37	14.68	20.3	19.73	41.95	42.53	42.02	30.13	29.84	0.01	0	0	0.01	0.02	0	0.03	0	0.02	0.01	0.02
V2O3	0.25	0.16	0.23	0.02	0.23	0.29	0.25	0.38	0.31	0.34	0.47	0.45	0.02	0.01	0	0.1	0.12	0.11	0.13	0.1	0.08	0.19	0.13
FeO	61.79	37.42	63.61	38.79	69.98	61.76	62.82	30.64	30.19	30.49	48.79	50.29	76.67	92.62	92.85	91.84	90.82	88.77	87.25	86.82	87.62	87.45	85.88	92.22
MnO	1.92	1.04	1.74	1.35	1.48	0.34	0.26	0.45	0.45	0.43	0.56	0.49	0.02	0.1	0.09	0.1	0.14	0.25	0.4	0.17	0.21	0.08	1.11	0.06
MgO	0.41	3.17	0.35	1.46	0.17	3.4	3.34	6.09	5.77	6.09	3.04	3.02	0.23	0.14	0.09	2.15	2.42	2.96	2.03	1.32	1.72	3.71	4.46	0.62
CaO	0.05	0.05	0.02	0.07	0.02	0.01	0	0.02	0.01	0	0	0.01	0.5	0.17	0.08	0	0	0	0	0	0	0	0	0
ZnO	0.58	0.56	0.8	0.43	0.61	0.08	0.16	0.24	0.13	0.25	0.03	0.19	0.06	0.13	0.1	0.02	0.22	0.05	0	0.07	0.12	0.05	0.57	0.02
F	0.25	0.61	0.22	0.64	0.21	0.19	0	0.47	0.48	0.83	0.15	0.02	0.04	0.08	0	0.03	0.16	0.19	0	0.09	0	0.07	0.02	0.01
Na2O	0.03	0.02	0.08	0.01	0.03	0.01	0.02	0.01	0.02	0.02	0.02	0.02	0	0.02	0.03	0.01	0	0.03	0	0.05	0.01	0.02	0.01	0.06
P2O5	0	0	0	0	0	0	0.04	0	0.09	0.05	0.04	0.06	0.03	0.14	0	0	0	0	0	0.13	0.02	0.14	0.02	0.06
Cl	0	0	0	0	0	0	0	0	0	0	0	0	0.04	0	0	0	0	0.01	0	0.01	0	0	0	0.01
K2O	0.01	0.01	0.01	0	0.02	0.01	0	0	0.01	0	0	0	0	0.01	0	0.01	0.01	0.01	0	0.02	0.01	0.02	0.01	0
CaO	0.28	0.14	0.26	0.17	0.14	0.19	0.14	0.16	0.06	0.07	0.06	0.16	0.77	0.23	0.2	0.24	0.16	0.21	0.09	0.18	0.2	0.19	0.16	0.24
NiO	0.34	0.06	0.31	0.07	0.33	0.35	0.39	0.17	0.06	0.15	0.25	0.23	0.14	0.03	0.09	0.11	0.06	0	0.05	0.01	0.01	0.07	0.04	0.07
CuO	0	0.05	0.05	0.05	0.05	0.03	0.02	0.01	0.04	0.05	0.01	0.01	0.64	0.04	0.11	0.05	0.17	0.02	0.05	0.11	0.01	0.15	0.02	0.03
Total	94.99	98.54	94.87	98.74	93.96	98.02	95.87	98.99	98.3	99.38	96.26	97.38	85.01	93.41	93.75	95.34	94.81	94.86	94.45	94.22	93.55	94.63	94.8	94.97
# oxygene cations	32	32	32	32	32	32	32	32	32	32	32	32	32	32	32	32	32	32	32	32	32	32	32	32
Si	0.01	0.46	0.03	0.02	0.02	0.00	0.00	0.00	0.00	0.02	0.00	0.02	1.97	0.00	0.01	0.01	0.01	0.02	0.00	0.00	0.01	0.00	0.01	0.01
Ti	0.29	0.07	0.16	0.05	0.06	0.17	0.26	0.30	0.30	0.30	0.47	0.44	0.01	0.00	0.15	0.15	0.21	0.27	1.00	0.82	0.79	0.83	1.58	0.21
Al	3.30	2.58	3.07	2.12	2.04	2.83	2.77	5.33	5.25	5.38	3.56	3.55	0.02	0.01	0.06	0.06	0.09	0.34	0.01	0.03	0.04	0.02	0.02	0.01
Cr	4.31	10.25	4.14	11.82	3.52	4.60	4.47	8.86	9.13	8.87	6.80	6.61	0.00	0.00	0.00	0.00	0.00	0.00	0.00	0.01	0.00	0.00	0.00	0.00
V	0.06	0.04	0.05	0.00	0.06	0.07	0.06	0.08	0.07	0.07	0.11	0.10	0.01	0.00	0.02	0.02	0.03	0.03	0.03	0.03	0.02	0.05	0.03	0.03
Fe(III)	7.73	2.08	8.36	1.91	10.26	8.16	8.31	1.13	0.95	1.05	4.59	4.83	12.01	15.98	15.60	15.60	15.45	15.05	13.96	14.30	14.34	14.67	12.76	15.61
Fe(II)	7.50	6.81	7.42	6.97	7.48	6.84	6.67	5.72	5.86	5.76	7.04	7.03	8.67	7.86	7.18	7.18	7.06	6.91	7.99	6.16	7.04	6.96	7.22	7.83
Mn	0.48	0.25	0.44	0.34	0.38	0.08	0.06	0.10	0.10	0.10	0.14	0.12	0.00	0.03	0.03	0.03	0.04	0.06	0.10	0.04	0.05	0.02	0.28	0.02
Mg	0.18	1.34	0.15	0.65	0.08	1.45	1.43	2.43	2.32	2.41	1.29	1.27	0.12	0.08	0.05	0.05	0.07	1.31	0.91	0.80	0.78	1.64	1.97	0.37
Ca	0.02	0.01	0.01	0.02	0.01	0.00	0.00	0.01	0.00	0.00	0.00	0.00	0.18	0.06	0.00	0.00	0.00	0.00	0.00	0.00	0.00	0.00	0.00	0.00
Zn	0.13	0.12	0.18	0.09	0.14	0.00	0.03	0.05	0.03	0.05	0.00	0.04	0.01	0.00	0.00	0.00	0.05	0.01	0.00	0.02	0.03	0.01	0.12	0.00
TOTAL	24	24	24	24	24	24	24	24	24	24	24	24	24	24	24	24	24	24	24	24	24	24	24	24
Mg#	0.02	0.16	0.02	0.08	0.01	0.18	0.18	0.30	0.28	0.30	0.16	0.15	0.01	0.01	0.12	0.12	0.13	0.16	0.10	0.07	0.09	0.19	0.21	0.05
Fe/Fe+Mg	0.99	0.968783	0.99603864	0.9322011	0.99546876	0.9106218	0.9130364	0.7383536	0.7458516	0.7383696	0.800001	0.8033894	0.9948801	0.997731	0.959935	0.959935	0.958435	0.954504	0.64389	0.960171	0.9741	0.966619	0.929568	0.913049	0.984439
Cr/Cr+Al	0.57	0.799649	0.5744628	0.8477168	0.6329824	0.6193065	0.6171699	0.6246515	0.6256572	0.6224201	0.625681	0.6501362	0.1182564	0	0.037963	0.037963	0.050933	0	0.26117	0.2223	0	0.21156	0.10056	0.30602

Annex F. Electron microprobe analyses of sulphides.

elem wt%	BH1_1	BH1_2	BH1_3	BH1_4	BH1_5	BH1_6	CL2_1	CL2_2	VSKM_1	VSKM1_2	VSKM2_1	VSKM2_2	RR580_1	RR580_2	RR580_3	RR580_4
Zn	<d.l.	<d.l.	<d.l.	<d.l.	<d.l.	<d.l.	<d.l.	<d.l.	<d.l.	<d.l.	<d.l.	<d.l.	<d.l.	<d.l.	<d.l.	<d.l.
Ag																
Co	1,27	0,63	0,03	0,02	0,11	0,46	0,10	0,10	0,02	0,02	0,02	0,02	0,02	0,02	0,02	0,65
Bi																
Ni	0,19	0,16	0,16	0,12	0,17	0,18	0,13	0,15	0,15	0,13	0,16	0,14	0,13	0,14	0,14	32,89
Fe	45,98	47,05	30,55	30,66	47,22	47,15	59,33	59,53	30,25	30,44	30,18	30,52	30,43	30,72	30,71	34,09
Mn																
Cu	0,20	0,21	34,86	35,11	0,21	0,17	0,20	0,18	35,29	35,21	34,92	35,24	35,66	35,50	35,30	0,21
Cd																
Sn																
Sb	<d.l.	<d.l.	<d.l.	<d.l.	<d.l.	<d.l.	<d.l.	<d.l.	<d.l.	<d.l.	<d.l.	<d.l.	<d.l.	<d.l.	<d.l.	<d.l.
Pb	0,13	0,13	0,07	0,08	0,14	0,15	0,13	0,14	0,07	0,08	0,09	0,09	0,09	0,08	0,10	0,09
As	0,08	0,10	0,09	0,10	0,09	0,08	0,18	0,15	0,11	0,09	0,07	0,10	0,08	0,10	0,07	0,09
S	54,12	54,47	34,63	35,42	54,19	54,16	40,17	40,69	35,65	35,54	35,81	35,88	35,70	35,56	35,54	34,04
Total	101,91	102,67	100,37	101,49	102,10	102,31	100,20	100,87	101,52	101,49	101,22	101,95	102,09	102,12	101,86	101,97
Zn	0,000	0,000	0,000	0,000	0,000	0,000	0,000	0,000	0,000	0,000	0,000	0,000	0,000	0,000	0,000	0,000
Ag	0,000	0,000	0,000	0,000	0,000	0,000	0,000	0,000	0,000	0,000	0,000	0,000	0,000	0,000	0,000	0,000
Co	0,008	0,004	0,000	0,000	0,001	0,003	0,001	0,001	0,000	0,000	0,000	0,000	0,000	0,000	0,000	0,005
Bi	0,000	0,000	0,000	0,000	0,000	0,000	0,000	0,000	0,000	0,000	0,000	0,000	0,000	0,000	0,000	0,000
Ni	0,001	0,001	0,001	0,001	0,001	0,001	0,001	0,001	0,001	0,001	0,001	0,001	0,001	0,001	0,001	0,249
Fe	0,324	0,329	0,251	0,248	0,332	0,331	0,457	0,455	0,245	0,246	0,244	0,246	0,245	0,247	0,248	0,272
Mn	0,000	0,000	0,000	0,000	0,000	0,000	0,000	0,000	0,000	0,000	0,000	0,000	0,000	0,000	0,000	0,000
Cu	0,001	0,001	0,252	0,250	0,001	0,001	0,001	0,001	0,251	0,251	0,249	0,249	0,252	0,251	0,250	0,001
Cd	0,000	0,000	0,000	0,000	0,000	0,000	0,000	0,000	0,000	0,000	0,000	0,000	0,000	0,000	0,000	0,000
Sn	0,000	0,000	0,000	0,000	0,000	0,000	0,000	0,000	0,000	0,000	0,000	0,000	0,000	0,000	0,000	0,000
Sb	0,000	0,000	0,000	0,000	0,000	0,000	0,000	0,000	0,000	0,000	0,000	0,000	0,000	0,000	0,000	0,000
Pb	0,000	0,000	0,000	0,000	0,000	0,000	0,000	0,000	0,000	0,000	0,000	0,000	0,000	0,000	0,000	0,000
As	0,000	0,001	0,001	0,001	0,001	0,000	0,001	0,001	0,001	0,000	0,000	0,001	0,000	0,001	0,000	0,001
S	0,665	0,664	0,495	0,500	0,664	0,663	0,539	0,541	0,502	0,501	0,505	0,503	0,501	0,499	0,500	0,472
Min. phase	*FeS2*	*FeS2*	*FeCuS*	*FeCuS*	*FeS2*	*FeS2*	*pyrr*	*pyrr*	*FeCuS*	*FeCuS*	*FeCuS*	*FeCuS*	*FeCuS*	*FeCuS*	*FeCuS*	*NiFeS*

elem wt%	RR580_5	RR580_6	RR580_7	RR580_8	RR580_9	PGM501_1	PGM501_2	PH4_1	PH4_2	PH8_1	PH8_2	PH8_3	PH8_4	PH8_5	PH8_6	PH20_1	PH20_2
Zn	<d.l.	<d.l.	<d.l.	<d.l.	<d.l.	<d.l.	<d.l.	<d.l.	<d.l.	<d.l.	<d.l.	<d.l.	<d.l.	<d.l.	<d.l.	<d.l.	<d.l.
Ag																	
Co	0,67	0,67	0,05	0,05	0,06	0,91	0,02	0,02	0,02	-0,01	-0,01	-0,01	0	-0,01	0,01	0,02	0,02
Bi																	
Ni	32,82	32,66	0,41	0,38	0,37	44,45	0,26	0,16	0,13	0,15	0,16	0,15	0,16	0,18	0,24	0,14	0,19
Fe	34,24	34,33	60,6	60,82	60,38	5,57	26,47	30,63	30,7	0,13	0,46	9,97	10,38	27,39	25,91	30,57	30,31
Mn																	
Cu	0,22	0,25	0,21	0,21	0,22	3,66	30,7	35,46	35,41	80,56	80,61	66,28	64,34	38,61	38,69	35,72	35,68
Cd																	
Sn																	
Sb	<d.l.	<d.l.	<d.l.	<d.l.	<d.l.	<d.l.	<d.l.	<d.l.	<d.l.	<d.l.	<d.l.	<d.l.	<d.l.	<d.l.	<d.l.	<d.l.	<d.l.
Pb	0,09	0,06	0,12	0,14	0,09	0,15	0,07	0,06	0,09	<d.l.	<d.l.	<d.l.	0,06	0,09	0,12	0,09	0,08
As	0,09	0,12	0,17	0,19	0,16	<d.l.	0,08	0,08	0,11	<d.l.	<d.l.	<d.l.	0,02	0,05	0,08	0,08	0,09
S	34,04	33,82	38,95	39,29	39,1	38,02	31,7	35,83	35,79	20,99	21,56	25,83	25,64	33,64	33,33	35,35	35,67
Total	102,08	101,82	100,48	101,05	100,31	92,52	89,29	102,20	102,21	101,78	102,73	102,21	100,60	99,95	98,38	101,52	101,99
Zn	0,000	0,000	0,000	0,000	0,000	0,000	0,000	0,000	0,000	0,000	0,000	0,000	0,000	0,000	0,000	0,000	0,000
Ag	0,000	0,000	0,000	0,000	0,000	0,000	0,000	0,000	0,000	0,000	0,000	0,000	0,000	0,000	0,000	0,000	0,000
Co	0,005	0,005	0,000	0,000	0,000	0,007	0,000	0,000	0,000	0,000	0,000	0,000	0,000	0,000	0,000	0,000	0,000
Bi	0,000	0,000	0,000	0,000	0,000	0,000	0,000	0,000	0,000	0,000	0,000	0,000	0,000	0,000	0,000	0,000	0,000
Ni	0,249	0,248	0,003	0,003	0,358	0,002	0,001	0,001	0,001	0,001	0,001	0,001	0,001	0,001	0,002	0,001	0,001
Fe	0,273	0,274	0,469	0,468	0,467	0,047	0,243	0,246	0,247	0,001	0,004	0,088	0,093	0,228	0,219	0,247	0,244
Mn	0,000	0,000	0,000	0,000	0,000	0,000	0,000	0,000	0,000	0,000	0,000	0,000	0,000	0,000	0,000	0,000	0,000
Cu	0,002	0,002	0,001	0,001	0,001	0,027	0,247	0,250	0,250	0,658	0,650	0,514	0,506	0,282	0,287	0,254	0,253
Cd	0,000	0,000	0,000	0,000	0,000	0,000	0,000	0,000	0,000	0,000	0,000	0,000	0,000	0,000	0,000	0,000	0,000
Sn	0,000	0,000	0,000	0,000	0,000	0,000	0,000	0,000	0,000	0,000	0,000	0,000	0,000	0,000	0,000	0,000	0,000
Sb	0,000	0,000	0,000	0,000	0,000	0,000	0,000	0,000	0,000	0,000	0,000	0,000	0,000	0,000	0,000	0,000	0,000
Pb	0,000	0,000	0,000	0,000	0,000	0,000	0,000	0,000	0,000	0,000	0,000	0,000	0,000	0,000	0,000	0,000	0,000
As	0,001	0,001	0,001	0,001	0,001	0,000	0,001	0,000	0,001	0,000	0,000	0,000	0,000	0,000	0,001	0,000	0,001
S	0,472	0,470	0,525	0,526	0,527	0,561	0,507	0,502	0,501	0,340	0,345	0,397	0,400	0,488	0,491	0,498	0,501
Min. phase	*NiFeS*	*NiFeS*	*pyrr*	*pyrr*	*pyrr*	*violarite*	*FeCuS*	*FeCuS*	*FeCuS*	*CuZS*	*CuZS*	*CuZS*	*CuZS*	*CuZS*	*FeCuS*	*FeCuS*	*FeCuS*

Annex G. SIMS analyses – O isotopes of apatite.

	$\delta^{18}O_{cor}$	+/-
BH1@1	6,56	0,21
BH1@2	6,03	0,19
BH1@3	6,10	0,38
BH1@4	6,13	0,32
BH1@5	5,96	0,24
RR510@1	3,21	0,32
RR510@2	3,32	0,23
RR510@3	*2,01*	0,27
RR510@4	3,06	0,24
RR510@5	2,73	0,24
Ph2@1	7,78	0,19
Ph2@2	7,25	0,23
Ph2@3	7,71	0,23
Ph2@4	7,65	0,27
Ph2@5	7,38	0,21
Ph2@6	7,42	0,23
Ph6@1	6,62	0,37
Ph6@2	6,01	0,23
Ph6@3	6,00	0,28
Ph6@4	6,47	0,33
Ph6@5	6,28	0,41
Ph6@6	6,40	0,27

Annex H. First page of the papers published in the frame of the DESIRED project.

The Meteoritical Society

Meteoritics & Planetary Science 59, Nr 11, 2956–2980 (2024)
doi: 10.1111/maps.14258

Fe, Zn, and Mg stable isotope systematics of acapulcoite lodranite clan meteorites

Stepan M. CHERNONOZHKIN[1,2*], Lidia PITTARELLO[3], Genevieve HUBLET[4], Philippe CLAEYS[5], Vinciane DEBAILLE[4], Frank VANHAECKE[1], and Steven GODERIS[5]

[1]Atomic & Mass Spectrometry—A&MS Research Unit, Department of Chemistry, Ghent University, Ghent, Belgium
[2]Isotope Ratio Analysis Research Group, Chair of General and Analytical Chemistry, Montanuniversität Leoben, Leoben, Austria
[3]Naturhistorisches Museum Wien – NHMW, Vienna, Austria
[4]Laboratoire G-Time, Université Libre de Bruxelles, Brussels, Belgium
[5]Archaeology, Environmental Changes, and Geo-Chemistry (AMGC), Vrije Universiteit Brussel, Brussels, Belgium

***Correspondence**
Stepan M. Chernonozhkin, Atomic & Mass Spectrometry—A&MS Research Unit, Department of Chemistry, Ghent University, Campus Sterre, Krijgslaan, 281-S12, Ghent 9000, Belgium.
Email: stepan.chernonozhkin@gmail.com

(Received 15 November 2023; revision accepted 05 August 2024)

Abstract–The processes of planetary accretion and differentiation, whereby an unsorted mass of primitive solar system material evolves into a body composed of a silicate mantle and metallic core, remain poorly understood. Mass-dependent variations of the isotope ratios of non-traditional stable isotope systems in meteorites are known to record events in the nebula and planetary evolution processes. Partial melting and melt separation, evaporation and condensation, diffusion, and thermal equilibration between minerals at the parent body (PB) scale can be recorded in the isotopic signatures of meteorites. In this context, the acapulcoite–lodranite meteorite clan (ALC), which represents the products of thermal metamorphism and low-degree partial melting of a primitive asteroid, is an attractive target to study the processes of early planetary differentiation. Here, we present a comprehensive data set of mass-dependent Fe, Zn, and Mg isotope ratio variations in bulk ALC species, their separated silicate and metal phases, and in handpicked mineral fractions. These non-traditional stable isotope ratios are governed by mass-dependent isotope fractionation and provide a state-of-the-art perspective on the evolution of the ALC PB, which is complementary to interpretations based on the petrology, trace element composition, and isotope geochemistry of the ALC. None of the isotopic signatures of ALC species show convincing co-variation with the oxygen isotope ratios, which are considered to record nebular processes occurring prior to the PB formation. Iron isotopic compositions of ALC metal and silicate phases broadly fall on the isotherms within the temperature ranges predicted by pyroxene thermometry. The isotope ratios of Mg in ALC meteorites and their silicate minerals are within the range of chondritic meteorites, with only accessory spinel group minerals having significantly different compositions. Overall, the Mg and Fe isotopic signatures of the ALC species analyzed are in line with their formation as products of high-degree thermal metamorphism and low-degree partial melting of primitive precursors. The $\delta^{66/64}$Zn values of the ALC meteorites demonstrate a range of ~3.5‰ and the Zn is overall isotopically heavier than in chondrites. The superchondritic Zn isotopic signatures have possibly resulted from evaporative Zn losses, as observed for other meteorite parent bodies. This is unlikely to be the result of PB differentiation processes, as the Zn isotope ratio data show no covariation with the proxies of partial melting, such as the mass fractions of the platinum group and rare earth elements.

Geochemical Perspectives Letters

Metal differentiation on asteroids recorded in Zn and Fe isotopic signatures of ureilites

S.M. Chernonozhkin[1,2,3*], L. Pittarello[4,5], G. Hublet[6], S. Weyer[7], I. Horn[7], P. Claeys[8], V. Debaille[6], F. Vanhaecke[1], S. Goderis[8]

OPEN ACCESS

https://doi.org/10.7185/geochemlet.2501

Abstract

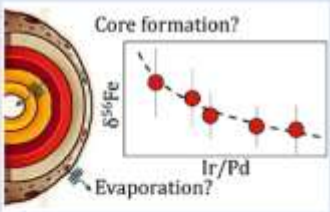

Ureilites are meteorites that represent mantle restites of a planetesimal likely disrupted before the magma ocean stage and then reaccreted. Historically, it was speculated that evaporation shifts the Zn isotope ratios in ureilites toward heavier compositions. The fact that the ureilite parent body (UPB) is depleted in some moderately volatile elements (MVEs) makes ureilites an appealing target to study isotopic fractionation by evaporation in the early Solar System. Here, we show that Fe and Zn isotope ratios of bulk ureilites and their metal and silicate components rather record metal melting and extraction of Fe-FeS melts in the UPB, which also resulted in isotopic disequilibrium between the silicate and metal parts. This finding underlines that the isotopic evolution of MVEs in the early Solar System is not only affected by evaporation, but also by planetary differentiation processes due to the chalcophile and/or siderophile behaviour of many MVEs. It shows that to avoid interpretational bias due to undersampling of planetesimal reservoirs in meteorite collections, and to distinguish planetary differentiation from evaporation, isotopic compositions of MVEs should be combined with common geochemical proxies.

Received 15 January 2024 | Accepted 27 November 2024 | Published 3 January 2025

Introduction

The chemical pathways of moderately volatile elements (MVEs) in the Solar System and, ultimately, the compositions of the terrestrial planets, strongly depend on the processes of evaporation and condensation. As kinetic processes under extreme heating regimes drive isotope fractionation, in the recent decade the isotope ratios of MVEs (*e.g.*, K, Fe, Si) have been found to be a useful proxy to unravel the evaporation histories of the planetary materials (Pringle *et al.*, 2014; Dauphas *et al.*, 2015; Wang and Jacobsen, 2016). Ureilites form a group of achondrites particularly interesting in this context due to their depletion in siderophile (*e.g.*, Ag and Ge) and lithophile (K, Rb) volatile elements compared to the Solar System abundances. At the same time Zn, one of the most volatile elements among MVEs known for chalcophile and lithophile properties, is present in higher concentrations than that in chondrites (Goodrich, 1992), and although the exact precursors and delivery mechanisms of Zn on the ureilite parent body (UPB) are not known, isotopically heavy Zn signatures have been interpreted to result from evaporation (Moynier *et al.*, 2010; Bruger *et al.*, 2019).

The main group ureilites are coarse-grained, ultramafic olivine-pyroxene rocks with interstitial refractory components, including carbon-rich material, Fe-Ni metal and accessories (Mittlefehldt *et al.*, 1998). Petrography and geochemistry of ureilites record high degree melting and melt extraction from an unknown lithology similar to a carbonaceous chondrite (Rankenburg *et al.*, 2008; Collinet and Grove, 2020). Ureilites are thought to have formed on a heterogeneously accreted planetesimal as mantle restites after extraction of metal and silicate partial melts at 1120–1280 °C (Mittlefehldt *et al.*, 1998). A diversity among the nebular components that accreted into the heterogeneous UPB is supported by non-equilibrated oxygen isotopic signatures of ureilites, plotting along the carbonaceous chondrite anhydrous minerals line (Clayton and Mayeda, 1988), and correlation of mineral and O-isotopic compositions (Rai *et al.*, 2020). Non-equilibrated oxygen isotope ratios indicate that the UPB differentiation did not reach the magma ocean stage (Rai *et al.*, 2020).

Mass-dependent variations in the isotope ratios of "non-traditional" systems in meteorites record not only the evaporation/condensation processes, but have also been applied to study

1. Atomic & Mass Spectrometry – A&MS Research Unit, Department of Chemistry, Ghent University, Campus Sterre, Krijgslaan, 281 – S12, B-9000 Ghent, Belgium
2. Chair of General and Analytical Chemistry, Research group - Isotope ratio analysis, Montanuniversität Leoben, Franz Josef-Straße 18, 8700 Leoben, Austria
3. Geological Survey of Finland, P.O. Box 96, 02151 Espoo, Finland
4. Naturhistorisches Museum Wien – NHMW, Mineralogisch-Petrographische Abteilung, Burgring 7, 1010 Vienna, Austria
5. University of Vienna, Department of Lithospheric Research, Josef-Holaubek-Platz 2, 1090 Vienna, Austria
6. Laboratoire G-Time, Université Libre de Bruxelles, 50, Av. F.D. Roosevelt CP 160/02, B-1050 Brussels, Belgium
7. Institute of Earth System Sciences, Section Mineralogy, Leibniz Universität Hannover, Callinstr. 3, 30167 Hannover, Germany
8. Archaeology, Environmental Changes, and Geo-Chemistry (AMGC), Vrije Universiteit Brussel, Pleinlaan 2, 1050 Brussels, Belgium
* Corresponding author (email: Stepan.Chernonozhkin@gmail.com)

12

—報告—
Report

Comprehensive report of the BELARE 2022–2023 meteorite reconnaissance expedition in the Sør Rondane area, East Antarctica

Vinciane Debaille[1], Maria Schönbächler[2], Maria Valdes[3,4], Ryoga Maeda[3,5*], Manu Poudelet[6], Steven Goderis[5], Philipp R. Heck[3,4], Veronica Tollenaar[7], Harry Zekollari[7,8,9] and Philippe Claeys[5]

(Received June 23, 2023; Accepted September 14, 2023)

Abstract: We provide a comprehensive overview of a reconnaissance expedition aimed at identifying new possible meteorite stranding zones in the surrounding of the Belgian Princess Elisabeth Antarctica (PEA) station in the Sør Rondane Mountains during the BELARE 2022–2023 field season. The team was composed of four scientists and one field guide. Several areas of interest were identified and daily searches occurred in two phases, first from a base camp and then from PEA. The first phase was in the Nils Larsenfjellet area, and a camp, accessible from the H.E. Hansenbreen (S72° 13.260' E22° 37.779'; altitude 1640 m), was set up from December 21 to 27, 2022. Systematic searches were performed in moraines and on blue ice areas (BIAs) during day trips, including the Verheyefjellet BIA, several BIAs surrounding an alignment of nunataks south of PEA, centered on S72° 18.403' E23° 13.191', and the Røysane nunatak at the eastern edge of Nils Larsenfjellet. Four meteorites were recovered during the first phase of the expedition, and another one in the second phase, also in the Nils Larsenfjellet area. In addition, nine surface ice samples and 18 kg of micrometeorite-bearing sediments were collected.

Preliminary classification, performed on-site using magnetic susceptibility, tentatively indicated H and L chondrites. The recovered meteorites were transported in frozen state to the Royal Belgian Institute of Natural Sciences in Brussels to be thawed in vacuum conditions and classified based on their mineralogy. The Nils Larsenfjellet is identified as a potential new Dense Collection Area.

Keywords: blue ice area, meteorites, Sør Rondane Mountains

[1] Laboratoire G-Time, Université libre de Bruxelles, CP 160/02, 50, Av. F.D. Roosevelt, 1050 Brussels, Belgium.
[2] Institute of Geochemistry and Petrology, ETH Zürich, Clausiusstrasse 25, 8092 Zürich, Switzerland.
[3] Robert A. Pritzker Center for Meteoritics and Polar Studies, Negaunee Integrative Research Center, The Field Museum of Natural History, 1400 S DuSable Lake Shore Drive, Chicago, IL 60605, USA.
[4] Department of the Geophysical Sciences, The University of Chicago, 5734 S. Ellis Ave, Chicago, IL 60637, USA.
[5] Archeology, Environmental Changes, and Geo-Chemistry, Vrije Universiteit Brussel, Pleinlaan 2, BE-1050 Brussels, Belgium.
[6] International Polar Guide Association.
[7] Laboratoire de Glaciologie, Université libre de Bruxelles, CP 160/03, 50, Av. F.D. Roosevelt, B-1050 Brussels, Belgium.
[8] Laboratory of Hydraulics, Hydrology and Glaciology (VAW), ETH Zürich, Zürich, Switzerland.
[9] Swiss Federal Institute for Forest, Snow and Landscape Research (WSL), Birmensdorf, Switzerland.
* Corresponding author. Now at Submarine Resources Research Center (SRRC), Japan Agency for Marine-Earth Science and Technology (JAMSTEC), 2-15 Natsushima-cho, Yokosuka 237-0061. E-mail: maedar@jamstec.go.jp

南極資料, Vol. 67, 12–27, 2023
Nankyoku Shiryô (Antarctic Record), Vol. 67, 12–27, 2023

Ore Geology Reviews 150 (2022) 105130

Contents lists available at ScienceDirect

Ore Geology Reviews

journal homepage: www.elsevier.com/locate/oregeorev

In-situ trace element and Sr isotope signature of apatite: A new key to unravelling the genesis of polymetallic mineralisation in black shales of the Early Cambrian Niutitang Formation, Southern China

Sophie Decrée [a,*], Jan Pašava [b], Jean-Marc Baele [c], Julien Mercadier [d], Delia Rösel [e], Hartwig Frimmel [f]

[a] Royal Belgian Institute of Natural Sciences-Geological Survey of Belgium, Brussels, Belgium
[b] Czech Geological Survey, Prague, Czech Republic
[c] Department of Geology and Applied Geology, University of Mons, Mons, Belgium
[d] Université de Lorraine, CNRS, CREGU, GeoRessources Lab, Vandoeuvre-lès-Nancy, France
[e] Department of Earth Sciences, University of Göteborg, Göteborg, Sweden
[f] Bavarian Georesources Centre, Dept. of Geodynamics and Geomaterials Research, Institute of Geography and Geology, University of Würzburg, Germany

ARTICLE INFO

Keywords:
Phosphocite
Ni-Mo-PGE sulphide ore
Rare Earth Elements
Mafic affinity
Hydrothermal brines

ABSTRACT

The Early Cambrian Mo-Ni-PGE sulphidic black shale in the Niutitang Formation on the margin of the Yangtze Craton (Southern China) is known for its extremely high metal concentrations. It is also very rich in phosphate that formed contemporaneously with the sulphides. Detailed petrological as well as in-situ trace element and Sr isotope analyses of authigenic apatite revealed new information on the metallogenesis of this enigmatic rock unit. In the ore bed, apatite forms nodules or is found in phosphatic (phoslithoclasts) and sulphide clasts. In the latter, the replacement of organic matter and sulphides by apatite microspherules suggests a microbially mediated phosphogenesis. Enrichment in middle rare earth elements emphasizes the role played by Fe-oxyhydroxides and organic matter in element scavenging. Moderately reducing conditions are supported by a lack of Ce and Eu anomalies. The trace element signature of apatite and its initial $^{87}Sr/^{86}Sr$ (0.7032–0.7190), which is - for a group of analyses - well below the signature of Lower Cambrian seawater, points to some contribution from mafic rock-sourced hydrothermal brines. This effectively explains the exceptional enrichment of Ni and PGE in the sulphides. Seawater remains, however, the preferred source for other elements such as P and Mo.

1. Introduction

The polymetallic Mo-Ni-PGE sulphide and phosphate-rich bed within the black shale unit of the Lower Cambrian Niutitang Formation (Huangjiawan mine, Zunyi region, northern part of the Guizhou Province, Southern China) is well-known for its extreme metal concentrations (e.g. Chen et al., 1982; Coveney and Chen, 1991; Fan, 1983; Han et al., 2015; Jiang et al., 2006; Lehmann et al., 2007; Li et al., 2013; Mao et al., 2002; Pašava et al., 2008, 2013, 2017; Xu et al., 2013). For instance, Mo and Ni are enriched over 1000 times compared to the average continental crust (with at least 4 wt% Mo and 2 wt% Ni) and Au-Pt-Pd contents in the ore bed reach 100 times the average content in this reservoir (1–249 ppm of precious metals, including Au, Pt, Pd, and Os) (e.g. Fan, 1983; Mao et al., 2002; Pašava et al., 2008, 2013, 2017). The metalliferous black shale occurs along a belt extending about 1600 km across South China (Steiner et al., 2001). The ore bed mostly contains sulphides and phosphate as mineralised clasts. The latter have been interpreted to represent remnants of a shallow-water hardground horizon rich in metals, which was reworked, transported (at least over short distances) and re-deposited in the deeper part of the basin (e.g. Murowchick et al., 1994; Pašava et al., 2008).

A lot of effort has been made to identify the source of the metals and to understand the complex genesis of the mineralisation in the Niutitang ore bed. As a general assumption, the timing of the mineralisation is synsedimentary to early diagenetic (e.g. Orberger et al., 2005; Pašava et al., 2008), and sulphides and phosphate replaced organic material,

* Corresponding author.
E-mail addresses: sophie.decree@naturalsciences.be (S. Decrée), jan.pasava@geology.cz (J. Pašava), jean-marc.baele@umons.ac.be (J.-M. Baele), julien.mercadier@univ-lorraine.fr (J. Mercadier), delia.rosel@gu.se (D. Rösel), hartwig.frimmel@uni-wuerzburg.de (H. Frimmel).

https://doi.org/10.1016/j.oregeorev.2022.105130
Received 26 October 2021; Received in revised form 3 September 2022; Accepted 26 September 2022
Available online 27 September 2022

ARTICLE IN PRESS

Geochimica et Cosmochimica Acta xxx (xxxx) xxx

Contents lists available at ScienceDirect

Geochimica et Cosmochimica Acta

journal homepage: www.elsevier.com/locate/gca

Loss and accretion of moderately volatile elements K and Na in Australasian microtektites from Antarctica

M. Del Rio [a,b,*], L. Folco [a,c], E. Mugnaioli [a,c], S. Goderis [d], M. Masotta [a,c]

[a] Dipartimento di Scienze della Terra, Università di Pisa, Via Santa Maria, 53, 56126 Pisa, Italy
[b] Dipartimento di Matematica, Informatica e Geoscienze, Università di Trieste, Via Weiss, 2, 34128 Trieste, Italy
[c] Center for the Instrument Sharing of the University of Pisa, CISUP, Lungarno Pacinotti 43/44, 56126 Pisa, Italy
[d] Archaeology, Environmental Changes & Geo-Chemistry, Vrije Universiteit Brussel, Pleinlaan 2, BE-1050 Brussels, Belgium

ARTICLE INFO

Associate editor: Tomas Magna

Keywords:
Microtektites
Tektites
Impact melting
MVE uptake
Antarctica

ABSTRACT

Recent studies on alkali metals, Ar-, Fe- and K-isotope distribution in Australasian microtektites have revealed the complex interplay of multiple fractionation processes in establishing their moderately volatile elements record, particularly in those deposited in Antarctica, most distal from the hypothetical source crater. To provide a better understanding of moderately volatile elements fractionation during microtektite formation, we studied the distribution of K, Na, Rb and Cs in twenty-seven Australasian microtektites from Antarctica ranging in size from 180 to 680 μm. Compositional profiles were determined using electron probe microanalyses (major elements) and laser ablation-inductively coupled plasma-mass spectrometry (trace elements), following a petrographic study at the nanoscopic scale by means of scanning and transmission electron microscopy. The Australasian microtektites from Antarctica contain nanometer-sized, partly digested lechatelierite inclusions and rare vesicles, and record significant moderately volatile elements depletion ($Na_2O = 0.30 \pm 0.07$ (1σ) wt%; $K_2O = 0.94 \pm 0.25$ (1σ) wt%) relative to: i) upper continental crust ($Na_2O = 3.46$ wt%; $K_2O = 3.45$ wt%), ii) microtektites from deep sea sediments ($Na_2O = 1.15 \pm 0.43$ (1σ) wt%; $K_2O = 2.47 \pm 0.32$ (1σ) wt%), and iii) Australasian tektites ($Na_2O = 1.20 \pm 0.19$ (1σ) wt%; $K_2O = 2.43 \pm 0.24$ (1σ) wt%). They are also characterized by moderately volatile elements enrichments at their rims (up to ~2x for K_2O; ~1.6x for Na_2O), and the enrichment factor typically decreases with increasing diameter. Lastly, there is an inverse correlation between bulk Na_2O content (but not K_2O) and diameter. We propose that the most distal Antarctic microtektites originated as impact melt droplets and not as vapor condensate spherules. Their moderately volatile elements geochemical budget was established through three subsequent stages of fractionation in the context of a hypervelocity impact. 1) Gross Na and K and other moderately volatile elements loss which occurred during the melting and vaporization of the target precursor materials. 2) Re-accretion of Na, K and other moderately volatile elements from the condensation of a hot gas envelope of vaporized target materials onto volatile depleted droplets cores. 3) Size-controlled partial evaporation of (mainly) Na, caused by aerodynamic drag heating, during deceleration from high ejection velocities either during the decoupling from the hot gas envelope in ambient air, or during atmospheric re-entry, as suggested by alkalis and Fe-isotope data in the literature. The late accretion of K vapor also provides plausible explanations for the contamination by extraneous Ar and K-isotopic systematics reported in the literature.

1. Introduction

Tektites and microtektites are high–velocity, distal impact ejecta distributed in strewn fields extending for thousands of kilometers (Glass and Simonson, 2013). They are generated by melting and vaporization of the Earth's continental crust during large-scale impacts of asteroidal or cometary bodies (Artemieva, 2002). Tektites are natural siliceous glass objects up to several tens of centimeters in size with splash/flanged aerodynamic forms or blocky shapes with layered structure, i.e., the Muong Nong-type (Glass, 1990; Koeberl, 1992, 1994). Microtektites are their microscopic counterparts, as they typically occur in the form of spherules of less than 1 mm in diameter. Both tektites and microtektites have bulk chemical composition similar to the average composition of the upper continental crust (Taylor and McLennan, 1995; Wedepohl,

* Corresponding author at: Dipartimento di Scienze della Terra, Università di Pisa, Via Santa Maria, 53, 56126 Pisa, Italy.
E-mail address: matteo.delrio@phd.units.it (M. Del Rio).

https://doi.org/10.1016/j.gca.2025.03.005
Received 12 November 2024; Accepted 9 March 2025
Available online 12 March 2025

COSMOCHEMISTRY

Ruthenium isotopes show the Chicxulub impactor was a carbonaceous-type asteroid

Mario Fischer-Gödde[1]*, Jonas Tusch[1], Steven Goderis[2], Alessandro Bragagni[3,4], Tanja Mohr-Westheide[5], Nils Messling[6], Bo-Magnus Elfers[7], Birger Schmitz[8], Wolf U. Reimold[9], Wolfgang D. Maier[10], Philippe Claeys[2], Christian Koeberl[11], François L. H. Tissot[12], Martin Bizzarro[13], Carsten Münker[1]

An impact at Chicxulub, Mexico, occurred 66 million years ago, producing a global stratigraphic layer that marks the boundary between the Cretaceous and Paleogene eras. That layer contains elevated concentrations of platinum-group elements, including ruthenium. We measured ruthenium isotopes in samples taken from three Cretaceous-Paleogene boundary sites, five other impacts that occurred between 36 million to 470 million years ago, and ancient 3.5-billion- to 3.2-billion-year-old impact spherule layers. Our data indicate that the Chicxulub impactor was a carbonaceous-type asteroid, which had formed beyond the orbit of Jupiter. The five other impact structures have isotopic signatures that are more consistent with siliceous-type asteroids, which formed closer to the Sun. The ancient spherule layer samples are consistent with impacts of carbonaceous-type asteroids during Earth's final stages of accretion.

Several mass extinction events occurred on Earth during the Phanerozoic era, the geologic time period from 539 million years ago (Ma) to the present (*1*, *2*). The most recent mass extinction occurred simultaneously with the Cretaceous-Paleogene (K-Pg) geologic boundary at 66 Ma, during which ≥60% of all species were extinguished (*3*). The geologic signature of the K-Pg boundary was produced by the impact on Earth of a >10-km-diameter asteroid at Chicxulub, Mexico (*3*, *4*). Samples taken from the K-Pg boundary layers have elevated concentrations of platinum-group elements (PGE)—iridium, ruthenium, osmium, rhodium, platinum, and palladium (*5*–*7*)—which are rare in Earth's crustal rocks (*8*). Meteorites, which are fragments of asteroids, have orders-of-magnitude-higher PGE concentrations than Earth's crust (*9*). The PGE enrichment of K-Pg boundary layer samples, along with other terrestrial impact-related rocks and deposits, has been interpreted as derived from the extraterrestrial impactors.

Elevated PGE concentrations have been identified in many samples from globally distributed K-Pg boundary sites (*10*–*12*), indicating that the fallout produced by the impact extended worldwide. The PGE data have been interpreted as indicating that the impactor was an asteroid with composition similar to the class of meteorites known as chondrites (*13*). Further evidence for extraterrestrial material in the K-Pg boundary layer includes chromium (Cr) isotope data (*14*, *15*) and the presence of a fossil meteorite fragment in a sample of the K-Pg boundary in the Pacific Ocean (*16*).

An alternative hypothesis for the origin of PGE in K-Pg boundary layer deposits is that they are derived from global ash fall originating from extensive volcanic eruptions in the Deccan Trap, India (*17*). However, the abundance ratios of PGEs in the K-Pg boundary differ from those in the Deccan Trap volcanic basalts (*18*); the K-Pg PGE relative abundances are more consistent with those of chondritic meteorites (*13*), not with Deccan basalts.

The abundance ratios of PGEs and osmium isotope compositions have been used to constrain the nature of the extraterrestrial impactors that produced the impact structures at Brent (*19*), Clearwater East (*20*), Morokweng (*21*, *22*), and Popigai (*23*), and the impactors responsible for ancient 3.5-billion- to 3.2-billion-

Table 1. Ruthenium isotope measurements. Isotope data are listed for five ruthenium isotope ratios, measured from the samples of the K-Pg boundary layer, other Phanerozoic impact structures, Archean spherule layers, two meteorites, and a terrestrial reference sample (UG2 chromitite). *n* is the number of analyses of the same sample solution. Ruthenium isotope data have been internally normalized to $^{99}Ru/^{101}Ru$ and are expressed in ε notation as deviations from the Alfa Aesar Ru standard solution (*33*). Uncertainties for all samples are identical because they are dominated by the systematic uncertainty (*33*), which is expressed as twice the standard deviation (2 SD) of repeated measurements of reference sample UG2 (UG2_average), calculated from 11 individual analyses of two replicate digestions (table S2).

Sample	*n*	$\varepsilon^{96}Ru$	$\varepsilon^{98}Ru$	$\varepsilon^{100}Ru$	$\varepsilon^{102}Ru$	$\varepsilon^{104}Ru$
K-Pg boundary layer						
Caravaca	1	−0.0 ± 0.27	2.29 ± 0.46	−0.94 ± 0.11	−0.36 ± 0.15	0.18 ± 0.25
Fonte D'Olio	13	0.25 ± 0.27	0.07 ± 0.46	−1.02 ± 0.11	−0.43 ± 0.15	−0.01 ± 0.25
Stevns Klint-1	2	0.68 ± 0.27	0.58 ± 0.46	−1.02 ± 0.11	−0.35 ± 0.15	0.17 ± 0.25
Stevns Klint-2	1	0.07 ± 0.27	0.92 ± 0.46	−0.98 ± 0.11	−0.44 ± 0.15	0.09 ± 0.25
Stevns Klint-3	1	0.38 ± 0.27	1.41 ± 0.46	−0.95 ± 0.11	−0.45 ± 0.15	−0.12 ± 0.25
Phanerozoic impact structures						
Popigai	1	0.52 ± 0.27	1.01 ± 0.46	−0.36 ± 0.11	−0.19 ± 0.15	−0.06 ± 0.25
Morokweng	5	0.14 ± 0.27	0.66 ± 0.46	−0.36 ± 0.11	−0.14 ± 0.15	0.04 ± 0.25
Rochechouart	3	0.20 ± 0.27	0.43 ± 0.46	−0.40 ± 0.11	−0.20 ± 0.15	−0.07 ± 0.25
Brent	2	0.15 ± 0.27	1.43 ± 0.46	−0.35 ± 0.11	−0.09 ± 0.15	−0.08 ± 0.25
Clearwater East	2	0.26 ± 0.27	0.29 ± 0.46	−0.37 ± 0.11	−0.26 ± 0.15	−0.08 ± 0.25
Archean impact spherule layers						
BARB5_SL2	1	0.40 ± 0.27	0.03 ± 0.46	−0.33 ± 0.11	−0.16 ± 0.15	−0.01 ± 0.25
CT3-1_SL9	7	0.12 ± 0.27	0.27 ± 0.46	−0.27 ± 0.11	−0.16 ± 0.15	−0.04 ± 0.25
CT3-2_SL13	8	0.09 ± 0.27	0.10 ± 0.46	−0.30 ± 0.11	−0.12 ± 0.15	0.05 ± 0.25
Terrestrial reference samples						
UG2_1	7	−0.09 ± 0.27	0.11 ± 0.46	0.01 ± 0.11	−0.06 ± 0.15	−0.11 ± 0.25
UG2_2	4	−0.12 ± 0.27	−0.12 ± 0.46	0.01 ± 0.11	0.03 ± 0.15	−0.11 ± 0.25
UG2_average	11	−0.10 ± 0.27	0.03 ± 0.46	0.01 ± 0.11	−0.02 ± 0.15	−0.11 ± 0.25
Meteorites						
Allende (CV)	1	0.52 ± 0.27	0.53 ± 0.46	−0.73 ± 0.11	−0.25 ± 0.15	0.21 ± 0.25
Orgueil (CI)	1	1.52 ± 0.27	0.99 ± 0.46	−0.38 ± 0.11	−0.18 ± 0.15	0.01 ± 0.25

[1]Institut für Geologie und Mineralogie, University of Cologne, 50674 Cologne, Germany. [2]Archeology, Environmental Changes and Geochemistry Research Group, Vrije Universiteit Brussel, 1050 Brussels, Belgium. [3]Department of Earth Sciences, University of Florence, 50121 Firenze, Italy. [4]Institute of Marine Sciences, National Research Council, 40129 Bologna, Italy. [5]Museum für Naturkunde, Leibniz-Institut für Evolutions- und Biodiversitätsforschung, 10115 Berlin, Germany. [6]Geochemistry and Isotope Geology Department, Geoscience Center, University of Göttingen, 37073 Göttingen, Germany. [7]Zentrallabor, Technical University Hamburg, 21073 Hamburg, Germany. [8]Astrogeobiology Laboratory, Lund University, SE-22100 Lund, Sweden. [9]Laboratório de Geocronologia e Geoquímica Isotópica, Instituto de Geociências, Universidade de Brasília, CEP 70910-900 Brasília, DF, Brazil. [10]School of Earth and Ocean Sciences, Cardiff University, Cardiff CF10 3AT, UK. [11]Department of Lithospheric Research, University of Vienna, A-1090 Vienna, Austria. [12]Division of Geological and Planetary Sciences, California Institute of Technology, Pasadena CA 91125, USA. [13]Center for Star and Planet Formation, Globe Institute, University of Copenhagen, DK-1350 Copenhagen, Denmark. *Corresponding author. Email: mfisch48@uni-koeln.de

The Meteoritical Society

Meteoritics & Planetary Science 1–22 (2024)
doi: 10.1111/maps.14145

Oxygen isotopic compositions of fresh rooftop micrometeorites from the Budel collection—Insights into the contemporary cosmic dust flux

Guido JONKER [1]*, Flore van MALDEGHEM [2], Matthias van GINNEKEN [3], Lisa KRÄMER RUGGIU[2], and Steven GODERIS [2]

[1]Department of Earth Sciences, Faculty of Science, Vrije Universiteit Amsterdam, Amsterdam, The Netherlands
[2]Archaeology, Environmental Changes, and Geo-Chemistry, Vrije Universiteit Brussel, Brussels, Belgium
[3]Centre for Astrophysics and Planetary Science, School of Physical Sciences, University of Kent, Canterbury, UK
*Correspondence
Guido Jonker, Department of Earth Sciences, Faculty of Science, Vrije Universiteit Amsterdam, De Boelelaan 1085, Amsterdam 1081HV, The Netherlands.
Email: guidojonker.vua@gmail.com

(Received 15 March 2023; revision accepted 24 January 2024)

Abstract–Cosmic dust particles originate from a wide variety of solar system and interstellar objects, including sources not identified among meteorite collections. Particles that survive atmospheric entry are retrieved on the Earth's surface as micrometeorites. The recovery of these micrometeorites has recently advanced to rooftop sites. Here, we present the results of an extensive isotopic study on this type of rooftop micrometeorite from the Budel collection, the Netherlands, accreted to the Earth between October 31, 2018 and June 16, 2021. The triple oxygen isotopic compositions of 80 silica-dominated cosmic spherules (CSs) with diameters ranging between 105 and 515 μm are obtained relying on 213 in situ spot analyses determined using ion microprobe. Our analyzed population spans a large range of isotopic compositions and is dominated by carbonaceous chondritic sources. In situ measurements on several CSs support a possible continuum between ^{16}O-rich and ^{16}O-poor compositions following the CM mixing line, showing that ^{16}O-poor CSs may be genetically related to aqueously altered carbonaceous chondrites. We demonstrate that weathering in the terrestrial environment has negligible effects on the isotopic compositions of the studied CSs and attempt to quantify the effects of kinetic mass-dependent fractionation and admixture of terrestrial oxygen during atmospheric entry. The results further corroborate previously suggested relations between CS texture and the duration and intensity of the heating pulse experienced during atmospheric deceleration. Finally, the young and well-constrained terrestrial age of the collection provides insights into the most recent flux of cosmic dust. Our results indicate no major recent changes in the global flux compared with collections sampled over thousand- to million-year time scales and demonstrate that ^{16}O-poor material is still represented in the modern-day cosmic dust flux at a relative abundance of ~13%–15%. As such, rooftop micrometeorites represent a valuable reservoir to study the characteristics of the contemporary cosmic dust flux.

INTRODUCTION

Micrometeorites are particles of extraterrestrial origin ~50–2000 μm in size collected on the Earth's surface (Genge et al., 2008; Taylor et al., 2016). During atmospheric entry, micrometeoroids decelerate and experience frictional heating. If peak temperatures remain sufficiently low, then micrometeorites may retain some of their preatmospheric textures and mineralogy, forming unmelted and partially melted scoriaceous micrometeorites, or relict-bearing spherules (Genge et al., 2008). Higher peak temperatures will result in melting and degassing, leading to

Icarus 418 (2024) 116143

Contents lists available at ScienceDirect

Icarus

journal homepage: www.elsevier.com/locate/icarus

Identification of Earth's late accretion by large impactors through mass independent Cr isotopes

Yogita Kadlag [a,b,*], Aryavart Anand [c,d], Mario Fischer-Gödde [e], Klaus Mezger [d], Kristoffer Szilas [f], Steven Goderis [g], Ingo Leya [b]

[a] Geosciences Division, Physical Research Laboratory, Navrangpura, Ahmedabad, Gujarat 380009, India
[b] Space Science and Planetology, Physics Institute, Universität Bern, Sidlerstrasse 5, 3012 Bern, Switzerland
[c] Max-Planck-Institut für Sonnensystemforschung, Justus-von-Liebig-Weg 3, 37077 Göttingen, Germany
[d] Institut für Geologie, Universität Bern, Baltzerstrasse 1+3, 3012 Bern, Switzerland
[e] Institut für Geologie und Mineralogie, University of Cologne, Zülpicher Straße 49b, 50674 Köln, Germany
[f] Department of Geosciences and Natural Resource Management, University of Copenhagen, Øster Voldgade 10, 1350 Copenhagen, Denmark
[g] Archaeology, Environmental Changes, and Geo-Chemistry (AMGC) Research Group, Department of Chemistry, Vrije Universiteit Brussel, Pleinlaan 2, 1050 Brussels, Belgium

ARTICLE INFO

Keywords:
Impacts
Late accretion
Chromium isotopes
Archean

ABSTRACT

The late addition of extra-terrestrial material may represent an important source of Earth's volatiles. The composition of impactors can be reconstructed using ^{54}Cr abundances in impact related rocks preserved in the terrestrial record. The average ε^{53}Cr and ε^{54}Cr of Earth's mantle determined from mantle rocks of 3.8 Ga to present are 0.03 ± 0.02 and 0.05 ± 0.04, respectively. Impact melt rocks and spherule beds linked to impact structures larger than 50 km that formed between 3.4 Ga and 66 Ma have ε^{53}Cr ranging from −0.04 to 0.17, and ε^{54}Cr ranging from −0.64 to 1.41. A carbonaceous chondrite-like impactor contribution dominated the Meso- to Paleoarchean spherule layers (> 3.0 Ga), whereas a mixed chondrite flux composed of carbonaceous and non-carbonaceous chondrites, with a possible contribution of differentiated meteorites is observed in the younger spherule layers (2.5 Ga to 66 Ma). This likely reflects the break-up of distinct asteroid families through time. Although available impact materials are limited, the Cr isotope signatures of materials related to large impacts suggest a change in the composition of crater-forming impactors on Earth, from predominantly carbonaceous chondrite-like more oxidized material during the Archean to predominantly non-carbonaceous -like more reduced and volatile poor material in recent times. Chromium isotopes suggest that not more than 0.01 wt % of CC-like material added to the Earth's mantle after the Archean. Thus, it is inferred that the mass accreted after 3.0 Ga contributed insignificantly to the water and other volatile element budget of the Earth.

1. Introduction

The mass that accreted to Earth can be chronologically divided into three major events: i) accretion of the proto-Earth within the first few Ma after the formation of the solar system (Halliday and Canup, 2023), ii) accretion during/subsequent to the Moon forming giant impact within the first 60 Ma (Wood and Halliday, 2005; Barboni et al., 2017), and iii) the late veneer (~ 0.5% of the Earth's Mass, Dauphas and Marty, 2002; Walker, 2009; Bottke et al., 2010) and late accretion (accretion after the giant impact, Morbidelli and Wood, 2015) in the form of micrometeorites to large crater forming impactors. The evidence of the late accretion is recorded at different times throughout Earth's history in the form of impacts. The main mass and chemical composition of the bulk Earth is dominantly shaped by the first two events (Mezger et al., 2021; Halliday and Canup, 2023). The current annual flux of extra-terrestrial material (large impactors as well as micrometeorites) on Earth represents $<6 \times 10^{-10}$ times the mass of Earth (Peucker-Ehrenbrink and Ravizza, 2000; Zolensky et al., 2006), i.e., $<6 \times 10^{-16}$% of the mass of Earth. Extending these estimates to over to 4.5 Ga, gives the limit of 0.000002% of the mass accreted to the Earth through impacts. Nevertheless, it was likely much more significant in Earth's earlier history (Fig. 1, Johnson et al., 2016). The combined flux of late accreted material after Earth's core formation is estimated to be ~0.5% of the Earth's mass based on the refractory and volatile element abundances

* Corresponding author at: Geosciences Division, Physical Research Laboratory, Navrangpura, Ahmedabad, Gujarat 380009, India.
E-mail address: yogita@prl.res.in (Y. Kadlag).

https://doi.org/10.1016/j.icarus.2024.116143
Received 11 February 2024; Received in revised form 10 May 2024; Accepted 10 May 2024
Available online 31 May 2024

Geochimica et Cosmochimica Acta 405 (2025) 114–131

Contents lists available at ScienceDirect

Geochimica et Cosmochimica Acta

journal homepage: www.elsevier.com/locate/gca

Diversity among fossil micrometeorites in the late Devonian

Lisa Krämer Ruggiu [a,*], Johan Villeneuve [b], Anne-Christine Da Silva [c], Vinciane Debaille [d], Sophie Decrée [e], Lutz Hecht [f], Felix E.D. Kaufmann [f], Steven Goderis [a]

[a] Archaeology, Environmental Changes & Geo-Chemistry, Vrije Universiteit Brussel, Brussels, Belgium
[b] CRPG, CNRS, Université de Lorraine, UMR 7358, Vandoeuvre-lès-Nancy 54501, France
[c] SedCCIm Laboratory, Geology Department, Liège University, Liège, Belgium
[d] Laboratoire G-Time, Université Libre de Bruxelles, Brussels, Belgium
[e] Institute of Natural Sciences, Geological Survey of Belgium, Brussels, Belgium
[f] Museum für Naturkunde, Leibniz-Institut für Evolutions- und Biodiversitätsforschung, Invalidenstrasse 43, Berlin 10115, Germany

ARTICLE INFO

Associate editor: Martin Robert Lee

Keywords:
Micrometeorites
Fossil micrometeorites
Oxygen isotopes
Late Devonian
Major element composition

ABSTRACT

A total of 1222 Micrometeorites (MMs) from the late Devonian period were extracted from 26 kg of carbonates host rock fragments from the Chanxhe section in Belgium, from the Latest Famennian around 360 Myr, through magnetic separation and optical picking following dissolution with mild HCl, making it one of the largest fossil MMs collection, the largest from the late Devonian. The collection shows a wide diversity of texture, comparable to modern day collection but with different distribution. The majority of the MMs were I-type (90 %), with G-type particles constituting 6 % and S-type particles at 1 %. Some of the S-types spherules are amongst the first silicate-type spherules, and amongst the most well-preserved in terms of texture and composition, to be described in fossil MMs collections. Additionally, intermediate type G/I representing <1 % of the sample are introduced for future fossil MMs classification.

Distinguishing extraterrestrial (ET) MMs from terrestrial spherules is challenging due to weathering effects that modify both texture and composition during long residency time on Earth. The $Na_2O + K_2O$ versus Fe/Si ratio plot is used for distinguishing ET from terrestrial spherules. Using textural and compositional data in combination creates a reliable ET spherule identification.

I-type spherules show significant terrestrial alteration with notable loss of Ni and Cr, also observed in S-type spherules, with their silicate phases recrystallized in palagonite. G-type spherules display a mix of characteristics from I-type and S-type MMs. The study also highlights the presence of smaller spherules (<125 μm) compared to modern micrometeorites (210–330 μm), attributed to the predominance of I- and G-type spherules and long-term dissolution effects.

Despite some alteration for some spherules, due diagenesis of the sedimentary host rocks, the collection shows extremely well-preserved spherules, with even some oxygen isotopes signature being preserved. Indeed, triple oxygen isotope analysis reveals that 5.8 % of the particles are related to ordinary chondrites (OC) and 33 % to carbonaceous chondrites (CCs), yielding a CC/OC ratio of approximately 5.6, with comparable distribution for all major types. Also, 9 % of I- and G/I-types are OC-related. Most I-type spherules likely originate from CM, CR, or H chondrites, with some possibly from iron meteorites. The findings suggest that the source materials of the ET flux have remained relatively consistent over the past 360 Myr, providing insights into historical Solar System events and Earth's environmental changes and extends the study of ET flux to Earth to CC compared to meteorites. In addition, combined with chemical and isotopic proxies and chrome spinel, the fossil MMs could assess the complete flux of cosmic dust to Earth. Finally, the use of fossil MMs could represent potential proxies for paleo-atmospheric oxygen levels and CO_2 contents.

* Corresponding author.
E-mail address: lisa.kramer.ruggiu@vub.be (L. Krämer Ruggiu).

https://doi.org/10.1016/j.gca.2025.07.016
Received 15 January 2025; Accepted 19 July 2025
Available online 26 July 2025

JAAS

ROYAL SOCIETY OF CHEMISTRY

PAPER

View Article Online
View Journal

Cite this: DOI: 10.1039/d2ja00317a

Quantitative elemental mapping of chondritic meteorites using laser ablation-inductively coupled plasma-time of flight-mass spectrometry (LA-ICP-TOF-MS)†

Ryoga Maeda, *[ab] Thibaut Van Acker, [c] Frank Vanhaecke, [c] Akira Yamaguchi, [d] Vinciane Debaille, [b] Phillippe Claeys [a] and Steven Goderis [a]

Fast elemental mapping using laser ablation-inductively coupled plasma-time of flight-mass spectrometry (LA-ICP-TOF-MS) was applied to a set of chondritic meteorite samples, more specifically H chondrites. LA-ICP-TOF-MS enables element distribution maps for both major and trace elements to be obtained at μm-order spatial resolution (5 × 5 μm square pixels in this study) in a (semi-)quantitative manner. To assess the reliability of the quantitative data as obtained using LA-ICP-TOF-MS mapping, the accuracy and precision as obtained using this fast elemental mapping approach were compared to those of the data obtained using the more conventional spot analysis with an electron probe micro analyzer and LA-ICP-sector field (SF)-MS for major and trace elements, respectively. The maps obtained using LA-ICP-TOF-MS visualize elemental distributions among the constituent minerals, while major and trace element abundances determined using LA-ICP-TOF-MS are overall in good agreement within up to 30% relative uncertainty with those obtained based on the spot analyses and with literature values. Yet, some analytical limitations of LA-ICP-TOF-MS mapping remain due to the limited ablated yield when using a small laser spot size for high spatial resolution mapping, while ICP-TOF-MS shows a lower sensitivity and narrower linear dynamic range than does ICP-SF-MS. On the other hand, the main host phase(s) of an element can be readily identified and the major and trace element abundances in the phase(s) can be quantified with an accuracy approaching that of the spot analyses. As such, this study demonstrates the potential of LA-ICP-TOF-MS for fast quantitative imaging of various types of samples, in particular geological samples.

Received 28th September 2022
Accepted 21st December 2022

DOI: 10.1039/d2ja00317a

rsc.li/jaas

Introduction

In situ spot analysis and elemental mapping in geological and geochemical research are commonly based on electron probe micro analysis (EPMA), scanning electron microscopy in combination with energy-dispersive X-ray spectrometry, micro-X-ray fluorescence spectrometry (μXRF), or secondary ion mass spectrometry (SIMS). Most of these techniques are valuable in the context of major element concentrations (generally >0.1% m m^{-1} level) for both spot analysis and mapping, but their application is more limited in relation to trace element analysis due to their relatively high limits of detection. For the determination of trace elemental abundances, laser ablation-inductively coupled plasma-mass spectrometry (LA-ICP-MS) is now widely used as a direct solid sampling micro-analytical technique.[1–3] The LA-ICP-MS technique not only determines the trace elemental abundances in mineral phases, but also provides spatially resolved information in the form of elemental maps for major, minor, and trace elements.[4,5] Recently, hardware developments focusing on low-dispersion ablation cells and aerosol transport systems, which reduce the duration of single pulse response profiles and boost the signal-to-noise ratio and speed of analysis, significantly improved the analytical capabilities of LA-ICP-MS elemental mapping.[6,7] Moreover, the launch of commercially available time-of-flight (TOF) based ICP-mass spectrometers, providing rapid quasi-simultaneous detection of nearly the entire elemental mass spectrum for each individual laser pulse, has boosted the use of LA-ICP-MS for elemental mapping applications in a wide variety of research fields. ICP-TOF-MS instruments can handle the short transient signals produced with low-dispersion LA setups and provide fast multi-elemental detection in contrast to sequential scanning-type ICP-mass

[a]Analytical-, Environmental-, and Geo-Chemistry, Vrije Universiteit Brussel, Pleinlaan 2, 1050 Brussels, Belgium. E-mail: Ryoga.Maeda@vub.be
[b]Laboratoire G-Time, Université libre de Bruxelles, CP 160/02, 50, Av. F. D. Roosevelt, 1050 Brussels, Belgium
[c]Atomic & Mass Spectrometry (A&MS) Research Unit, Department of Chemistry, Ghent University, Campus Sterre, Krijgslaan, 281 – S12, 9000 Ghent, Belgium
[d]National Institute of Polar Research, 10-3 Midori-cho, Tachikawa-shi, Tokyo 190-8518, Japan

† Electronic supplementary information (ESI) available. See DOI: https://doi.org/10.1039/d2ja00317a

The Meteoritical Society

Meteoritics & Planetary Science 1–21 (2023)
doi: 10.1111/maps.14034

Fluid mobilization of rare earth elements, Th, and U during the terrestrial alteration of H chondrites

Ryoga MAEDA[1,2,3,4]*, Steven GODERIS[1], Akira YAMAGUCHI[5], Thibaut VAN ACKER[6], Frank VANHAECKE[6], Vinciane DEBAILLE[2], and Phillippe CLAEYS[1]

[1]Analytical-, Environmental-, and Geo-Chemistry, Vrije Universiteit Brussel, Brussels, Belgium
[2]Laboratoire G-Time, Université libre de Bruxelles, Brussels, Belgium
[3]Submarine Resources Research Center (SRRC), Japan Agency for Marine-Earth Science and Technology (JAMSTEC), Yokosuka, Japan
[4]REE Smelting Unit, Development of Production Technology for REE, General Project Team for SIP, Japan Agency for Marine-Earth Science and Technology (JAMSTEC), Yokosuka, Japan
[5]National Institute of Polar Research, Tokyo, Japan
[6]Atomic & Mass Spectrometry (A&MS) Research Unit, Department of Chemistry, Ghent University, Ghent, Belgium
*Correspondence
Ryoga Maeda, Submarine Resources Research Center (SRRC), Japan Agency for Marine-Earth Science and Technology (JAMSTEC), 2-15 Natsushima-cho, Yokosuka 237-0061, Japan.
Email: maedar@jamstec.go.jp

(Received 24 October 2022; revision accepted 31 May 2023)

Abstract–The chemical effects of terrestrial alteration, with a particular focus on lithophile trace elements, were studied for a set of H chondrites displaying various degrees of weathering from fresh falls to altered finds collected from hot deserts. According to their trace element distributions, a considerable fraction of rare earth elements (REEs), Th, and U resides within cracks observed in weathered meteorite specimens. These cracks appear to accumulate unbound REEs locally accompanied by Th and U relative to the major element abundances, especially P and Si. The deposition of Ce is observed in cracks in the case of most of the weathered samples. Trace element maps visually confirm the accumulation of these elements in such cracks, as previously inferred based on chemical leaching experiments. Because the positive Ce anomalies and unbound REE depositions in cracks occur in all weathered samples studied here while none of such features are observed in less altered samples including falls (except for altered fall sample Nuevo Mercurio), these features are interpreted to have been caused by terrestrial weathering following chemical leaching. However, the overall effects on the bulk chemical composition remain limited as the data for all Antarctic meteorites studied in this work (except for heavily weathered sample A 09516, H6) are in good agreement with published data for unaltered meteorites.

INTRODUCTION

Meteorites are divided into "falls" and "finds" depending on how they were recovered: falls are recovered after observed fall events, while finds cannot be associated with observed fall events and include meteorites collected from cold and hot deserts mostly. As falls are usually collected shortly after the fall events, they are in general significantly fresher than finds, as the latter have been subjected to weathering to various degrees during their terrestrial residence (roughly of the order of tens of kyr in most hot deserts and up to a few Myr in Antarctica and Atacama: e.g., Al-Kathiri et al., 2005; Drouard et al., 2019; Nishiizumi et al., 1989; Zekollari et al., 2019). Terrestrial weathering may change the original mineralogy and chemical compositions of meteorites due to oxidation, hydration, and so on, that is, the alteration to phases that are more stable at the Earth's surface depending on environmental factors such as humidity and temperature (e.g., Bland et al., 2006;

Received: 27 May 2024 | Revised: 9 September 2024 | Accepted: 12 September 2024

DOI: 10.1002/rcm.9921

RESEARCH ARTICLE

Rapid Communications in Mass Spectrometry WILEY

Triple-oxygen isotopes of stony micrometeorites by secondary ion mass spectrometry (SIMS): Olivine, basaltic glass and iron oxide matrix effects for sensitive high-mass resolution ion microprobe-stable isotope (SHRIMP-SI)

Seann J. McKibbin[1,2,3,4] | Janaína N. Ávila[3,5] | Trevor R. Ireland[3,6] | Matthias Van Ginneken[1,7,8,9] | Bastien Soens[1] | Flore Van Maldeghem[1] | Matthew Huber[10] | Leonardo Baeza[3] | Aditya Patkar[3] | Frank Vanhaecke[11] | Vinciane Debaille[7] | Philippe Claeys[1] | Steven Goderis[1]

[1]Analytical, Environmental and Geo-Chemistry, Vrije Universiteit Brussel, Brussels, Belgium

[2]Geowissenschaftliches Zentrum, Abteilung Isotopengeologie, Georg-August-Universität Göttingen, Göttingen, Germany

[3]Research School of Earth Sciences, Australian National University, Acton, ACT, Australia

[4]Earth Atmosphere and Environment, Monash University, Clayton, Victoria, Australia

[5]Griffith Centre for Social and Cultural Research, Griffith University, Nathan, Queensland, Australia

[6]School of Earth and Environmental Sciences, The University of Queensland, St Lucia, Queensland, Australia

[7]Laboratoire G-Time, Université Libre de Bruxelles, Brussels, Belgium

[8]Belgian Geological Survey, Royal Belgian Institute of Natural Sciences, Brussels, Belgium

[9]Center for Astrophysics and Planetary Science, School of Physical Sciences, Ingram Building, University of Kent, Canterbury, UK

[10]Planetary Science Institute, Tucson, Arizona, USA

[11]Department of Chemistry, Universiteit Gent, Ghent, Belgium

Correspondence
Seann J. McKibbin, Earth Atmosphere and Environment, Monash University, 9 Rainforest Walk, Clayton, VIC 3800, Australia.
Email: seann.mckibbin@gmail.com

Funding information
Belgian Federal Science Policy Office; Fonds De La Recherche Scientifique - FNRS; Alexander von Humboldt-Stiftung; Fonds Wetenschappelijk Onderzoek; FVM, the Interuniversity Attraction Poles Program (IUAP) Planet Topers and the BRAIN-be BAMM, Grant/Award Number: 11C2520N; Belgian Science Policy Office and the FWO/FNRS Excellence of Science, Grant/Award Number: 30442502

Rationale: Micrometeorites are extraterrestrial particles smaller than ~2 mm in diameter, most of which melted during atmospheric entry and crystallised or quenched to form 'cosmic spherules'. Their parentage among meteorite groups can be inferred from triple-oxygen isotope compositions, for example, by secondary ion mass spectrometry (SIMS). This method uses sample efficiently, preserving spherules for other investigations. While SIMS precisions are improving steadily, application requires assumptions about instrumental mass fractionation, which is controlled by sample chemistry and mineralogy (matrix effects).

Methods: We have developed a generic SIMS method using sensitive high-mass resolution ion micro probe-stable isotope (SHRIMP-SI) that can be applied to finely crystalline igneous textures as in cosmic spherules. We correct for oxygen isotope matrix effects using the bulk chemistry of samples obtained by laser ablation inductively coupled plasma mass spectrometry (LA-ICP-MS) and model bulk chemical

The Meteoritical Society

Meteoritics & Planetary Science 1–14 (2023)
doi: 10.1111/maps.14091

The vesiculated layer in the anomalous diogenite Northwest Africa 12973

Lidia PITTARELLO[1,2]*, Ludovic FERRIÈRE[1,2], Stepan M. CHERNONOZHKIN[3,5], Frank VANHAECKE[3], and Steven GODERIS[4]

[1]Naturhistorisches Museum Wien, Mineralogisch-Petrographische Abteilung, Vienna, Austria
[2]Department of Lithospheric Research, University of Vienna, Vienna, Austria
[3]Atomic & Mass Spectrometry—A&MS Research Unit, Department of Chemistry, Ghent University, Ghent, Belgium
[4]Archaeology, Environmental Changes and Geo-Chemistry, Vrije Universiteit Brussel, Brussels, Belgium
[5]Present address: Lehrstuhl für Allgemeine und Analytische Chemie, Montanuniversität Leoben, Franz-Josef-Strasse 18, A-8700 Leoben, Austria
*Correspondence
Lidia Pittarello, Naturhistorisches Museum Wien, Mineralogisch-Petrographische Abteilung, Burgring 7, Vienna A-1010, Austria.
Email: lidia.pittarello@nhm-wien.ac.at

(Received 14 October 2022; revision accepted 29 September 2023)

Abstract–Diogenites, which are part of the howardite–eucrite–diogenite (HED) group, are considered to represent rocks from the lower crust and mantle of a differentiated planetary body, likely the asteroid 4 Vesta. The Northwest Africa 12973 (NWA 12973) meteorite was classified as an anomalous diogenite due to the occurrence of a vesiculated layer. This work reports on the petrographic and geochemical study of two fragments of this meteorite, aiming to better constrain the origin of the vesiculated layer. Whereas the interior of NWA 12973 (here called host) presents the typical characteristics of an olivine diogenite, that is, coarse-grained pyroxene, olivine ribbons, chromite, and accessory phases, the vesiculated layer presents a fine-grained pyroxene groundmass with local rounded relics of olivine and interstitial chromite and metal, and is characterized by abundant large vesicles. The contact between the vesiculated layer and the host is sharply defined. The composition of individual minerals does not show any significant differences between the host and the vesiculated layer, suggesting in situ melting. Geothermobarometry indicates a slightly higher crystallization temperature at lower pressure for the vesiculated layer, consistent with melting and crystallization under lower crustal conditions upon exhumation. The trigger for the local melting was likely a large impact event, which was responsible for adiabatic decompression in the central area or deep faulting and frictional melting.

INTRODUCTION

Diogenites are a relatively abundant type of achondrite meteorite, with in total 585 individuals (i.e., with distinct names) identified to date, but only 12 observed falls (Meteoritical Bulletin Database, consulted on October 3, 2022). Diogenites are petrologically highly diverse, including dunitic, harzburgitic, and noritic lithologies, in addition to the more traditional orthopyroxenites (e.g., Mittlefehldt, 2015; Mittlefehldt et al., 2012; Shearer et al., 2010, and references therein), and are petrogenetically associated with mafic magmatism in the lower crust of the parent body of the howardite–eucrite–diogenite (HED) meteorites (Shearer et al., 2010). The internal differentiation of the HED parent body was deduced from the magmatic relationship among the HEDs (e.g., Ruzicka et al., 1997). According to these authors, a fractional crystallization model is able to explain the formation of diogenites and eucrites from a unique magma source, even though the equilibrium could only be approached and not completely achieved. All the HEDs likely stem from the asteroid 4 Vesta, according to the relationship between their oxygen isotopic compositions, which define a precise fractionation line (e.g., Clayton & Mayeda, 1996; Greenwood et al., 2006). This common origin was already proposed based on spectroscopic investigations (e.g., Burbine et al., 2001 and

nature astronomy

Article

https://doi.org/10.1038/s41550-023-01968-0

Impact mixing among rocky planetesimals in the early Solar System from angrite oxygen isotopes

Received: 2 February 2022

Accepted: 6 April 2023

Published online: 15 May 2023

Check for updates

B. G. Rider-Stokes[1], R. C. Greenwood[1], M. Anand[1,2], L. F. White[1], I. A. Franchi[1], V. Debaille[3], S. Goderis[4], L. Pittarello[5,6], A. Yamaguchi[7], T. Mikouchi[8] & P. Claeys[4]

Angrite meteorites are thought to represent ancient basaltic igneous rocks that formed inward of Jupiter's orbit on the basis of their isotopic parameters such as ε^{50}Ti, ε^{54}Cr and Δ^{17}O in addition to Fe/Mn ratios of pyroxene. New bulk oxygen isotope measurements of nine angrites, and of olivine 'xenocrysts' and groundmass fractions from three quenched angrites, however, reveal clear isotopic disequilibrium, implying an impact melt origin. Groundmass fractions from Asuka 12209, Asuka 881371 and Northwest Africa 12320 quenched angrites demonstrate an average Δ^{17}O value of −0.003 ± 0.020‰. Here, excluding the bulk value and all groundmass fractions of Northwest Africa 12320, which is contaminated by an impactor, we determine a new well constrained average Δ^{17}O value for the angrite parent body (−0.066 ± 0.016‰). Microstructural investigations of Northwest Africa 12320 reveal the presence of both fully recrystallized and undeformed olivine xenocrysts, indicating that some xenocrysts underwent high-temperature processes. These results suggest that angrites bear signatures of impact-driven isotopic mixing, possibly in response to early giant planet migration. The evidence for impact mixing raises doubts about the utility of quenched angrites as a suitable Pb–Pb isotopic anchor, which in turn has consequences for accurately defining the timeline of other Solar System events.

Angrites are defined as a group of unshocked, alkali-depleted basaltic meteorites that are amongst the oldest igneous rocks in the Solar System[1,2]. On the basis of the mineral chemistry of pyroxene (Fe/Mn ratios) within angrites and the isotopic dichotomy between non-carbonaceous and carbonaceous chondrites, it is likely that angrites originate from the inner Solar System[3,4]. Evidence from Mn/Cr isotopic systematics indicates that the angrite parent body (APB) was larger than the asteroid 4 Vesta[5]. On the basis of differing textures and mineralogy, angrites have been principally divided into plutonic angrites (slowly cooled), with crystallization ages ranging from 4,560.74 ± 0.47 to 4,556.60 ± 0.26 million years ago (Ma), and quenched angrites (rapidly cooled), with crystallization ages ranging from 4,564.39 ± 0.24 to 4,562.2 ± 0.7 Ma

[1]School of Physical Sciences, The Open University, Milton Keynes, UK. [2]Department of Earth Sciences, The Natural History Museum, London, UK. [3]Laboratoire G-Time, Université Libre de Bruxelles, Brussels, Belgium. [4]Analytical–Environmental and Geo-Chemistry, Vrije Universiteit Brussel, Brussels, Belgium. [5]Mineralogisch-Petrographische Abteilung, Naturhistorisches Museum Wien, Vienna, Austria. [6]Department of Lithospheric Research, University of Vienna, Vienna, Austria. [7]National Institute of Polar Research, Tachikawa, Japan. [8]The University Museum, The University of Tokyo, Tokyo, Japan. e-mail: ben.rider-stokes@open.ac.uk

Talanta 263 (2023) 124714

Contents lists available at ScienceDirect

Talanta

journal homepage: www.elsevier.com/locate/talanta

Comparison of two gallium purification procedures for isotopic measurements by MC-ICP-MS in a set of silicate reference materials

Jérôme Roland [a,b,*], Vinciane Debaille [a], Jeroen de Jong [a], Steven Goderis [b]

[a] Laboratoire G-Time, Université Libre de Bruxelles 50, Av. F.D. Roosevelt CP 160/02, 1050, Brussels, Belgium
[b] Analytical-, Environmental-, and Geo-Chemistry (AMGC), Vrije Universiteit Brussel, Pleinlaan 2, 1050, Brussels, Belgium

ARTICLE INFO

Handling Editor: A Campiglia

Keywords:
Gallium
Ga
Moderately volatile elements
MVE
Fractionation
Stable isotopes

ABSTRACT

Gallium is a moderately volatile, moderately siderophile element with two stable isotopes: ^{69}Ga and ^{71}Ga. A general interest in Ga isotopes arose over the last few years, as its moderately volatile behavior potentially marks it as a useful tracer of various processes such as condensation and evaporation. Nevertheless, there is a lack of agreement between laboratories for consistent δ^{71}Ga values in geological reference materials. In this work, we have developed and evaluated two methods for purification protocols leading to precise analysis of gallium (Ga) isotopic composition in silicate rock materials. The first method is a three-step column chemistry using the resins AG1-X8, HDEHP, and AG50W-X12 whereas the second method uses only two columns, AG1-X8 and AG50W-X8. The two methods were applied to a range of both synthetic (multi-element) solutions and geological samples. Both methods show comparable results with no isotope fractionation occurring during purification chemistry, allowing us to define the δ^{71}Ga of selected USGS reference materials (BHVO-2, BCR-2, RGM-2). Similar to previously reported results, we also observe no Ga fractionation between distinct igneous terrestrial materials.

1. Introduction

Gallium (Z = 31) has two stable isotopes, ^{69}Ga and ^{71}Ga with natural abundances of 60.1079% and 39.8921% respectively [1,2]. The 50% condensation temperature of Ga is determined to be 968 K [3] and Ga is therefore classified as a moderately volatile element (MVE). Its volatility together with its siderophile properties makes Ga a useful tool to classify metal-rich materials. For example, the variations in Ga concentration have been used as an important parameter for meteorites classification, especially regarding iron meteorites, where gallium is usually enriched up to 100 ppm compared to chondrites (5–10 ppm) [4–9]. On Earth, the abundance of Ga in the crust is determined to be around 15 ppm [10]. Gallium is mainly present in its trivalent oxidation state at the Earth's surface. Due to their similar ionic radii, Ga^{3+} frequently substitutes for Al^{3+} and Fe^{3+} in various types of rock-forming minerals such as feldspars, micas and clay minerals [11,12]. Gallium also behaves similarly to Al during magmatic processes and is enriched in the crust compared to the mantle [6,13].

With the development of multi-collector inductively coupled plasma-mass spectrometry (MC-ICP-MS), a general interest has grown for the study of isotopic fractionation in stable isotopes, particularly of MVEs such as Zn [14], Cu [15], K [16], and Rb [17] which can be useful tools to investigate condensation and evaporation processes. Gallium has been a recent addition to this list with various studies published over the last six years [6,9,10–25]. Simultaneously, purification methods for Ga isotopes have been developed and adapted by different laboratories. Gallium isotopic compositions are usually reported as δ^{71}Ga in permil (‰) relative to a Ga reference material following the equation:

$$\delta^{71}Ga_{standard} = \left[\left(^{71}Ga/^{69}Ga\right)_{sample} / \left(^{71}Ga/^{69}Ga\right)_{standard} - 1\right] \times 1000$$

Most authors previously reported values relative to the high purity Ga metal NIST SRM-994 [10,19,21,22], except in Kato et al. [6,9,20] where a Ga ICP/DCP standard solution (Aldrich, catalog number 35623–9) was used. Up to now, reported δ^{71}Ga for terrestrial reference materials (RM) are not consistent between studies, even though the reasons for this remain unclear. Wimpenny et al. (2020) [22] suggested that the NIST SRM-994 is heterogeneous for its isotopic composition.

In this study, we have applied and evaluated two different purification methods for gallium, which were modified based on previous studies. We used the high purity Ga metal NIST SRM-994 as isotopic standard because it is the most used standard in previous studies and allows for more efficient interlaboratory comparison which is the main

* Corresponding author. Laboratoire G-Time, Université Libre de Bruxelles 50, Av. F.D. Roosevelt CP 160/02, 1050, Brussels, Belgium.
E-mail address: jerome.roland@ulb.be (J. Roland).

https://doi.org/10.1016/j.talanta.2023.124714
Received 16 February 2023; Received in revised form 16 May 2023; Accepted 22 May 2023
Available online 23 May 2023

Icarus 412 (2024) 115983

Contents lists available at ScienceDirect

Icarus

journal homepage: www.elsevier.com/locate/icarus

Moderately volatile elemental and isotopic variations in variably shocked equilibrated ordinary chondrites from Antarctica

Jérôme Roland [a,b,*], Vinciane Debaille [a], Hamed Pourkhorsandi [a], Steven Goderis [b]

[a] Laboratoire G-Time, Université Libre de Bruxelles, 50 Av. F.D. Roosevelt, CP 160/02, 1050 Brussels, Belgium
[b] Archaeology, Environmental Changes, and Geo-Chemistry (AMGC), Vrije Universiteit Brussel, Pleinlaan 2, 1050 Brussels, Belgium

ARTICLE INFO

Keywords:
Cosmochemistry
Meteorites
Impact processes

ABSTRACT

Volatile elements, crucial players in planetary evolution, condense at low temperatures from solar nebula. Despite extensive past research, gaps remain in understanding the volatile budget establishment and depletion mechanisms during the early stages of Solar System formation. This study investigates the role of shock events on multiple isotope systems in H6 ordinary chondrites with varying shock and weathering degrees. In this study, we classified fifteen H6 ordinary chondrites from Antarctica for their shock and weathering stages. We report the bulk trace elemental abundances of the samples and focus on Zn, Ga, Cu, and Fe isotope compositions, each with distinct 50% condensation temperatures at 726 K, 968 K, 1037 K, and 1334 K, respectively. Three of those elements (Zn, Ga, and Cu) are moderately volatile and trace elements whereas Fe is a moderately refractory and major element. Zinc, with the lowest condensation temperature in this suite, exhibits the widest range in isotopic fractionation (difference between maximum and minimum delta (δ) values in per mil, expressed as Δ hereafter) in our data set with $\Delta^{66}Zn = 2.60$ ‰. Gallium presents a much narrower range of fractionation with $\Delta^{71}Ga = 0.62$ ‰ while copper is three times lower at $\Delta^{65}Cu = 0.21$ ‰. Iron, with the highest condensation temperature, displays the lowest range with $\Delta^{56}Fe = 0.18$ ‰. Interestingly, we found that these variations in isotopic fractionation do not appear to correlate with the shock stage nor weathering grade of the samples. Our findings suggest that impacts cannot explain the observed isotopic fractionation. Evaporative loss due to thermal metamorphism on the parent body may account for Zn and Ga isotope fractionation but likely represents a minor process. Future research should investigate variously metamorphosed samples using in-situ techniques (e.g., laser ablation MC-IPC-MS or SIMS) to highlight condensation and accretion processes from the early solar nebula.

1. Introduction

Volatile elements are elements that condense at relatively low temperatures (≤1200K) from the solar gas (Grossman, 1972). They play a crucial role in the evolutionary processes of planets. However, our understanding of how the volatile budgets of planets are established and what are the mechanisms and extent of volatile depletion in planetary bodies during the early stages of Solar System formation still remains incomplete (e.g., Albarède, 2009; Mezger et al., 2021, 2020; Norris and Wood, 2017; Paniello et al., 2012; Wood et al., 2010). The uneven distribution of volatile elements throughout the evolution of the solar system remains a topic of considerable ongoing debate. A comparison between terrestrial planets, the solar photosphere, and CI chondrites reveals a depletion of volatile elements (e.g., Cl, K, Zn) in the terrestrial planets (Albarède, 2009; Dreibus and Palme, 1996; Jochum and Palme, 1993; Larimer and Anders, 1967; Pringle et al., 2017; Ringwood, 1966; Stevenson and Lunine, 1988; Wasson and Chou, 1974; Xu et al., 2023). Various origins to explain this depletion have been proposed either via nebular processes such as incomplete volatile condensation (Jochum and Palme, 1993; Wasson and Chou, 1974) or planetary processes such as accretion evaporation/condensation (Albarède, 2009; Moynier et al., 2017; Paniello et al., 2012; Pringle et al., 2017) and magma ocean degassing (Day and Moynier, 2014; Dhaliwal et al., 2018; Kato et al., 2015; Wimpenny et al., 2019). Those various processes did not affect early solar system bodies. Planetary bodies such as chondrites parent bodies, the Moon and Mars present a non-chondritic Mn/Na ratio (O'Neill and Palme, 2008) that was supposedly caused by evaporation from silicate melts under high fO_2 conditions (Sossi et al., 2019). This evaporation was favored on planetesimals with respect to larger planetary bodies due to their lower escape velocities (Hin et al., 2017; Young

* Corresponding author at: Laboratoire G-Time, Université Libre de Bruxelles, 50 Av. F.D. Roosevelt, CP 160/02, 1050 Brussels, Belgium.
E-mail address: jerome.roland@ulb.be (J. Roland).

https://doi.org/10.1016/j.icarus.2024.115983
Received 4 October 2023; Received in revised form 30 January 2024; Accepted 31 January 2024
Available online 1 February 2024

ACS EARTH AND SPACE CHEMISTRY

http://pubs.acs.org/journal/aescoq

Article

Assessing the Effect of Aqueous Alteration on Soluble Organic Matter in Primitive Carbonaceous Chondrites: The Case of Asuka 12236

Coline Serra,* Vassilissa Vinogradoff,* Pauline Poinot, Quentin Blancart Remaury, Fabrice Duvernay, Louis Le Sergeant d'Hendecourt, Grégoire Danger, Philippe Claeys, Steven Goderis, and Philippe Schmitt-Kopplin

Cite This: ACS Earth Space Chem. 2023, 7, 1980−1991

Read Online

ACCESS | Metrics & More | Article Recommendations | Supporting Information

ABSTRACT: Carbonaceous chondrites (CCs) are considered the closest solid material to the composition of the early Solar System and can provide information about the origin of organic matter (OM) in the system and on Earth. Despite being primitive, their parent bodies have undergone secondary processes shortly after their formation (hydrothermal or metamorphism alterations) that blur their initial organic or mineral composition. The most primitive CC members are hence very precious to study the original composition. Here, we report the characterization of the soluble organic matter (SOM) of Asuka 12236, classified among the most primitive members of the CM group in comparison with the SOM from other CM chondrites: Paris, Murchison, and Aguas Zarcas. Analysis of these SOM were performed using several analytical techniques, including elemental analysis, high-resolution mass spectrometry, and liquid chromatography coupled to different mass spectrometers. Our results show that Asuka 12236 has the lowest H content among the CMs studied here and presents heterogeneity in its C content, likely indicating variable degrees of aqueous alteration. High-resolution mass spectrometry analysis reveals that Asuka 12236 has a molecular diversity similar to the SOM of Murchison and Aguas Zarcas but with a higher abundance of sulfur compounds, more similar to Paris SOM. The content of organomagnesium compounds indicates no high-pressure or -temperature stress but rather mid-temperature aqueous alteration for Asuka 12236, like Murchison SOM, but unlike Paris or Aguas Zarcas SOM. From liquid chromatography coupled with mass spectrometry analysis, we observed the highest concentration of amino acids in Asuka 12236 compared to the other CM chondrites considered here. Amino acids are mainly of α forms, witnessing a Strecker formation or a formose-type reaction under low amounts of water, in agreement with the low H content recorded in this peculiar chondrite. This study of the SOM of chondrites with different degrees of alteration highlights that organic compounds may be transformed much more rapidly than the minerals during hydrothermal alteration. This OM evolution depends on the amount of water and/or the temperature and/or pressure, leading toward significant transformation from one chondrite to another, while the mineralogy can indicate a low degree of alteration. In addition, to better assess the initial OM in chondrites, the impact of aqueous alteration on organic matter calls for additional laboratory experimentation.

KEYWORDS: *meteorites, aqueous alteration, soluble organic matter, amino acids, FTICR, liquid chromatography, extraterrestrial carbon*

1. INTRODUCTION

Carbonaceous chondrites (CCs), considered the most primitive meteorites, can contain up to 5% of organic matter (OM).[1] They can thus provide insight into the initial composition of OM in the protoplanetary disk (see the reviews by Remusat et al.[2] and Alexander et al.[3]). Their parent bodies, the asteroids, were formed among the first bodies of the solar system 4.56 billion years ago and have remained virtually unchanged over time from the planets. However, mineralogical studies have revealed that secondary alteration processes have occurred in the CC parent bodies during the first tens of thousands of years after their formation.[4] These traces of alteration processes range from aqueous alteration (liquid fluid) to metamorphism (high temperature/pressure), which could have blurred the initial organic signatures in the same way as the minerals have been transformed. In this line, the less-altered CCs are particularly interesting to study this secondary alteration and obtain clues about the initial composition of the accreted OM. The Mighei-subtype CC group (CM) contains some meteorites having low alteration degrees with an ~2 wt % abundance of carbon, making them

Received: April 21, 2023
Revised: September 6, 2023
Accepted: September 8, 2023
Published: September 25, 2023

https://doi.org/10.1021/acsearthspacechem.3c00106
ACS Earth Space Chem. 2023, 7, 1980−1991

nature climate change

Brief Communication

https://doi.org/10.1038/s41558-024-01954-y

Antarctic meteorites threatened by climate warming

Received: 28 June 2023

Accepted: 8 February 2024

Published online: 08 April 2024

Check for updates

Veronica Tollenaar[1,12], Harry Zekollari[1,2,3,4,12], Christoph Kittel[5,6], Daniel Farinotti[2,3], Stef Lhermitte[7,8], Vinciane Debaille[9], Steven Goderis[10], Philippe Claeys[10], Katherine Helen Joy[11] & Frank Pattyn[1]

More than 60% of meteorite finds on Earth originate from Antarctica. Using a data-driven analysis that identifies meteorite-rich sites in Antarctica, we show climate warming causes many extraterrestrial rocks to be lost from the surface by melting into the ice sheet. At present, approximately 5,000 meteorites become inaccessible per year (versus ~1,000 finds per year) and, independent of the emissions scenario, ~24% will be lost by 2050, potentially rising to ~76% by 2100 under a high-emissions scenario.

Meteorites are unique samples of extraterrestrial bodies and provide crucial information on the origin and evolution of our Solar System[1,2]. Antarctica is the world's most prolific site for collecting meteorites, with more than 60% of all ~80,000 meteorites ever found on Earth being collected at the surface of the ice sheet. Antarctic meteorites are found in blue ice areas, which are atypical zones (~1% of the Antarctic surface area) where layers of snow and ice are removed from the surface through a combination of ice flow processes and local meteorological conditions, exposing meteorites that were once embedded in the ice[1,3]. Not all blue ice areas contain meteorites: only where processes interact favourably, a concentration of meteorites is built up over tens to hundreds of thousands of years, resulting in so-called meteorite stranding zones (Fig. 1a)[4–6]. Meteorites found in Antarctica are a few centimetres in diameter on average, but are easily detectable given their visual contrast with the underlying ice[7,8]. Over past decades, an average of ~1,000 meteorites per year have been collected through numerous field campaigns (Fig. 2a) and the potential of Antarctic meteorites remains far from exhausted: a data-driven approach[9] recently identified over 600 meteorite-rich areas in Antarctica. Many of the identified meteorite stranding zones are not yet (fully) explored, and an estimated 300,000 to 850,000 meteorites remain to be collected from the surface of the ice sheet (Fig. 2b)[9].

Once exposed at the surface, meteorites can stay there for thousands of years due to stagnant ice flow and the lack of weathering in the cold, dry conditions[3,5]. While most of the indicators for the presence of meteorites—for example, ice flow velocity, elevation, mountains—are thought to be stable on multidecadal to centennial timescales, the concentration of meteorites is also directly influenced by temperature[4,9,10]. Even when temperatures are well below zero, meteorites, with their characteristic dark crust, warm when exposed to solar radiation[11] and can melt the underlying ice. The warmed meteorite generates a small water melt pocket below the stone, resulting in a surface depression that deepens over time into a hole, which (in conjunction with refreezing meltwater) results in the disappearance ('sinking') of the meteorite from the surface (Fig. 1)[10,12,13]. The sensitivity of meteorite presence to temperature is apparent from various independent lines of evidence:

(1) Field observations: entrapped meteorites have been found covered by superimposed (refrozen) ice after the meteorite sank into the ice (Fig. 1)[14–16].
(2) Data on meteorite retrieval locations[9,17] indicate that almost no meteorites (<1% of all finds) are found in locations where surface temperatures of the ice are higher than −9 °C even very rarely (this near-maximum value of the surface temperature is

[1]Laboratoire de Glaciologie, Université libre de Bruxelles, Brussels, Belgium. [2]Laboratory of Hydraulics, Hydrology and Glaciology (VAW), ETH Zürich, Zurich, Switzerland. [3]Swiss Federal Institute for Forest, Snow and Landscape Research (WSL), Birmensdorf, Switzerland. [4]Department of Water and Climate, Vrije Universiteit Brussel, Brussels, Belgium. [5]Department of Geography, UR SPHERES, University of Liège, Liège, Belgium. [6]Institut des Géosciences de l'Environnement (IGE), Université Grenoble Alpes/CNRS/IRD/G-INP, Grenoble, France. [7]Department of Earth and Environmental Sciences, KU Leuven, Leuven, Belgium. [8]Department of Geoscience and Remote Sensing, Delft University of Technology, Delft, the Netherlands. [9]Laboratoire G-Time, Université libre de Bruxelles, Brussels, Belgium. [10]Archaeology, Environmental Changes and Geo-Chemistry, Vrije Universiteit Brussel, Brussels, Belgium. [11]Department of Earth and Environmental Sciences, University of Manchester, Manchester, UK. [12]These authors contributed equally: Veronica Tollenaar, Harry Zekollari. e-mail: Veronica.Tollenaar@ulb.be; zharry@ethz.ch

Earth Planet. Sci. Lett. 627 (2024) 118562

Contents lists available at ScienceDirect

Earth and Planetary Science Letters

journal homepage: www.elsevier.com/locate/epsl

The identification of airbursts in the past: Insights from the BIT-58 layer

Matthias van Ginneken [a,*], Ralph P. Harvey [b], Steven Goderis [c], Natalia Artemieva [d,e], Mark Boslough [f], Ryoga Maeda [g], Jérôme Gattacceca [h], Luigi Folco [i], Akira Yamaguchi [j], Corinne Sonzogni [h], Penelope Wozniakiewicz [a]

[a] Centre for Astrophysics and Planetary Science, School of Physical Sciences, University of Kent, Ingram Building, Canterbury CT2 7NH, UK
[b] Department of Geological Sciences, 112 A. W. Smith Building, Case Western Reserve University, Cleveland OH 44106-7216, USA
[c] Archaeology, Environmental Changes & Geo-Chemistry, Vrije Universiteit Brussel, Pleinlaan 2, Brussels BE1050, Belgium
[d] Planetary Science Institute, 1700 East Fort Lowell, Suite 106, Tucson AZ 85719, USA
[e] Russian Academy of Sciences, Institute of Geosphere Dynamics, Moscow 119334, Russian Federation
[f] Earth and Planetary Sciences, University of New Mexico, Albuquerque, NM 87131, USA
[g] Submarine Resources Research Center (SRRC), Japan Agency for Marine-Earth Science and Technology (JAMSTEC), 2-15 Natsushimacho, Yokosuka, Kanagawa 237-0061, Japan
[h] CNRS, Aix-Marseille Univ, IRD, INRAE, CEREGE, Aix-en-Provence, France
[i] Dipartimento di Scienze della Terra, Università di Pisa, Via S. Maria 53, Pisa, Italy
[j] National Institute of Polar Research, Tokyo 190-8518 Japan

ARTICLE INFO

Editor: Dr. F. Moynier

ABSTRACT

Airbursts are estimated to be the most frequent type ofdestructive impact events. Yet, confirmation of these events is elusive, resulting in a major gap in the impact record of Earth. The recent discovery of igneous chondritic spherules produced during a new type of touchdown airburst 430 thousand years (kyr) ago over Antarctica, in which a projectile vapor jet interacts with the Antarctic ice sheet, provided the first trace of such an impact in the geological record. In terms of petrology and geochemistry, particles constituting the BIT-58 dust horizon, which was found in surface ice at near Allan Hills in Antarctica, are almost identical to those produced 430 kyr ago. We demonstrate here that BIT-58 particles were indeed formed during a touchdown event between 2.3 and 2.7 million years (Myr) ago. This represents the oldest record of an airburst on Earth identified to date. Slight geochemical differences with 430 kyr old airburst spherules provide additional constraints on spherule condensation in large airburst plumes. Finding confirmation of airbursts in the paleorecord can provide insight into the frequency of the most hazardous impacts and, thus, has implications for planetary defence.

1. Introduction

Airbursts are the sharp release of impact energy when asteroids less than 200 m in size are disrupted in the lower atmosphere (Artemieva and Shuvalov, 2016; Boslough et al., 2015). Shockwaves and thermal radiation produced by airbursts result in massive damage at ground level, as evidenced by the 2013 Chelyabinsk small-scale airburst that resulted from the atmospheric entry of a stony asteroid approximately 20 metres in size (Popova et al., 2013). Surveys of the population of Near-Earth Asteroids smaller than 140 m, along with numerical models simulating effects at ground level, suggest that airbursts are currently the biggest cosmic threat to populations and infrastructures by combining their destructive potential and calculated frequency (Artemieva and Shuvalov, 2019; Boslough, 2014; Boslough et al., 2015). However, contrary to cratering events that can be identified using a set of well-defined geomorphological, mineralogical and geochemical criteria, evidence for past airbursts are poorly constrained (Glass and Simonson, 2012; Osinski et al., 2012). This is partly due to the lack of easily recognizable impact structures created by such events, but also a limited knowledge of physical and geochemical processes leading to the formation of potential residues.

The recent discovery of airburst spherules from Antarctica demonstrates that past airburst events can be identified on the grounds of petrological and geochemical evidences (Van Ginneken et al., 2021; 2016). So far, two spherule populations have been reported to have originated from large airbursts approximately 430 and 480 thousand

* Corresponding author.
E-mail address: m.van-ginneken@kent.ac.uk (M. van Ginneken).

https://doi.org/10.1016/j.epsl.2023.118562
Received 19 October 2023; Received in revised form 18 December 2023; Accepted 27 December 2023
Available online 9 January 2024

PHILOSOPHICAL TRANSACTIONS A

royalsocietypublishing.org/journal/rsta

Review

Cite this article: van Ginneken M *et al.* 2024 Micrometeorite collections: a review and their current status. *Phil. Trans. R. Soc. A* **382**: 20230195.
https://doi.org/10.1098/rsta.2023.0195

Received: 15 October 2023
Accepted: 23 January 2024

One contribution of 9 to a theme issue 'Dust in the Solar System and beyond'.

Subject Areas:
astrochemistry, solar system

Keywords:
micrometeorites, cosmic dust, planetary science

Author for correspondence:
Matthias van Ginneken
e-mail: m.van-ginneken@kent.ac.uk

THE ROYAL SOCIETY PUBLISHING

Micrometeorite collections: a review and their current status

Matthias van Ginneken[1], Penelope J. Wozniakiewicz[1], Donald E. Brownlee[2], Vinciane Debaille[3], Vincenzo Della Corte[4], Lucie Delauche[5], Jean Duprat[5,6], Cecile Engrand[5], Luigi Folco[7], Marc Fries[8], Jérôme Gattacceca[9], Matthew J. Genge[10], Steven Goderis[11], Matthieu Gounelle[5], Ralph P. Harvey[12], Guido Jonker[13], Lisa Krämer Ruggiu[11], Jon Larsen[14], James H. Lever[15], Takaaki Noguchi[16], Scott Peterson[17], Pierre Rochette[9], Julien Rojas[5,18], Alessandra Rotundi[4,19], N. G. Rudraswami[20], Martin D. Suttle[7,21], Susan Taylor[15], Flore Van Maldeghem[11] and Michael Zolensky[8]

[1]Centre for Astrophysics and Planetary Science, School of Physics and Astronomy, University of Kent, Canterbury CT2 7NH, UK
[2]Department of Astronomy, University of Washington, Seattle, WA 98195, USA
[3]Laboratoire G-Time, Université Libre de Bruxelles, Brussels 1050, Belgium
[4]Istituto di Astrofisica e Planetologia Spaziali—INAF, Roma, Italy
[5]IJCLab, Université Paris-Saclay, CNRS/IN2P3, Orsay 91405, France
[6]IMPMC, CNRS-MNHN-Sorbonne Universités, UMR7590, 57 rue Cuvier, Paris 75005, France
[7]Dipartimento di Scienze della Terra, Università di Pisa, Pisa, Italy
[8]NASA Johnson Space Center, Astromaterials Research and Exploration Science (ARES), Houston, TX 77058, USA
[9]CEREGE, CNRS, Aix-Marseille Univ, IRD, INRAE, Aix-en-Provence, France
[10]Impacts and Astromaterials Research Centre, Department of Earth Science and Engineering, Imperial College London, UK
[11]Archaeology, Environmental Changes and Geo-Chemistry, Vrije Universiteit Brussel, Brussels BE 1050, Belgium
[12]Department of Geological Sciences, 112 A. W. Smith Building, Case Western Reserve University, Cleveland, OH 44106-7216, USA

Earth Planet. Sci. Lett. 641 (2024) 118837

Contents lists available at ScienceDirect

Earth and Planetary Science Letters

journal homepage: www.elsevier.com/locate/epsl

Chrome-rich spinels in micrometeorites from modern Antarctic sedimentary deposits

Flore Van Maldeghem [a,b,*], Ryoga Maeda [a,c], Bastien Soens [a], Martin D. Suttle [d,e], Lisa Krämer Ruggiu [a], Carole Cordier [f], Akira Yamaguchi [g], Birger Schmitz [h], Philippe Claeys [a], Luigi Folco [e], Steven Goderis [a]

[a] Archaeology, Environmental changes, and Geo-chemistry (AMGC), Vrije Universiteit Brussel, Pleinlaan 2, Brussels B-1050, Belgium
[b] Center for Star and Planet Formation, Globe Institute, University of Copenhagen, Oster Voldgade 5, 1350 Copenhagen K, Denmark
[c] Submarine Resources Research Center (SRRC), Japan Agency for Marine-Earth Science and Technology (JAMSTEC), 2-15 Natsushimacho, Yokosuka, Kanagawa 237-0061, Japan
[d] School of Physical Sciences, The Open University, Walton Hall, Milton Keynes MK7 6AA, UK
[e] Dipartimento di Scienze della Terra, Università di Pisa, Via S. Maria 53, Pisa 56126, Italy
[f] CNRS, IRD, Université Grenoble Alpes, Université Savoie Mont Blanc, Université Gustave Eiffel, ISTerre, Grenoble 38000, France
[g] National Institute of Polar Research, 10-3 Midori-cho, Tachikawa-Shi, Tokyo 190-8518, Japan
[h] Astrogeobiology Laboratory, Department of Physics, Lund University, P.O. Box 118, Lund 22100, Sweden

ARTICLE INFO

Edited by: Dr. F. Moynier

Keywords:
Micrometeorites
Cosmic spherules
Cr-spinel
Parent bodies
Chromite
Oxygen isotope ratios

ABSTRACT

Each year, approximately 5000 tons of extraterrestrial material reaches the Earth's surface as micrometeorites, cosmic dust particles ranging from 10 to 2000 μm in size. These micrometeorites, collected from diverse environments, mainly deep-sea sediments, Antarctic ice, snow and loose sediments, and hot deserts, are crucial in understanding our Solar System's evolution. Chrome-rich spinel (Cr-spinel) minerals have gained attention as proxies for studying the extraterrestrial flux in sedimentary deposits, because these robust minerals occur, in various extraterrestrial materials, with compositions characteristic of their parent bodies. A total of 27 Cr-spinel bearing micrometeorites within the size range of 185–800 μm, were identified from approximately 6000 micrometeorites from the Transantarctic Mountains ($n = 23$) and the Sør Rondane Mountains ($n = 4$), in Antarctica, containing Cr-spinel (5–120 μm), were examined in this study for geochemical composition and high-precision oxygen isotope ratios to assess alteration and identify potential parent bodies.

Oxygen isotopes in the micrometeorite groundmass and in Cr-spinel grains reveal a predominance of ordinary chondritic precursors, with only 1 in 10 micrometeorites containing Cr-spinel minerals showing a carbonaceous chondritic signature. This may be further confirmed by an elevated Al content (> 12 wt% Al_2O_3) in Cr-spinel from specific carbonaceous chondrite types, but a more extensive dataset is required to establish definitive criteria. The first Cr-spinel bearing particle, in an Antarctic micrometeorite, that can be linked to R-chondrites based on oxygen isotopes, has been documented, demonstrating the potential for R-chondrites as a source of chrome-rich spinels. The study also highlights the potential for chemical modifications and alteration processes that Cr-spinel minerals may undergo during their time on the parent body, atmospheric entry, and terrestrial residence.

In the context of the broader micrometeorite flux, the results align with previous findings, showing a consistent contribution of micrometeorites containing Cr-spinel minerals related to ordinary chondrites over the past 2 to 4 million years. This is however a small fraction (~ 1 %) of the total micrometeorite flux. The study further confirms that Cr-spinel minerals recovered from sedimentary deposits serve as valuable proxies for tracking events related to ordinary chondritic or achondritic materials. However, it is emphasized that Cr-spinel minerals alone cannot serve as exclusive indicators of the overall extraterrestrial flux, especially during periods dominated by carbonaceous chondritic dust in the inner Solar System. To comprehensively understand the complete extraterrestrial flux, additional proxies are needed to trace dust-producing events associated with various Solar System objects. The intricate nature of Cr-spinel compositions, and the potential for alteration processes emphasize the need for further research to refine our understanding of these extraterrestrial markers.

* Corresponding author.
E-mail address: flore.maldeghem@sund.ku.dk (F. Van Maldeghem).

https://doi.org/10.1016/j.epsl.2024.118837
Received 3 January 2024; Received in revised form 29 May 2024; Accepted 5 June 2024